

MICROCOPY RESOLUTION TEST CHART

NATIONAL BUREAU OF STANDARDS-1963-A

AD A089651

**SECRET**

①  
B.S.

⑥

**TIME-DOMAIN SONAR TARGET RESPONSE MODELING**

⑩

H. Mieras and C. L. Bennett

Sperry Research Center, Sudbury, MA 01776 ✓

**FINAL REPORT**

Contract No. N61331-78-C-0049 ✓

⑪

① 101

⑭

SRC-CR-79-74 ✓

October 1979

⑪

**SECRET**  
SEP 29 1980  
**A**

Prepared for  
**NAVAL COASTAL SYSTEMS LABORATORY**  
PANAMA CITY, FLORIDA 32407

**DISTRIBUTION STATEMENT A**

Approved for public release;  
Distribution Unlimited

**SPERRY**  
RESEARCH CENTER

J.C.B.

DDC FILE COPY

4/23/79

80 9 15 003

## LIST OF ILLUSTRATIONS

<u>Figure</u>		<u>Page</u>
2-1	Scattering geometry.	4
2-2	Frequency response of sphere: (a) hard, (b) aluminum, and (c) brass.	10
2-3	Frequency response of aluminum sphere with (a) $c_1 = 9300$ , (b) $c_1 = 6200$ , and (c) $c_1 = 4130$ .	11
2-4	Frequency response of aluminum sphere with (a) $c_2 = 4650$ , (b) $c_2 = 3100$ , and (c) $c_2 = 2065$ .	12
2-5	Frequency response of aluminum sphere with (a) $\rho = 2.7$ and (b) $\rho = 1.5$ .	13
2-6	Frequency response of aluminum sphere, fluid approximation, with (a) $c_1 = 9300$ , (b) $c_1 = 6200$ , and (c) $c_1 = 4130$ .	14
2-7	Smoothed impulse response of aluminum sphere: (a) hard, (b) aluminum, and (c) brass.	17
2-8	Smoothed impulse response of aluminum sphere with (a) $c_1 = 9300$ , (b) $c_1 = 6200$ , and (c) $c_1 = 4130$ .	18
2-9	Smoothed impulse response of aluminum sphere with (a) $c_2 = 4650$ , (b) $c_2 = 3100$ , and (c) $c_2 = 2065$ .	19
2-10	Smoothed impulse response of aluminum with (a) $\rho = 2.7$ and (b) $\rho = 1.5$ .	20
2-11	Smoothed impulse response of aluminum sphere, fluid approximation, for (a) $c_1 = 9300$ , (b) $c_1 = 6200$ , and (c) $c_1 = 4130$ .	21
2-12	Time reference for scattering from unit sphere.	22
2-13	Aluminum variations — responses vs. $c_{2t}$ with $c_1 = 6200$ .	24
2-14	Aluminum variations — responses vs. $c_{2t}$ with $c_1 = 9300$ .	25
3-1	Plane wave refraction at plane boundary.	27
3-2	Impulse response of hard sphere (leading edge).	32
3-3	Local influence theory: reflection and refraction.	42
3-4	Glory paths for sphere.	43
3-5	Glory wave model — fluid sphere response.	46
3-6	Glory wave model — aluminum and variations.	47
3-7	Glory wave model — brass and variations.	48
3-8	Principal scattering modes involving shear waves.	49
3-9	Simplified impulse response.	51

Accession For	
NRS - G. K. I.	<input checked="" type="checkbox"/>
EDS - S. S.	<input type="checkbox"/>
Unprocessed	<input type="checkbox"/>
Ju. - refraction	<input type="checkbox"/>
By _____	
Date _____	
Av. _____	
Dist	# call and/or special
A	

## LIST OF ILLUSTRATIONS (Cont.)

<u>Figure</u>		<u>Page</u>
3-10	Aluminum response model – time domain.	53
3-11	Aluminum response model – frequency domain.	54
3-12	Brass response model – time domain.	55
3-13	Brass response model – frequency domain.	56
4-1	STIE response for fluid aluminum right circular cylinder.	64
4-2	STIE response for fluid brass right circular cylinder.	65
4-3	STIE response – small angle deviation.	66
4-4	Surface pressure for elastic sphere – classical and STIE.	70
4-5	Status of elastic STIE calculation – far field response.	72
4-6	Shell scattering problem.	72
4-7	STIE solution – scattering from spherical membrane.	76
5-1	Shell responses as a function of thickness – frequency domain, thick shell.	83
5-2	Shell responses as a function of thickness – frequency domain, thin shell.	84
5-3	Shell responses as a function of thickness – frequency domain, very thin shell.	85
5-4	Shell responses as a function of thickness – time domain, $a_n = 4$ , thick shell.	86
5-5	Shell responses as a function of thickness – time domain, $a_n = 4$ , thin shell.	87
5-6	Shell responses as a function of thickness – time domain, $a_n = 4$ , very thin shell.	88
5-7	Responses of very thin shell with variations in elastic parameters, $h = 0.001$ .	90
5-8	Responses of very thin shell with variations in $\rho$ and $h$ , keeping $\rho_1 h$ constant.	91
5-9	Comparison of responses of soft sphere and soft core (gas-filled) spherical shell – frequency domain.	91
5-10	Comparison of responses of soft sphere and soft core (gas-filled) spherical shell – time domain.	92
5-11	Frequency and time domain responses of heavy core (glycerin-filled) spherical shell.	92

SECTION 1  
INTRODUCTION

The acoustic response of simple metallic targets submerged in water is studied under this contract. The aim is to develop an interpretation of the process which would permit its characterization by a simple model. This work is a continuation of a previous contract [1], which should be referred to for the general background of this problem and for greater detail of the space-time integral equation approach.

The classical solution for acoustic scattering from a penetrable homogeneous sphere is studied first in Section 2. It is seen that hard or soft target approximations are not valid for metallic targets (except at very low frequencies), but that resonances are present which are characteristic of the interior composition. Viewed in the time domain, the impulse response of a target consists of a sequence of pulses following the specular impulse. The arrival times of these pulses can be related directly to the elastic constants of the target and medium. Moreover they can be interpreted simply as pulse traversal times at the several speeds along certain paths. The description of this model (the 'glory-wave' model) is the subject of Section 3, along with the first steps toward a complete quantitative theory. A semi-quantitative computer program which generates time and frequency domain responses is given in an appendix.

In Section 4, the space-time integral equation approach is described. Whereas classical solutions can only be found for targets conforming to separable coordinate systems, the integral equation approach is applicable to targets of arbitrary shape. An exact solution is presented for a fluid right circular cylinder. The space-time integral equation formulation is presented for elastic targets (which exhibit interior shear waves as well as compression waves), although numerical difficulties have so far prevented computational results. A procedure is described whereby the scattering

next page

center responses can be computed for use in the simple model of Section 3.

In Section 5, the results of previous sections are extended to the hulled target. The classical solution is derived for the thick spherical shell. Results for the shell are given as functions of elastic parameters and shell thickness, including the very-thin shell limit. It is seen that the thick shell response is much more complicated than the already complicated homogeneous sphere, but that in the limit of the thin shell the response becomes a stepped sinusoid with exponential decay. Also given, in subsection 4.3, is the space-time integral equation formulation for the thin hulled target of general geometry.

SECTION 2  
ANALYSIS OF HOMOGENEOUS SPHERE RESPONSE

The solution for scattering from a homogeneous penetrable sphere was first given by Anderson in 1950 for the fluid sphere [2] and by Faran in 1951 for the elastic sphere [3]. These were classical solutions; found by expanding interior and exterior fields as sums of eigenfunctions and equating these at the boundary. The applicability of the method is limited to simple shapes which form constant surfaces in separable coordinate systems. However, the advantage is that the solution is straightforward. The only numerical difficulty arises in the evaluation of the spherical Bessel functions at large order and argument. In this section, the classical solution for the sphere, transformed to the time domain, will be used as a starting point for understanding acoustic scattering.

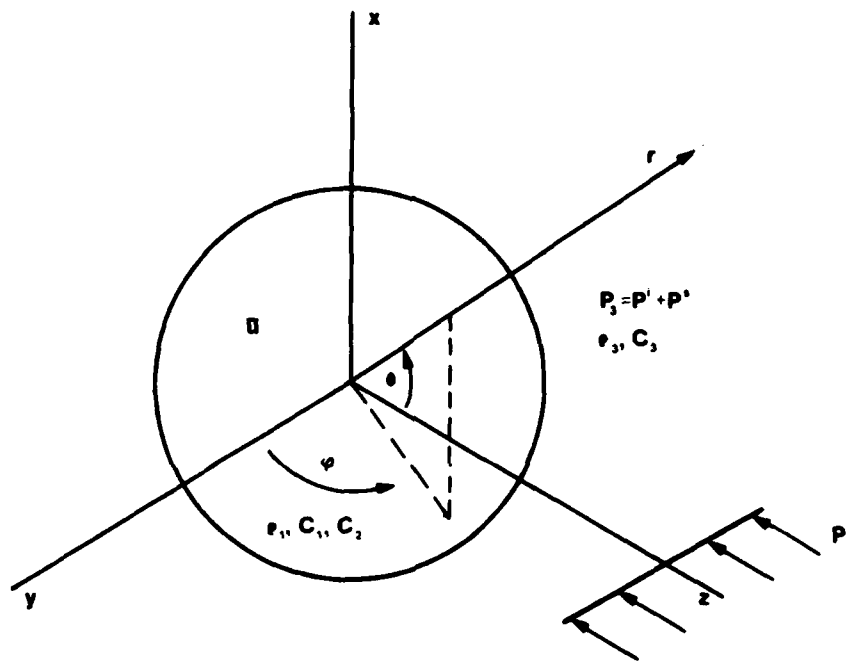
2.1 CLASSICAL SOLUTION FOR HOMOGENEOUS SPHERE

The elastic sphere is completely characterized by its radius,  $a$ , and three elastic constants: density  $\rho_1$ , compression speed  $c_1$ , and shear speed  $c_2$  (see Appendix 8.1). It is embedded in a fluid with density  $\rho_3$  and speed of sound  $c_3$ . Let a monochromatic plane wave  $p^i(\vec{r}, t)$  be incident upon it from the positive  $z$  direction (Fig. 2-1). The incident plane wave can be expanded, for  $r \geq a$ :

$$p^i(\vec{r}, t) = P_0 \sum_{n=0}^{\infty} (2n+1) (-i)^n P_n(\cos \theta) j_n(kr) e^{-i\omega t} \quad (2-1)$$

The time dependence  $e^{-i\omega t}$  will be suppressed in the equations to follow. The scattered pressure is given by

$$p^s(\vec{r}) = P_0 \sum_{n=0}^{\infty} c_n h_n^{(1)}(kr) P_n(\cos \theta) \quad (2-2)$$



79-888

FIG. 2-1 Scattering geometry.

Here,

$P_n(\cos \theta)$  are the Legendre polynomials;

$j_n(kr)$ ,  $n_n(kr)$ ,  $h_n^{(1)}(kr)$  are the spherical Bessel functions of the first, second and third kind;

$P_0$  is an arbitrary constant, or could represent  $P_0(\omega)$ , the frequency content of the incident pulse;

$k = 2\pi/\lambda = \omega/c_3$ , the wave number; and

$c_n$  is the coefficient which is to be found.

Note that  $p^S$  satisfies the radiation condition, since asymptotically  $h_n^{(1)}(kr) e^{-i\omega t} \rightarrow (-i)^{n+1} (1/kr) e^{i(kr - \omega t)} \rightarrow 0$  as  $r \rightarrow \infty$  and is outward traveling.

Following Faran, it can be argued that the displacement  $\vec{u}$  inside the target can be written

$$\vec{u} = -\nabla\psi + \nabla \times \vec{A}, \quad (2-3)$$

where  $\psi$ ,  $\vec{A}$  are of the form

$$\psi = \sum_{n=0}^{\infty} a_n j_n(k_1 r) P_n(\cos \theta) \quad (2-4)$$

$$\vec{A} = \hat{\phi} A_\phi = \hat{\phi} \sum_{n=0}^{\infty} b_n j_n(k_2 r) \frac{d}{d\theta} P_n(\cos \theta), \quad (2-5)$$

with unknowns  $a_n$  and  $b_n$ . The latter two equations are the results of symmetry arguments. These expressions are now evaluated at the boundary;  $r = a$ , and related via the boundary conditions, such as to permit solution for the unknown coefficients  $a_n$ ,  $b_n$ , and  $c_n$ .

The boundary conditions are continuity of normal stress, normal

displacement and tangent shear stress. Or, in order, in spherical coordinates at  $r = a$ :

$$-(p^i + p^s) = \lambda(\nabla \cdot \vec{u}) + 2\mu \frac{\partial u_r}{\partial r} ; \quad (2-6)$$

$$-\frac{1}{\rho_3} \left( \frac{\partial p^i}{\partial r} + \frac{\partial p^s}{\partial r} \right) = \ddot{u}_r ; \quad (2-7)$$

$$\left. \begin{aligned} 0 &= \frac{\partial u_\theta}{\partial r} - \frac{u_\theta}{r} + \frac{1}{r} \frac{\partial u_r}{\partial \theta} , \\ 0 &= \frac{1}{r \sin \theta} \frac{\partial u_r}{\partial \phi} + \frac{\partial u_\phi}{\partial r} - \frac{u_\phi}{r} . \end{aligned} \right\} \quad (2-8)$$

(The last of these is trivially satisfied due to axial symmetry.) See Appendix 8.1 for the relationships between the Lamé coefficients  $\lambda$ ,  $\mu$  and other elastic constants and for the relationships between pressure and displacement. The equation of motion in the solid is (see [1] for discussion)

$$\rho_1 \ddot{\vec{u}} = (\lambda + 2\mu) \nabla(\nabla \cdot \vec{u}) - \mu \nabla \times \nabla \times \vec{u} , \quad (2-9)$$

so that  $(\nabla \cdot \vec{u})$  and  $(\nabla \times \vec{u})$  inside as well as  $p = p^i + p^s$  outside satisfy their respective wave equations with velocities  $c_1$ ,  $c_2$ , and  $c_3$ .

The equations (2-6) through (2-8) must be satisfied for each mode  $n$ . We thus obtain the following set of three equations (in the same order) for each value of  $n$ , by direct substitution of (2-1) through (2-3) in the boundary condition equations:

$$\left. \begin{aligned} M_{11}^n a_n + M_{12}^n b_n + M_{13}^n c_n &= v_1^n \\ M_{21}^n a_n + M_{22}^n b_n + M_{23}^n c_n &= v_2^n \\ M_{31}^n a_n + M_{32}^n b_n &= 0 \end{aligned} \right\} \quad (2-10)$$

where  $M_{11}^n = (\alpha(n^2 + n) - x_1^2) j_n(x_1) - 2\alpha x_1 j_n'(x_1)$  (2-11)

$$M_{12}^n = (n^2 + n) \alpha (x_2 j_n'(x_2) - j_n(x_2))$$

$$M_{13}^n = \beta D_0 a^2 h_n^{(1)}(x)$$

$$M_{21}^n = x x_1 j_n'(x_1)$$

$$M_{22}^n = (n^2 + n) x j_n(x_2)$$

$$M_{23}^n = -D_0 a^2 h_n^{(1)'}(x)$$

$$M_{31}^n = x_1 j_n'(x_1) - j_n(x_1)$$

$$M_{32}^n = (n^2 + n - 1 - x_2^2/2) j_n(x_2) - x_2 j_n'(x_2)$$

$$M_{33}^n = 0$$

$$V_1^n = -\beta D_0 (2n+1) (-i)^n a^2 j_n(x)$$

$$V_2^n = D_0 (2n+1) (-i)^n a^2 j_n'(x)$$

$$V_3^n = 0$$

and where

$$x = ka = \omega a/c_3 ,$$

$$x_1 = k_1 a = \omega a/c_1 ,$$

$$x_2 = k_2 a = \omega a/c_2 .$$

It was useful in the above to note that the Bessel functions  $j_n$ ,  $n_n$ , and  $h_n$  all satisfy

$$x^2 f_n''(x) = (n^2 + n - x^2) f_n(x) - 2x f_n'(x) \quad (2-12)$$

The following constants were defined in conformance with [1]

$$\beta = \frac{\rho_3 c_3^2}{\rho_1 c_1^2}$$

$$\alpha = \frac{2c_2^2}{c_1^2} \quad (2-13)$$

$$D_o = - \frac{P_o}{\rho_3 c_3^2}$$

We can now solve for the coefficients  $a_n$ ,  $b_n$ ,  $c_n$  by inverting the matrix  $M^n$ . This must be done for all modes  $n$ .

By trial and error it is found that the number of modes  $n = NMAX$  required to achieve convergence is about  $NMAX = 2 + 8\sqrt{ka}$  for low values of  $ka$  and about  $NMAX = ka + 15$  for  $ka$  greater than 5. The applications considered in the following pages required  $ka$  up to 40 and  $NMAX$  up to 55. The evaluation of Bessel functions for such high order and argument is non-trivial. In these calculations Univac subroutines were used, which were based on the work by Goldstein and Thaler [4]. These utilize forward recurrence for  $n_n$  and backward recurrence for  $j_n$ . There are still difficulties with these evaluations which occur when  $n$  is large but the argument  $x_1$  is small. Overflows in the computation of  $n_n$  then limit the calculations to lower values of  $n$  and  $x$ . This situation arises when  $c_1/c_3$  is very large. For the materials considered here (brass and aluminum), it was found that the calculations could be made for  $ka$  up to 60. Since the

effect of parameter changes was also considered, the calculations of frequency responses were generally limited to  $ka = 40$ . Further, the solution was found at about 200 or 500 equally spaced points on the frequency scale.

The normalized far scattered field can be found from a simplification of (2-2), namely

$$\frac{r_0 i^s \vec{r}}{a} = P_0 H(\omega) ,$$

$$H(\omega, \theta) = \sum_{n=0}^{\infty} \frac{c_n (-i)^{n+1}}{k} P_n(\cos \theta) . \quad (2-14)$$

This is obtained from the asymptotic form of  $h_n^{(1)}$  which is

$$h_n^{(1)}(kr) \rightarrow \frac{(-i)^{n+1}}{kr} e^{ikr} \quad \text{as} \quad kr \rightarrow \infty$$

(Note that dropping the factor  $e^{ikr}$  in (2-14) is equivalent, in the time domain, to referencing the far field time origin to the space origin or sphere center. That is, a pulse scattered from the origin arrives in the far field at time  $t = 0$ .)

The magnitude of the frequency response,  $|H(\omega)|$ , in the back-scatter direction ( $\theta = 0$ ) is plotted in Figures 2-2 through 2-6. Some of these results were essentially previously obtained by Hickling [5]. (When making comparisons, see the note on "Scaling" Section 3.8 in [1].) Responses for sound-hard, aluminum, and brass spheres are given in Figure 2.2. In Figures 2-3 through 2-6 the responses of aluminum are given and compared with their modifications due to parameter changes. This will be discussed further in the next section. It is seen that a dominant feature of the elastic responses is the regular occurrence of deep nulls which is absent in the hard target and fluid target approximations. The spacing of the

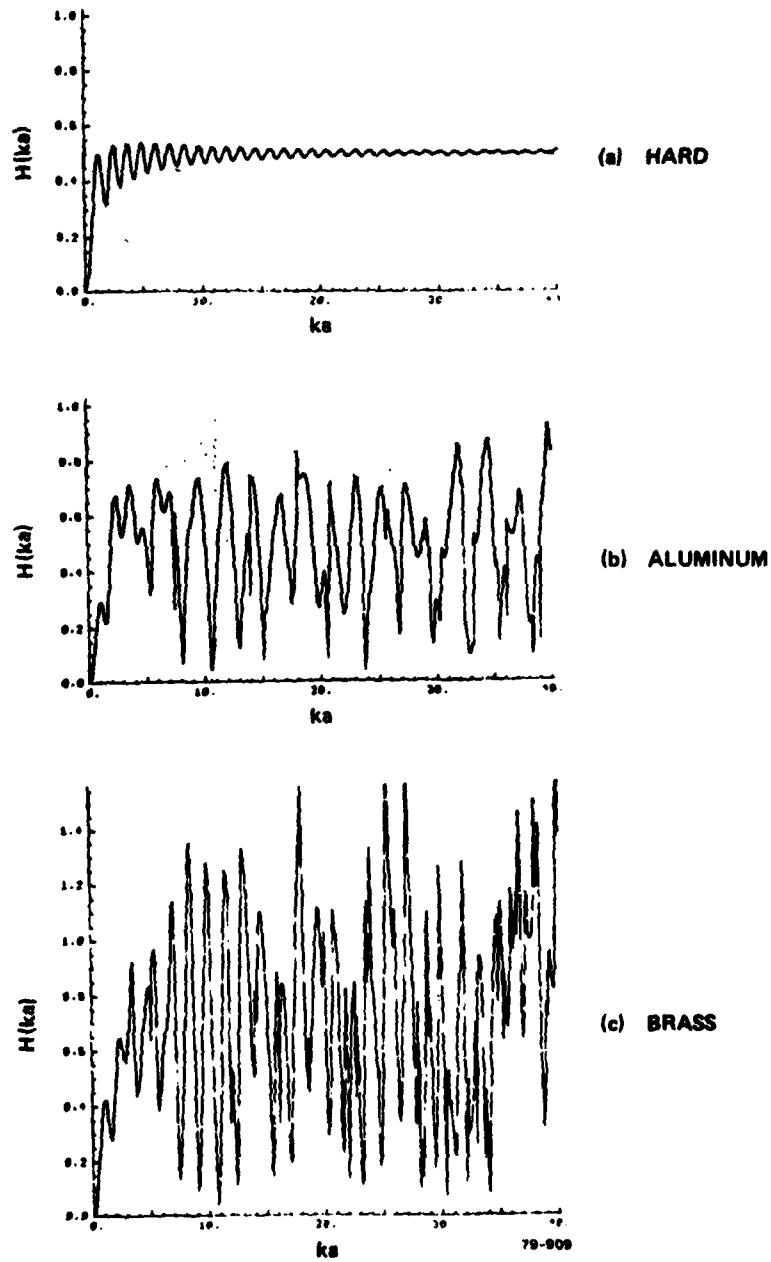


FIG. 2-2 Frequency response of sphere: (a) hard, (b) aluminum, and (c) brass.

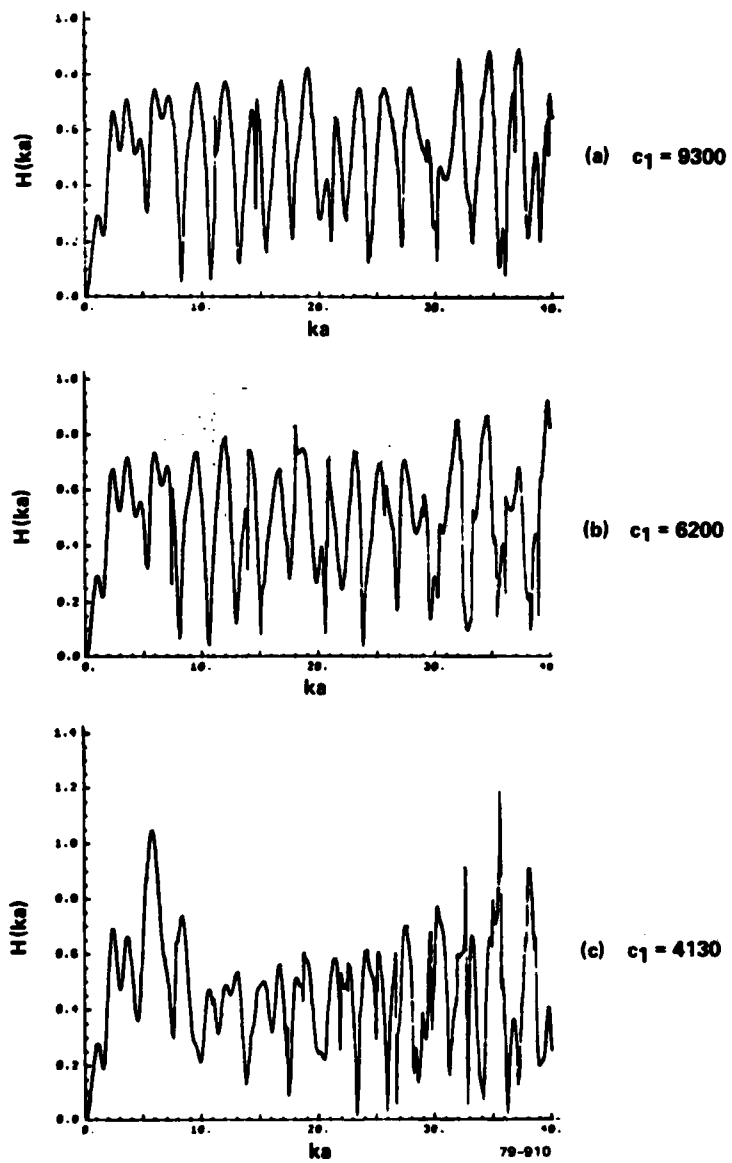


FIG. 2-3 Frequency response of aluminum sphere with (a)  $c_1 = 9300$ , (b)  $c_1 = 6200$ , and (c)  $c_1 = 4130$ .

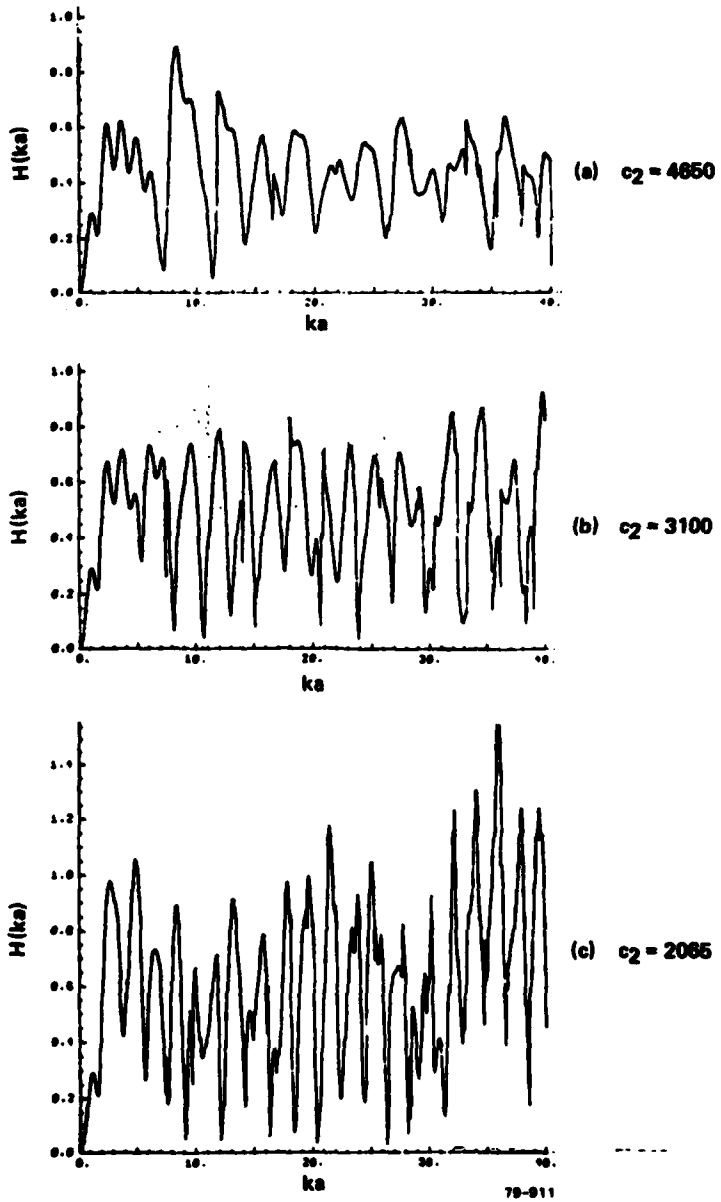


FIG. 2-4 Frequency response of aluminum sphere with (a)  $c_2 = 4650$ , (b)  $c_2 = 3100$ , and (c)  $c_2 = 2065$ .

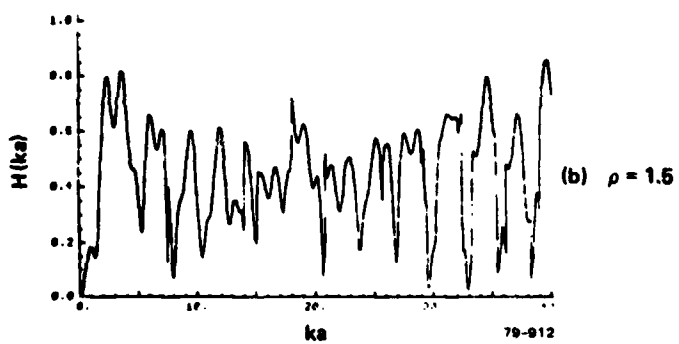
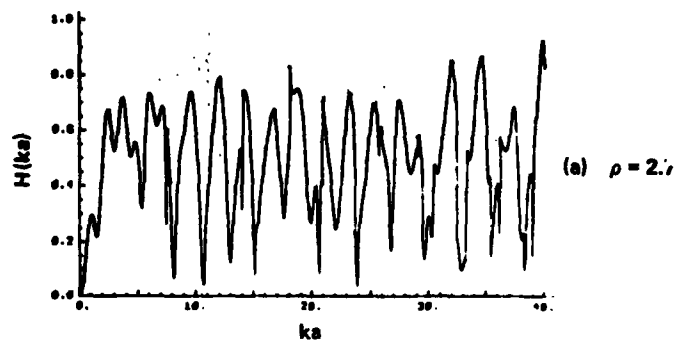


FIG. 2-5 Frequency response of aluminum sphere with (a)  $\rho = 2.7$  and (b)  $\rho = 1.5$ .

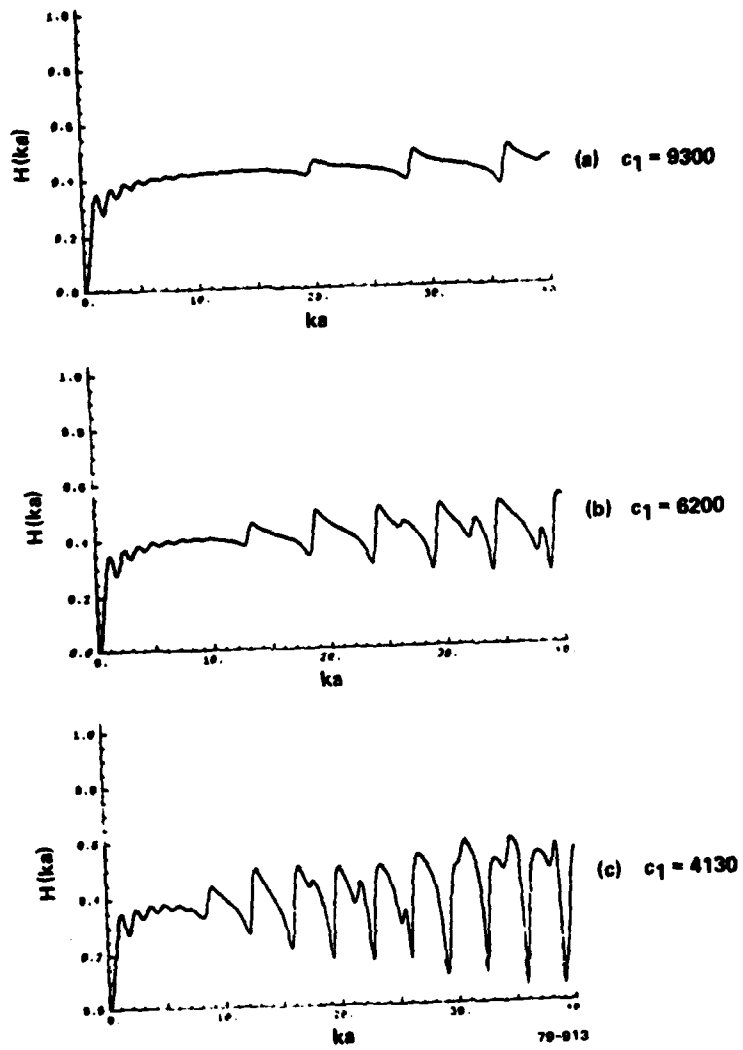


FIG. 2-6 Frequency response of aluminum sphere, fluid approximation, with (a)  $c_1 = 9300$ , (b)  $c_1 = 6200$ , and (c)  $c_1 = 4130$ .

nulls is affected by the velocities  $c_1$  and  $c_2$ , whereas the density affects mainly the amplitude of the response. The fluid response differs from the hard approximation mainly by amplitude at lower frequencies; although at higher frequencies a complex structure develops.

These features are difficult to explain in the frequency domain. After all, these pictures contain only half the available information, the phase of  $H(\omega)$  is as important (or more so) as the magnitude.

It is to be noted, that the aluminum and brass sphere responses have been well verified by measurement [1].

## 2.2 SMOOTHED IMPULSE RESPONSE FOR SPHERE

It is instructive to study the sphere response in the time domain. To do this, a band and time limited pulse is chosen, the "smoothed impulse":

$$e(t') = \frac{a_n}{\sqrt{\pi}} e^{-(a_n t')^2} \quad (2-15)$$

This pulse has been normalized to give unit time integral with the normalized time  $t' = c t_3/a$  and has a frequency domain representation

$$E(ka) = e^{-(ka/2a_n)^2} \quad (2-16)$$

(Refer to [6] appendix for a discussion on normalization.) In equation (2-14),  $P_0$  is replaced by  $E(ka)$ : the product is then transformed to the time domain, resulting in the far field, normalized, "smoothed impulse response",  $r_0 p^s(r, \vec{t}')/a$ . The larger  $a_n$ , the sharper the smoothed impulse, but the higher the range of  $\omega$  for which the response must be computed. A practical value here (consistent with the considerations of Section 2.1) is  $a_n = 8$ , which requires the computation of  $H(ka)$  up to  $ka = 40$ .

### 2.3 EFFECT OF TARGET PARAMETERS ON SPHERE RESPONSE

The time domain responses corresponding to the cases already given in the frequency domain, are plotted in Figures 2-7 through 2-11. The time axes are in units of  $c_3 t/a$ .

Consider the hard sphere response of Figure 2-7a. The initial part is the specular return, an impulse at time  $t = -2$ . This is immediately followed by a negative step, a ramp, etc. decaying to zero. This is due to radiation from the region immediately surrounding the specular point (see Section 3.2). Then, centered at a time  $t = \pi$ , is the creep response. Note that the time of occurrence is just that of a pulse impinging on the target at  $z = 0$ , traveling at the speed of the medium  $c_3$  around the back-side of the sphere and reradiating tangentially at  $z = 0$ .

It is seen immediately that the hard target cannot be an adequate model for scattering of wideband radiation from an elastic target: there is a small change in the specular response amplitude and backswing. But mainly, there have appeared large pulses at times 0 through 2. (One can verify readily that interference between these pulses and the specular impulse causes the resonant structure of the frequency response.) Significantly, these pulses are also absent from the fluid model response (Fig. 2-11). The time of occurrence of these pulses is strongly affected by the shear velocity  $c_2$  (Figure 2-9) but only slightly by the compression velocity  $c_1$  (Figure 2-8): we thus identify these features as due mainly to internal propagation of shear waves. Also present, and particularly noticeable in the fluid model are smaller pulses with arrival times proportional to compression velocity. These features can be associated with internal compression waves.

Aiding this discussion, Figure 2-12 illustrates the time references for various reflection paths. Suppose the distances  $a_1$ ,  $a_2$ ,  $a_3$  are travelled by a plane wave at velocities  $c_1$ ,  $c_2$ ,  $c_3$  respectively

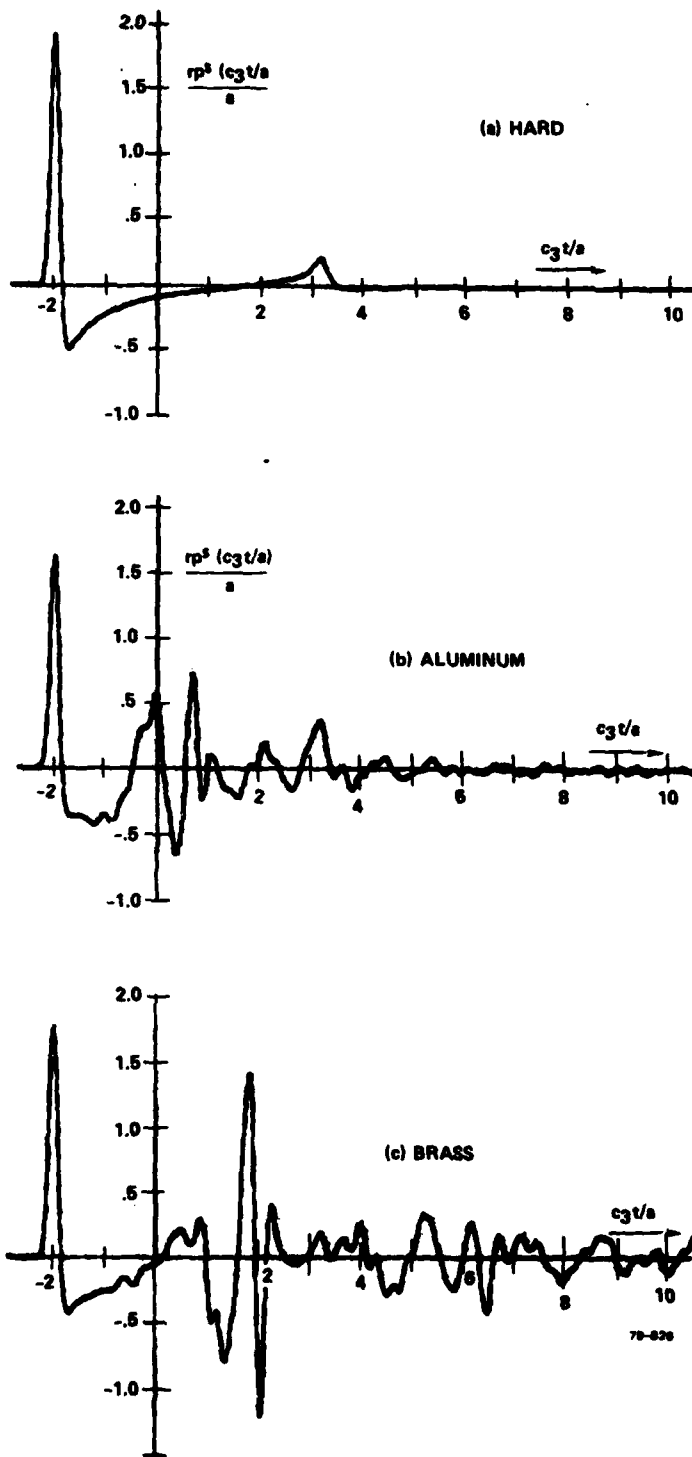


FIG. 2-7 Smoothed impulse response of aluminum sphere: (a) hard, (b) aluminum, and (c) brass.

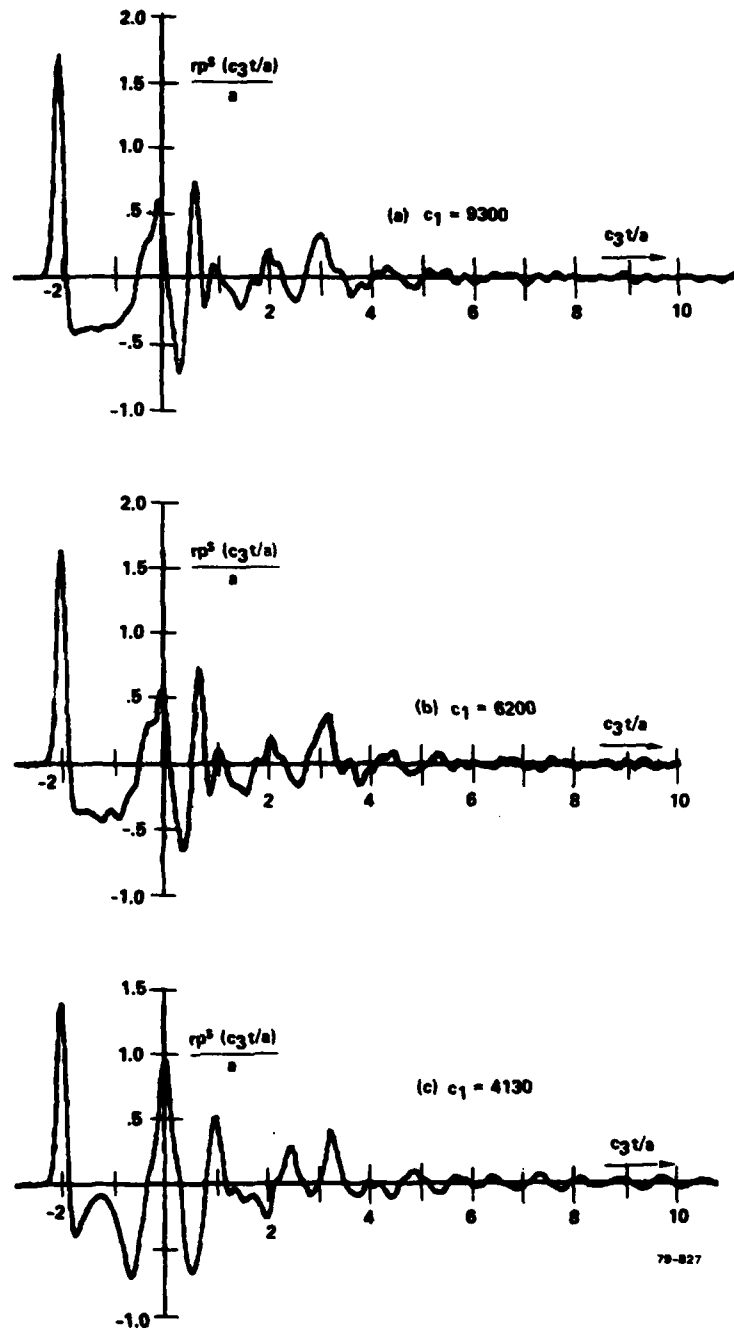


FIG. 2-8 Smoothed impulse response of aluminum sphere with (a)  $c_1 = 9300$ , (b)  $c_1 = 6200$ , and (c)  $c_1 = 4130$ .

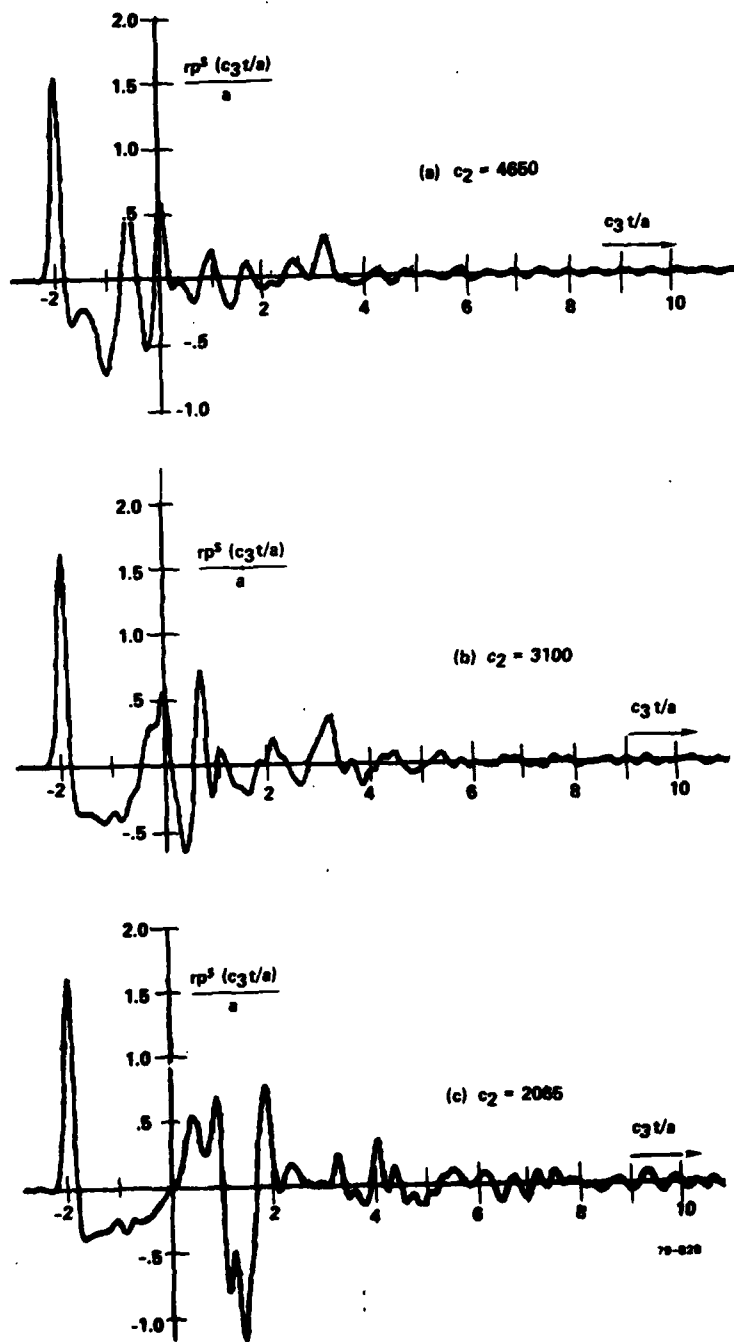


FIG. 2-9 Smoothed impulse response of aluminum sphere with (a)  $c_2 = 4650$ , (b)  $c_2 = 3100$ , and (c)  $c_2 = 2065$ .

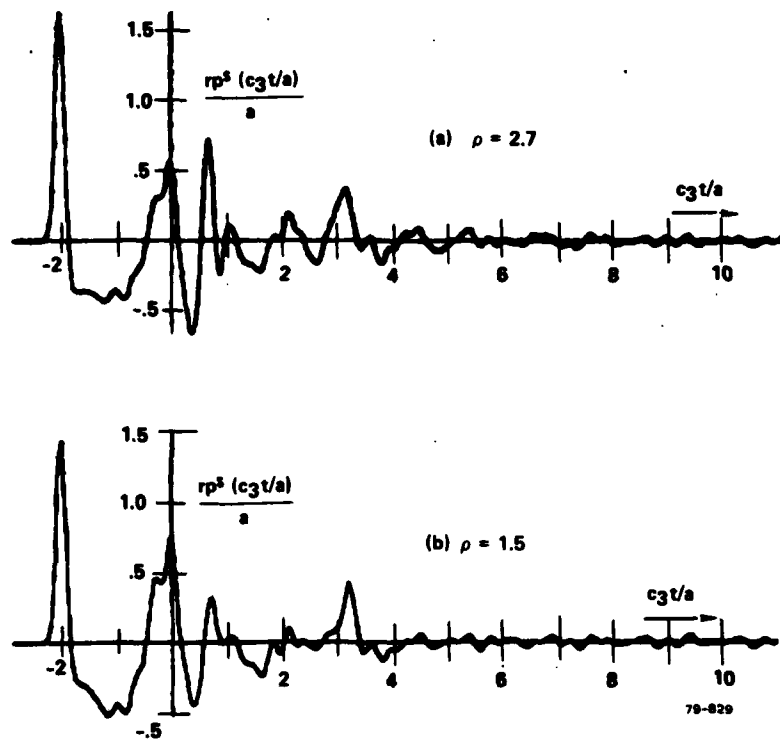


FIG. 2-10 Smoothed impulse response of aluminum with (a)  $\rho = 2.7$  and (b)  $\rho = 1.5$ .

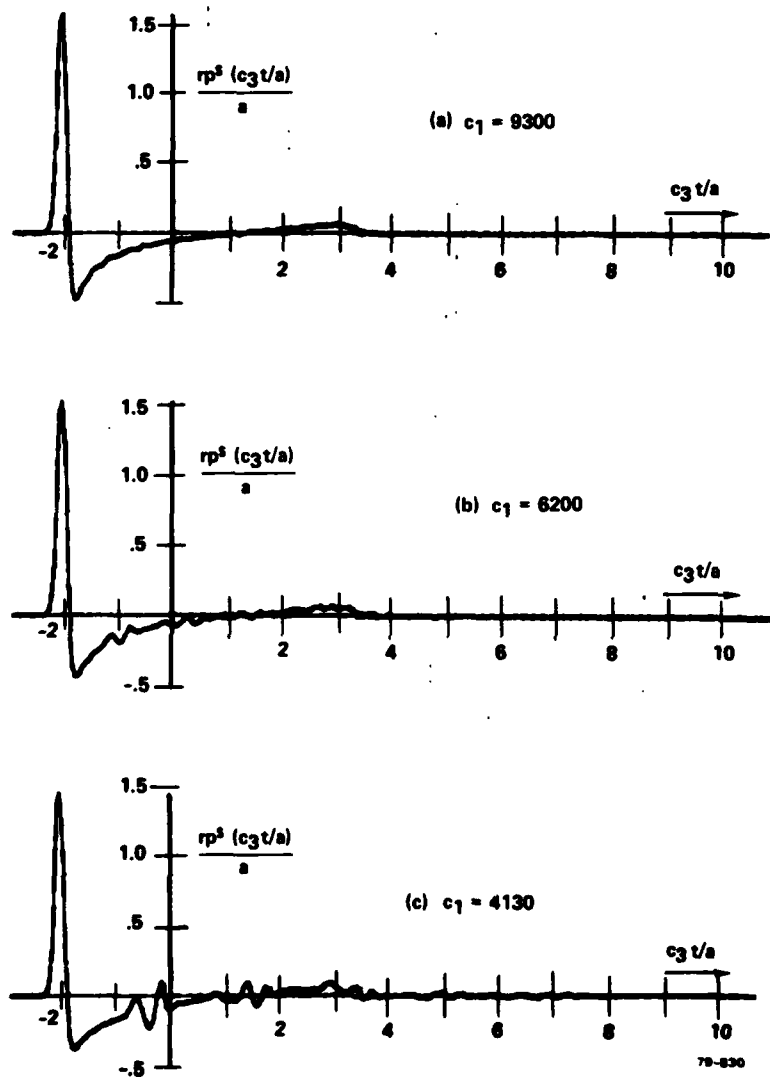
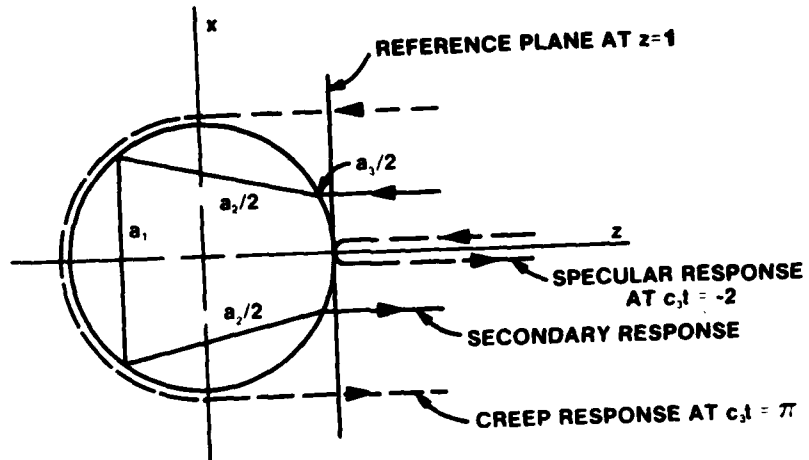


FIG. 2-11 Smoothed impulse response of aluminum sphere, fluid approximation, for (a)  $c_1 = 9300$ , (b)  $c_1 = 6200$ , and (c)  $c_1 = 4130$ .



SECONDARY RESPONSE AT  $c_1 t = -2 + \frac{a_1}{c_1} + \frac{a_2}{c_2} + \frac{a_3}{c_3}$

79-869

FIG. 2-12 Time reference for scattering from unit sphere.

(as compared with the specular wave for which the distance is  $a_3 = -2$ ).  
Then the time of arrival is

$$t = \frac{a_1}{c_1} + \frac{a_2}{c_2} + \frac{a_3}{c_3} . \quad (2-17)$$

In Figure 2-13 responses are plotted versus time scale  $c_2 t = c_2/c_1 a_1 + a_2 + c_2/c_3 a_3$ , for several values of  $c_2$ . If the path were entirely at speed  $c_2$  then the features would remain at the same value of  $c_2 t$ . This is nearly the case: while  $c_2$  is changed by a factor of 4, the time  $c_2 t$  at which the "shear wave features" appear is nearly the same. The slight variation of the arrival time in units of  $c_2 t$  associated with these features is then due to the fact that the paths of traversal are in small part at  $c_1$  and  $c_3$ . The vertical offset in Figures 2-13 and 2-14 is proportional to  $c_2$ . Figure 2-14 is the same as 2-13 but with a higher value for  $c_1$ . Only for large values of  $c_2$  is there a significant difference between the curves. These results are sufficient to allow estimating path lengths through the target at the various velocities for the principal features of the response. Physical considerations (Snell's law -- Section 3.1) then can give the likely path associated with these features. In Section 3.3 they will be identified as the principal modes of a glory-wave effect.

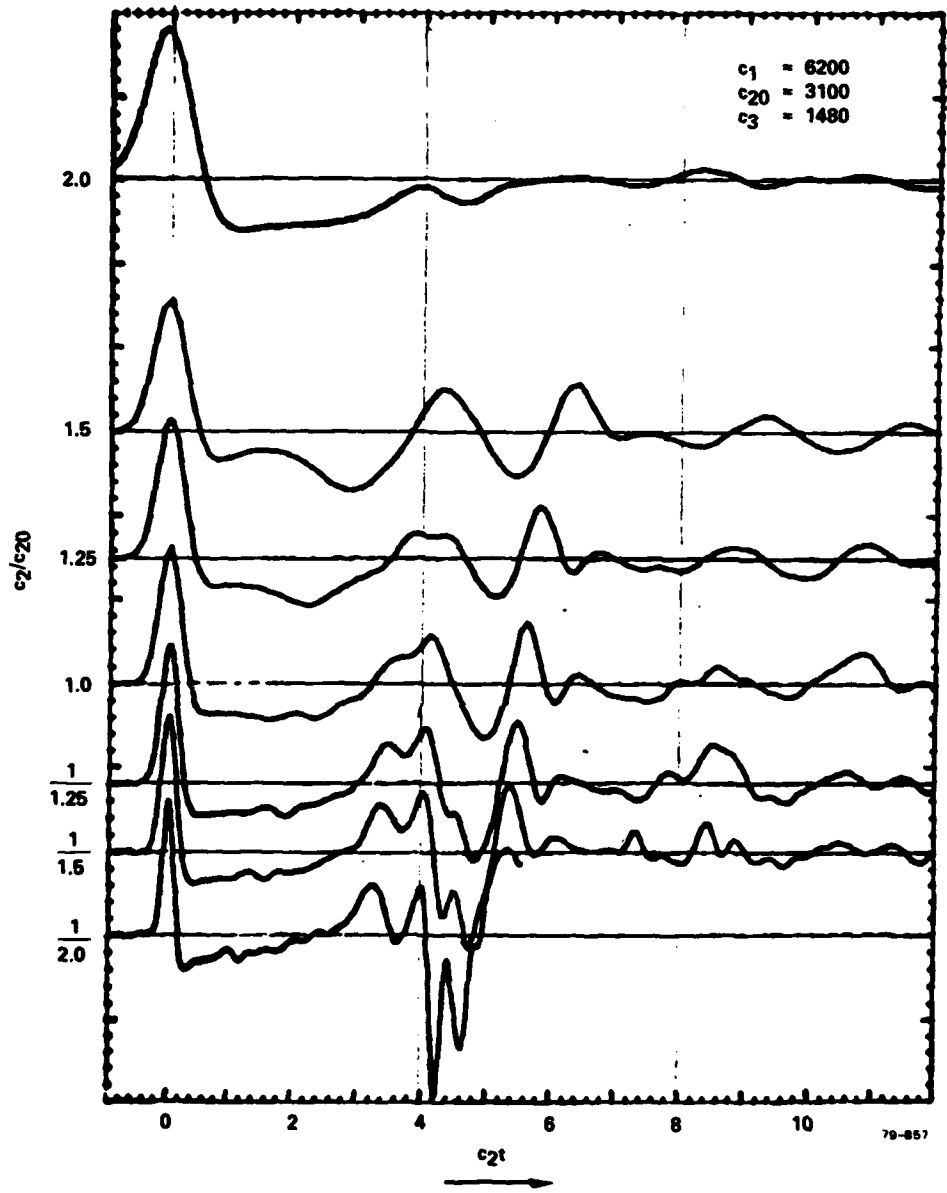


FIG. 2-13 Aluminum variations — response vs.  $c_2t$  with  $c_1 = 6200$ .

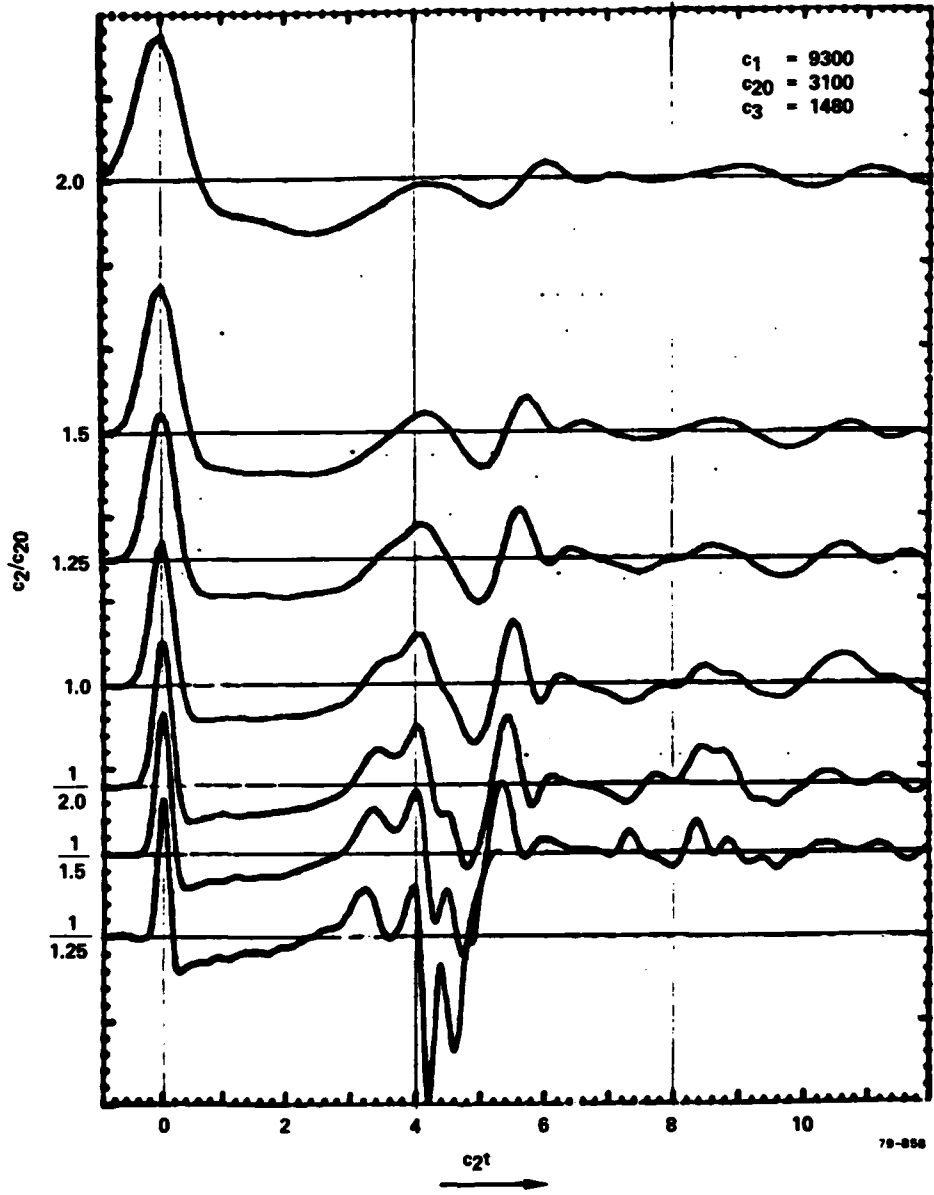


FIG. 2-14 Aluminum variations - response vs.  $c_2t$  with  $c_1 = 9300$ .

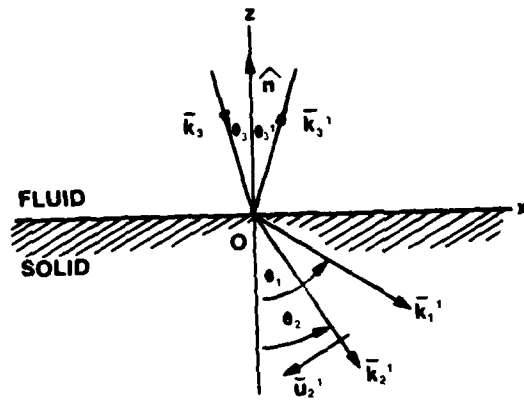
SECTION 3  
SCATTERING MODEL

It is apparent from both frequency and time domain points of view that the scattering process, for even such a simple target as a sphere, is inherently complicated. The aim of this section is to identify the essential attributes of the responses in order to obtain a reasonable approximation with a relatively simple model. Such a model is possible based on the glory-wave effect. This theory, developed originally for the scattering of light from water droplets, undergoes considerable complication (due to the existence of two sound speeds in the target) when applied to the acoustic case. However, the qualitative aspects of the theory, particularly when viewed in the time domain, are helpful in providing useful insight into the scattering process; it will be seen that the impulse response consists of a string of impulses which arrive after traveling through the target along the readily identifiable glory paths. On the other hand, quantitatively (i.e., for the magnitude of the impulse response) the theory is difficult to apply (see the extensive work of Uberall et al. [7]). It is suggested that a useful approach is a hybrid approximate method, using the quantitative considerations of the next two subsections together with the simple glory-path model.

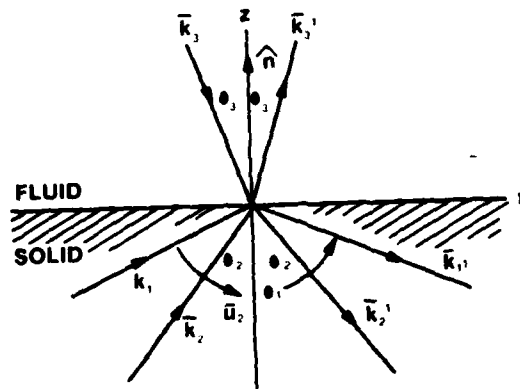
3.1 REFLECTION AND REFRACTION AT A PLANE ELASTIC BOUNDARY

The following is an exact treatment of the interaction of a plane compressional wave with a plane fluid-elastic interface, and of the reverse problem.

Let the displacement in a fluid medium be given by  $\vec{u}_3$ , and in the solid by  $\vec{u}_1$  and  $\vec{u}_2$  corresponding to compressional and shear waves respectively. Primes are used to denote the part of the wave after reflection or refraction. Consider the plane interface of Figure 3-1. Then we



(a) WAVE INCIDENT FROM FLUID



(b) GENERAL CASE

79-870

FIG. 3-1 Plane wave refraction at plane boundary.

have

$$\text{incident wave } \vec{u}_3 = \vec{u}_{30} e^{j\vec{k}_3 \cdot \vec{r} - j\omega t} , \quad (3-1)$$

$$\text{reflected wave } \vec{u}'_3 = \vec{u}'_{30} e^{j\vec{k}'_3 \cdot \vec{r} - j\omega t} , \quad (3-2)$$

$$\text{refracted wave } \vec{u}'_1 = \vec{u}'_{10} e^{j\vec{k}'_1 \cdot \vec{r} - j\omega t} , \quad (3-3)$$

$$\vec{u}'_2 = \vec{u}'_{20} e^{j\vec{k}'_2 \cdot \vec{r} - j\omega t} . \quad (3-4)$$

The zero subscript refers to the value at the origin. Assume that the wave normals are in the x,z plane so that:

$$\begin{aligned} \vec{k}_3 &= (\hat{x} \sin \theta_3 - \hat{z} \cos \theta_3) k_3 , \\ \vec{k}'_3 &= (\hat{x} \sin \theta'_3 + \hat{z} \cos \theta'_3) k'_3 , \\ k'_1 &= (\hat{x} \sin \theta_1 - \hat{z} \cos \theta_1) k'_1 , \\ k'_2 &= (\hat{x} \sin \theta_2 - \hat{z} \cos \theta_2) k'_2 \end{aligned} \quad (3-5)$$

where

$$k_i = \omega/c_i .$$

Snell's laws for reflection and refraction follow directly from these definitions, independent of the nature of the boundary conditions (see Jackson, p. 217 [8]): whatever boundary conditions prevail, the same conditions are satisfied at the point (0,0) as at every other point on the interface. Hence the variation in phase for (3-1) through (3-4) must be

the same for all under translation on the interface. That is:

$$k_1' \sin \theta_1 = k_2' \sin \theta_2 = k_3' \sin \theta_3' = k_3 \sin \theta_3 \quad (3-6)$$

(The same argument for phase variation with time can be used to establish that the frequencies,  $\omega$ , are the same for all waves.) Hence Snell's Law:

$$\sin \theta_3' = \sin \theta_3$$

$$\sin \theta_1 = \frac{c_1}{c_3} \sin \theta_3 \quad (3-7)$$

$$\sin \theta_2 = \frac{c_2}{c_3} \sin \theta_3$$

Note that for solids we generally have  $c_1 > c_2 > c_3$ , so that rays are refracted away from the normal after entering the solid, as in Figure 3-1. Also note that for some real incident angle,  $\theta_{3c1}$  (the critical angle), we will have  $\sin \theta_{1c} = c_1/c_3 \sin \theta_{3c1} = 1$ . There is no transmission at speed  $c_1$  for  $\theta_3 \geq \theta_{3c1}$ . Similarly, at  $\theta_{3c2}$  such that  $\sin \theta_{2c} = c_2/c_3 \sin \theta_{3c2} = 1$ , there is no transmission at  $c_2$  (nor at  $c_1$ ); so that there is total reflection for  $\theta_3 \geq \theta_{3c2}$ . At angles between these two critical angles, there is transmission only at  $c_2$ , that is as a shear wave. The boundary conditions can be satisfied through the existence of an evanescent wave which travels along the surface.

We will now derive the relative magnitudes of these waves, for which it is necessary to know the dynamics or boundary conditions. These are

- (1) continuity of normal stress,
- (2) continuity of normal displacement,
- (3) continuity of tangent shear stress.

In Cartesian coordinates these are written [1]:

$$\lambda_3 \left[ (\nabla \cdot \vec{u}_3) + (\nabla \cdot \vec{u}'_3) \right] = \lambda (\nabla \cdot \vec{u}) + 2\mu \frac{\partial u}{\partial n} ,$$

$$\hat{n} \cdot \left[ \vec{u}_3 + \vec{u}'_3 \right] = \hat{n} \cdot \vec{u} , \quad (3-8)$$

$$\mu \left[ \frac{\partial u}{\partial x} + \frac{\partial u}{\partial n} \right] = 0$$

where  $\vec{u} = \vec{u}_1 + \vec{u}_2$  and the elastic constants are

$$\lambda_3 / \rho_3 = c_3^2$$

$$(\lambda + 2\mu) / \rho = c_1^2 \quad (3-9)$$

$$\mu / \rho = c_2^2 .$$

Substituting equation (3-1) etc. into the boundary conditions, we obtain respectively

$$\lambda_3 k_3 (u_{30} + u'_{30}) = \lambda k_1 u'_{10} + 2\mu \left[ u'_{10} k_1 \cos^2 \theta_1 + u'_{20} k_2 \cos \theta_2 \sin \theta_2 \right] , \quad (3-10)$$

$$(u_{30} - u'_{30}) \cos \theta_3 = u'_{10} \cos \theta_1 + u'_{20} \sin \theta_2 , \quad (3-11)$$

$$2 u'_{10} k_1 \sin \theta_1 \cos \theta_1 - u'_{20} k_2 (\cos^2 \theta_2 - \sin^2 \theta_2) = 0 . \quad (3-12)$$

Solving simultaneously we obtain the transmitted amplitude (that is  $u'_{10}$ ,  $u'_{20}$ , and  $u'_{30}$ ) in terms of the incident amplitude  $u_{30}$ . It is convenient to define the quantities

$$A = \left( \frac{\rho_1 c_1}{\rho_3 c_3} \right) \left( \left( 1 - \alpha \sin^2 \theta_1 \right) + \alpha Q \sin \theta_1 \cos \theta_2 \right), \quad (3-13)$$

$$B = \frac{\cos \theta_1}{\cos \theta_3 \left( \cos^2 \theta_2 - \sin^2 \theta_2 \right)} \quad (3-14)$$

$$Q = \frac{2 c_2 \sin \theta_1 \cos \theta_1}{c_1 \left( \cos^2 \theta_2 - \sin^2 \theta_2 \right)} \quad (3-15)$$

where  $\alpha = 2 c_2^2 / c_1^2$ . Then the transmission coefficients are found to be

$$R_{33} = \frac{u'_{30}}{u_{30}} = \frac{A - B}{A + B}, \quad (3-16)$$

$$R_{31} = \frac{u'_{10}}{u_{30}} = \frac{2}{A + B}, \quad (3-17)$$

$$R_{32} = \frac{u'_{20}}{u_{30}} = \frac{2Q}{A + B}. \quad (3-18)$$

The first subscript of R refers to the incident wave, the second to the reflected or refracted wave.

The above derivation can be performed more generally, as indicated in Figure 3-2, to also permit waves incident from inside the solid. The results are as follows. For an incident compression wave in the solid,  $u_{10}$ , the refractions and reflections are

$$R_{11} = \frac{u'_{10}}{u_{10}} = \frac{B - C + QD}{A + B} \quad (3-19)$$

$$R_{12} = \frac{u'_{20}}{u_{10}} = - \frac{2QC}{A + B} \quad (3-20)$$

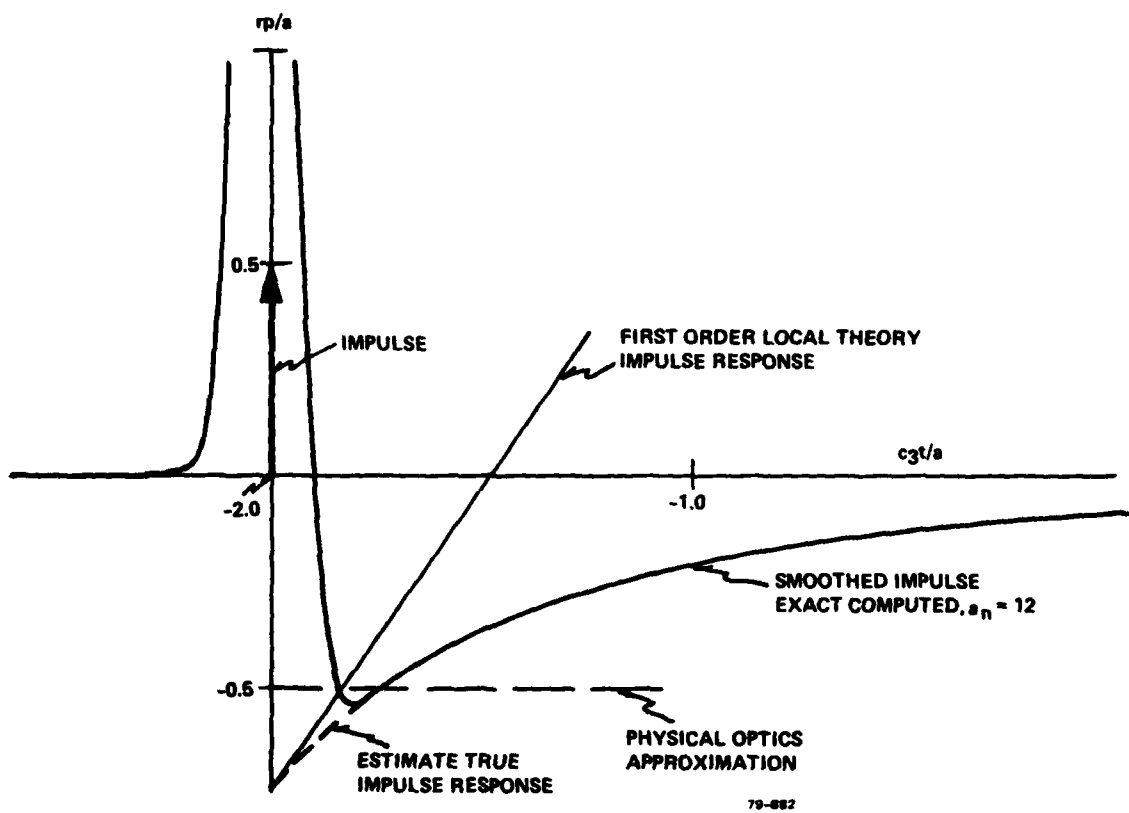


FIG. 3-2 Impulse response of hard sphere (leading edge).

$$R_{13} = \frac{u'_{30}}{u_{10}} = \frac{2BC}{A+B} \quad (3-21)$$

Here we have also used the definitions

$$C = \frac{\rho_1 c_1}{\rho_3 c_3} \left( \cos^2 \theta_2 - \sin^2 \theta_2 \right), \quad (3-22)$$

$$D = \frac{\rho_1 c_2}{\rho_3 c_3} \left( 2 \sin \theta_2 \cos \theta_2 \right). \quad (3-23)$$

For an incident shear wave,  $u_{20}$ , the refractions and reflections are

$$R_{21} = \frac{u'_{10}}{u_{20}} = \frac{2D}{A+B} \quad (3-24)$$

$$R_{22} = \frac{u'_{20}}{u_{20}} = \frac{2D - B - C}{A+B} \quad (3-25)$$

$$R_{23} = \frac{u'_{30}}{u_{20}} = -\frac{2BD}{A+B} \quad (3-26)$$

Note that  $R_{13}$ ,  $R_{23}$  represent energy transmitted from solid to fluid medium, while  $R_{12}$  and  $R_{21}$  represent mode conversions.

For normal incidence,  $\theta_1 = \theta_2 = \theta_3 = 0$ , these expressions simplify to

$$R_{33} = \frac{A-1}{A+1} = \frac{\rho_1 c_1 - \rho_3 c_3}{\rho_1 c_1 + \rho_3 c_3}$$

$$R_{31} = \frac{2}{A+1} = \frac{2\rho_3 c_3}{\rho_1 c_1 + \rho_3 c_3} \quad (3-27)$$

$$R_{32} = 0$$

Also, it is interesting to investigate the case of critical incidence for  $c_1$ , that is  $\theta_1 = 90^\circ$ . We then have that  $R_{33} = 1$ , that's total reflection. As the incident angle increases slightly and  $\theta_1$  becomes imaginary, there is transmission of energy as a shear wave at  $c_2$ , while on the surface there exists an evanescent compression wave at  $c_1$ .

In closing, it is noted that the fluid, hard, and soft cases are included in the analysis by appropriately letting the densities  $\rho_1, \rho_3$  go to zero or  $\infty$ .

### 3.2 TIME DOMAIN SPECULAR RESPONSE - LOCAL STIE

In the physical optics limit, the impulse response of a target is given by  $1/2\pi$  times the second derivative of its projected area function. This was given by Kennaugh & Cosgriff in 1958 [9] for the electromagnetic case and is valid, as will be seen, in the limit, for the acoustic case as well. For example, the projected area of a unit sphere with specular point at the origin (Figure 2-1) for an incident plane wave traveling in the z-direction is

$$S_p = \pi \rho^2 = \pi (2az - z^2). \quad (3-28)$$

Taking the speed of sound  $c = 1$ , we have that  $z = t/2$ . The area function is then

$$S_p(t) = \pi \left( at - \frac{t^2}{4} \right) u(t), \quad (3-29)$$

and

$$\frac{1}{2\pi} \frac{d^2 S_p}{dt^2} = \frac{1}{2} \delta(t) - \frac{1}{4} u(t) \quad (3-30)$$

is the physical optics impulse response. This can be considered to be the

first two terms of an expansion in singularity functions. An improvement to this approximation can be obtained by including the effect of surface interactions.

### 3.2.1 Sound Hard Convex Specular Point

For a sound hard target the far backscattered pressure is given by

$$\hat{r}_o p^s(t) = \frac{1}{4\pi} \int_S (\hat{r}_o \cdot \hat{n}') \frac{\partial p(\vec{r}', t')}{\partial t'} ds' , \quad (3-31)$$

where  $t' = t + (\hat{r}_o \cdot \vec{r}')$  and  $\hat{r}_o$  is the direction of observation. The pressure on the surface can be shown [1] to be

$$p(\vec{r}', t') = 2 p^i(z', t') + \frac{1}{2\pi} \int_S (\hat{R} \cdot \hat{n}'') \left( \frac{1}{R} + \frac{1}{R} \frac{\partial}{\partial t''} \right) p(\vec{r}'', t'') ds'' , \quad (3-32)$$

where  $t'' = t' - R$ ,  $\vec{R} = \vec{r} - \vec{r}'$ , and  $t$  is in units of sound-meters. It is easier to consider the step response first. Let the incident plane wave be a step traveling in the positive  $z$ -direction (i.e.,  $\hat{r}_o \cdot \vec{r}' = -z'$ )

$$p^i(z', t') = u(t' - z') ,$$

or

$$p^i(z', t) = u(t - 2z') . \quad (3-33)$$

As a first approximation we will consider the surface pressure,  $p(\vec{r}'', t'')$ , constant over the illuminated region (and zero outside). Then  $\partial p / \partial t'' = 0$ , except at the boundary of the illuminated region where

$$\frac{\partial p}{\partial t''}(\vec{r}'', t'') = p(\vec{r}'', t'') \delta(t'' - z'') ,$$

or

$$\frac{\partial p}{\partial t''}(\vec{r}'', t'') = p(\vec{r}'', t'') \delta(t' - z'' - R) .$$

We want to substitute this in the integral (3-32). To evaluate the integral we use the fact that for a circular patch  $\Delta S$  of radius  $\gamma$

$$\epsilon = \frac{1}{2\pi} \int_{\Delta S} dS'' \frac{(\hat{R} \cdot \hat{n}'')}{R^2} = \frac{\bar{\kappa}}{2} \int_0^\gamma dR = \frac{\gamma \bar{\kappa}}{2} , \quad (3-34)$$

where  $\kappa$  is the average curvature. This approximation applies to smooth convex surfaces. This was derived in [1] p. 16, but due to a typographical error, the value of  $\epsilon$  is given incorrectly in [1]. Here,  $\Delta S$  is the elliptical patch around  $\vec{r}'$  at time  $t'$  which is illuminated at the retarded times  $t'' = t' - R$ . Some reflection reveals that the approximate radius of  $\Delta S$  is given

$$\gamma = t - 2z' . \quad (3-35)$$

For the second term in (3-32) involving  $\partial p / \partial t''$  we need

$$\frac{1}{2\pi} \int_{\Delta S} dS'' \frac{(\hat{R} \cdot \hat{n}'')}{R} \delta(t' - z'' - R) = \frac{\bar{\kappa}}{2} \int_0^\gamma R \delta(t' - z'' - R) dR = \frac{\gamma \bar{\kappa}}{2} \quad (3-36)$$

This follows since  $\partial p / \partial t$  is nonzero at the boundary of the patch  $\Delta S$ . The result of the first order evaluation of (3-32) is thus

$$p(\vec{r}', t') = 2 p^i(z', t') + \gamma \bar{\kappa} p(\vec{r}', t') ,$$

where  $\gamma = t - 2z'$ . Solving for  $p$  and expanding  $1/(1 - \gamma \bar{\kappa})$  this can be

written

$$p(\vec{r}', t') = 2 p^i(z', t') \left\{ 1 + \bar{\gamma} \bar{\kappa} + \bar{\gamma}^2 \bar{\kappa}^2 + \dots \right\} ,$$

and making the substitution (3-33)

$$\frac{1}{2} p(\vec{r}', t') = u(t - 2z') \left\{ 1 + \bar{\kappa}(t - 2z') + \bar{\kappa}^2(t - 2z')^2 + \dots \right\} ; \quad (3-37)$$

$$\begin{aligned} \frac{1}{2} \frac{\partial p}{\partial t}(\vec{r}', t') &= \delta(t - 2z') \left\{ 1 + \bar{\kappa}(t - 2z') + \dots \right\} \\ &+ u(t - 2z') \bar{\kappa} \left\{ 1 + 2\bar{\kappa}(t - 2z') + \dots \right\} . \end{aligned} \quad (3-38)$$

This expression for the surface pressure can now be used to evaluate the far-scattered step response.

Using  $(\hat{r}'_o \cdot \hat{n}') dS' = 2\pi \rho a \cos \theta d\theta = 2\pi(a - z') dz'$ , the integral (3-31) can be rewritten

$$\begin{aligned} r_o p^S(t) &= \int_0^{t/2} (a - z') \delta(t - 2z') \left\{ 1 + \bar{\kappa}(t - 2z') + \bar{\kappa}^2(t - 2z')^2 + \dots \right\} dz' \\ &+ \int_0^{t/2} (a - z') u(t - 2z') \bar{\kappa} \left\{ 1 + 2\bar{\kappa}(t - 2z') + 3\bar{\kappa}^2(t - 2z')^2 + \dots \right\} dz' \end{aligned} \quad (3-39)$$

Direct evaluation and the substitution  $a\bar{\kappa} = -1$ , yields for the step response

$$r_o p^S = a \left\{ \frac{1}{2} - \frac{3}{4} (t/a) + \frac{5}{8} (t/a)^2 + \dots \right\} u(t) .$$

Differentiating and normalizing, the impulse response of the hard sphere is then

$$h(t/a) \equiv \frac{r_0 p^s(t/a)}{a} = \frac{1}{2} \delta(t/a) - \frac{3}{4} u(t/a) + \frac{5}{4} r_p(t/a) + \dots \quad (3-40)$$

The third term (ramp) of this expansion is inaccurate and could be improved upon by the use of (3-37) and (3-38) in (3-32) as the next approximation; and so on. The main result here is the correction of the step coefficient as given by the simpler physical optics theory in equation (3-30). The result of approximating the impulse response by the methods of Section 2, using  $a_n = 12$ , is plotted in Figure 3-2, superposed on the present results. The agreement, including the  $r_p$  term is seen to be excellent.

### 3.2.2 Fluid Sphere Convex Specular Point

Consider now the case where energy penetrates the target in the form of compression waves. We then have two integral equations (see Section 4) corresponding to pressure outside,  $p$ , and inside,  $p_1$ :

$$\begin{aligned} p(\vec{r}', t') &= 2 p^i(z', t) + \frac{1}{2\pi} \int_{\Delta S} (\hat{R} \cdot \hat{n}'') \left( \frac{1}{R} + \frac{1}{R} \frac{\partial}{\partial t''} \right) p(\vec{r}'', t'') ds'' \\ &\quad - \frac{1}{2\pi} \int_{\Delta S} \frac{1}{R} \frac{\partial}{\partial n''} p(\vec{r}'', t'') ds'' \\ p_1(\vec{r}', t') &= - \frac{1}{2\pi} \int_{\Delta S_1} (\hat{R} \cdot \hat{n}'') \left( \frac{1}{R} + \frac{1}{Rc_1} \frac{\partial}{\partial t''} \right) p_1(\vec{r}'', t_1'') ds'' \\ &\quad + \frac{1}{2\pi} \int_{\Delta S_1} \frac{1}{R} \frac{\partial}{\partial n''} p_1(\vec{r}'', t_1'') ds'' \end{aligned} \quad (3-41)$$

where  $t'' = t' - R$ ,  $t_1'' = t' - R/c_1$ . The patch  $\Delta S$  has radius  $\gamma = t - 2z'$  as before. The interior integral is over the larger patch  $\Delta S_1$  with radius

$\gamma_1 = c_1 t - 2z'_1$ . The above equations are related by the boundary conditions

$$p = p_1$$

$$\frac{\partial p}{\partial n} = \frac{\partial p_1}{\rho_1 \partial n} ; \quad (3-42)$$

$c_1, p_1$  are the sound speed and density inside relative to outside. The integrations over the surface patch are similar to that of the previous section and result in

$$p(\vec{r}', t') = 2p^i + \gamma \bar{\kappa} p - \gamma \frac{\partial p}{\partial n}$$

and

$$p(\vec{r}', t') = -c_1 \gamma \bar{\kappa} p + \gamma \rho_1 c_1 \frac{\partial p}{\partial n} ,$$

where the last equation is obtained from the last of (3-41) and the application of the boundary conditions. Again, we use a step function as the incident field. Solving, we obtain on the surface

$$p(\vec{r}', t') = 2 \left( \frac{\rho_1 c_1}{1 + \rho_1 c_1} \right) (1 + \epsilon + \epsilon^2 + \dots) u(t - 2z') ,$$

$$\frac{\partial p}{\partial n} (\vec{r}', t') = 2 \left( \frac{1}{1 + \rho_1 c_1} \right) (1 + \epsilon + \epsilon^2 + \dots) \left( \frac{1 + c_1 \bar{\kappa} \gamma}{\gamma} \right) u(t - 2z') , \quad (3-43)$$

where we have defined

$$\epsilon = \left( \frac{\rho_1 - 1}{1 + \rho_1 c_1} \right) \bar{\kappa} c_1 \gamma .$$

The integral equation for far field scattering from an elastic or fluid

target is

$$r_o p^s(t) = \frac{1}{4\pi} \int_s (\hat{r}_o \cdot \hat{n}') \frac{\partial p(\vec{r}', t')}{\partial t'} ds' - \frac{1}{4\pi} \int_s \frac{\partial p(\vec{r}', t')}{\partial n'} ds' \quad (3-44)$$

Substituting (3-43) into this, results in terms similar to that for the hard target step response except for constants. The result is that the impulse response of a smooth curved specular point for a fluid target is given by

$$h(t/a) = \left( \frac{\rho_1 c_1}{1 + \rho_1 c_1} \right) \left\{ \frac{1}{2} \delta(t/a) - \left[ \frac{1}{4} + \frac{\beta}{2} \right] u(t/a) + \dots \right\} \\ - \left( \frac{1}{1 + \rho_1 c_1} \right) \left\{ \frac{1}{2} \delta(t/a) - \left[ \frac{\beta + c}{2} \right] u(t/a) + \dots \right\}, \quad (3-45)$$

where

$$\beta = \frac{\rho_1 c_1 - c_1}{\rho_1 c_1 + 1}.$$

Note that as  $\rho_1 \rightarrow \infty$  (3-45) reduces to the sound-hard case. Also, the factor  $(\rho_1 c_1 - 1)/(\rho_1 c_1 + 1)$ , by which the impulse term differs from the sound-hard (perfectly reflecting) case, is the same as the reflection coefficient found in (3-27) for normal reflection from an elastic plane surface.

### 3.2.3 Extensions of These Techniques

At the next level of complexity it is possible to determine by these analytic methods the response of an elastic specular point. The expressions become very complicated however when shear wave effects are included; hence this approach was not pursued here. A direct approach is

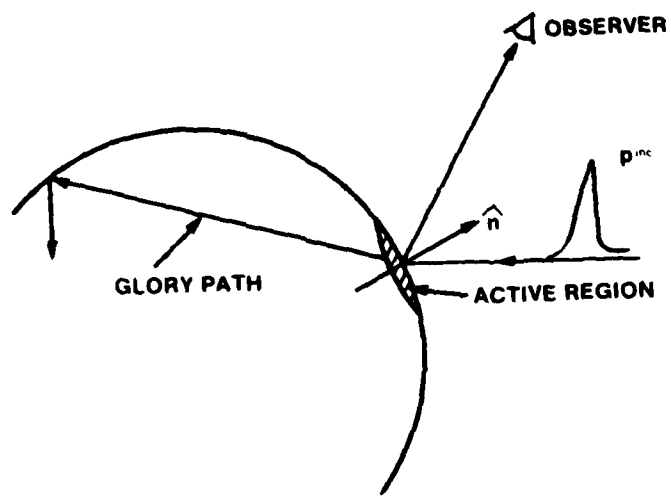
the numerical evaluation of the integrals of the preceding section using a very short smoothed impulse incident pressure. The result is the leading edge of the impulse response and requires the numerical integration over only a small part of the target surrounding the specular point. Furthermore, the technique may be applied to a bistatic configuration and also to refraction. This approach, known as the local influence theory, is based on the observation that at a given time only a few identifiable points are active as scatterers; see Figure 3-3. (The approach has been used successfully for the electromagnetic case [10].) Attempts to implement this technique for elastic targets have been, to date, thwarted by the numerical difficulties further described in Section 4. It is felt that, once these difficulties are removed, these calculations of scattering center responses, combined with the glory-wave model to be described, will yield a fully quantitative but greatly simplified scattering model.

### 3.3 GLORY-WAVE EFFECTS

The glory phenomenon is the halo surrounding the viewer's own shadow cast by the sun upon a mist (or a cloud, when observed by airplane). It is caused by light entering water droplets and, after multiple internal reflections, being returned to the observer [11][12]. It is a monostatic effect as distinguished from the rainbow effect which, although also involving internal reflections, is bistatic, resulting from local maxima in scattering intensity at certain bistatic angles. The phenomena involve surface (creep) waves as well as Snell's law reflection and refraction.

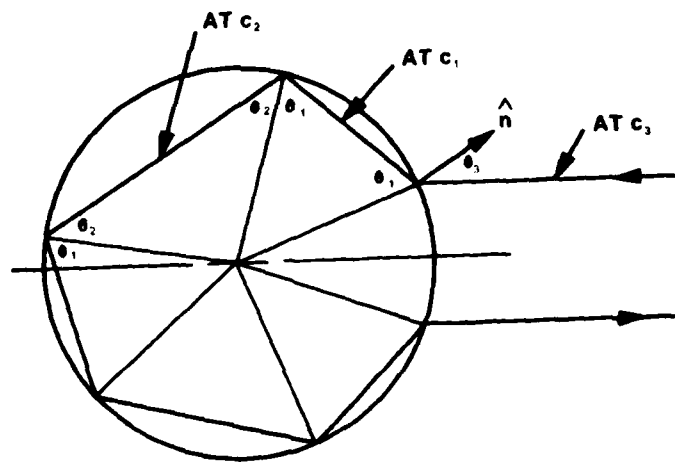
The nomenclature is here applied to the acoustic case. (Since the refractive index for most acoustical situations will be greater than 1 while for the optical case it is generally less than 1, there are some qualitative differences between the two cases.) A semiquantitative understanding of the phenomenon can be obtained using ray-optics theory.

Consider the glory path as illustrated in Figure 3-4 for a



79-871

FIG. 3-3 Local influence theory: reflection and refraction.



ILLUSTRATED FOR  $c_1 > c_2 > c_3$ ;  $m_1 = 4, m_2 = 1$

79-872

FIG. 3-4 Glory paths for sphere.

sphere. At each change in direction Snell's law is obeyed

$$\frac{\sin \theta_1}{c_1} = \frac{\sin \theta_2}{c_2} = \frac{\sin \theta_3}{c_3} \quad (3-46)$$

where  $c_1$ ,  $c_2$ ,  $c_3$  are the compression, shear, and external velocities respectively. Each chord of the path is thus the base of an isosceles triangle. The requirement is that after  $k$  traverses around the sphere the rays return to the source. Let  $m_1$  and  $m_2$  be the number of chords at  $c_1$  and  $c_2$  respectively. Then

$$2\theta_3 + m_1(\pi - 2\theta_1) + m_2(\pi - 2\theta_2) = 2\pi k \quad (3-47)$$

With the constraints (3-46), this equation has at most one solution  $\theta_3$  for each set  $(m_1, m_2, k)$ .

The extra time required to traverse this path compared to direct reflection from the center of the sphere is

$$t_{m_1 m_2 k} = 2a \left( \frac{m_1}{c_1} \cos \theta_1 + \frac{m_2}{c_2} \cos \theta_2 - \cos \theta_3 \right), \quad (3-48)$$

where  $a$  is the sphere radius.

The cases  $m_1$  or  $m_2 \rightarrow \infty$  are identified as creep waves along the (inner) surface of the sphere, which are launched when  $\theta_3$  is at one of the critical angles. By this model, then, the impulse response of an elastic sphere is a sequence of pulses occurring at the times  $t_{m_1, m_2, k}$ . The magnitudes and shapes of these pulses depend upon the detailed interaction of the local wavefront with the boundary at each of the reflection points.

### 3.4 GLORY MODEL EVALUATION

Consider first the fluid sphere response (that is, considering only compression waves). Figure 3.5 illustrates two cases, comparing the smoothed impulse response with the impulses predicted by the glory wave model. It is seen that the agreement is virtually perfect. All possible glory paths are observed with decreasing amplitude in proportion to the number of reflections.

In Figures 3.6 and 3.7 the model is compared with the elastic target response. First, note that the pure compression modes as observed for the fluid target are still observed (for the sake of clarity not all of them are indicated), though these effects are overwhelmed by the shear effects. The agreement between the glory modes and the main features of the response is only approximate. It is significant that the change in times of occurrence with changing  $c_2$  and  $c_1$  agree.

It is seen from the figures that the dominant modes are those with  $m_2 = 1$ ,  $m_2 = 2$ , or  $m_2 = \infty$  (creep). There is little time difference between  $(m_1, m_2) = (2,1)$  and  $(\infty,1)$  or between  $(1,2)$  and  $(\infty,2)$ , where  $m_1 = \infty$  means that the path at speed  $c_1$  is an internal creep path. A more quantitative theory is required to determine the relative contributions from those modes. These principal modes are illustrated in Figure 3-8.

### 3.5 SIMPLE MODEL

It is apparent that pure compressional modes can be neglected in a simple scattering model for elastic solids. We will base our model on the paths a, b, c, d of Figure 3-8. For path (a), the specular response, the return occurs at time

$$t_a = - \frac{2a}{c_3} \quad (3-49)$$

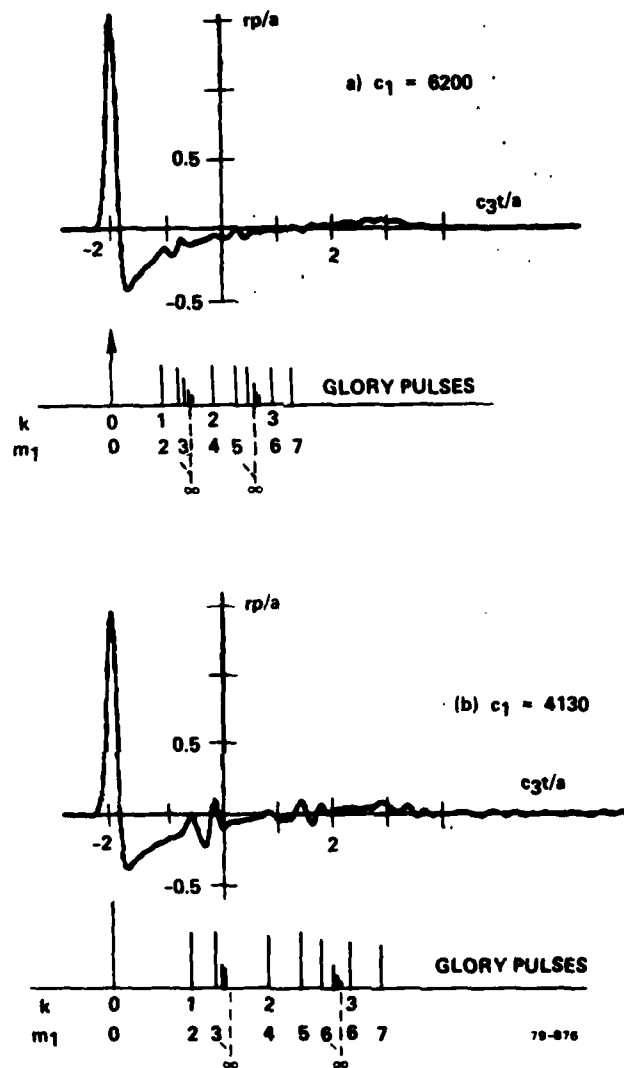


FIG. 3-5 Glory wave model — fluid sphere response.

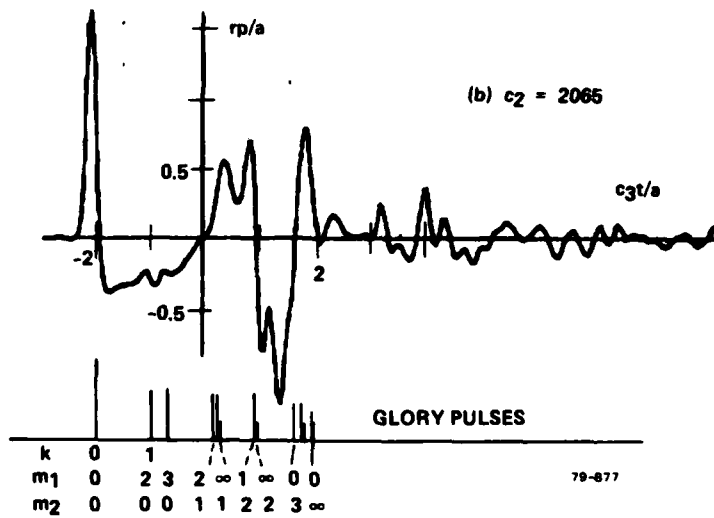
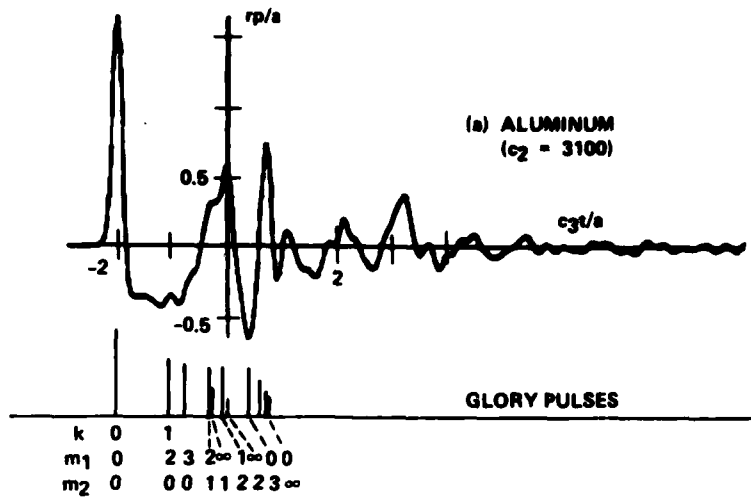


FIG. 3-6 Glory wave model — aluminum and variations.

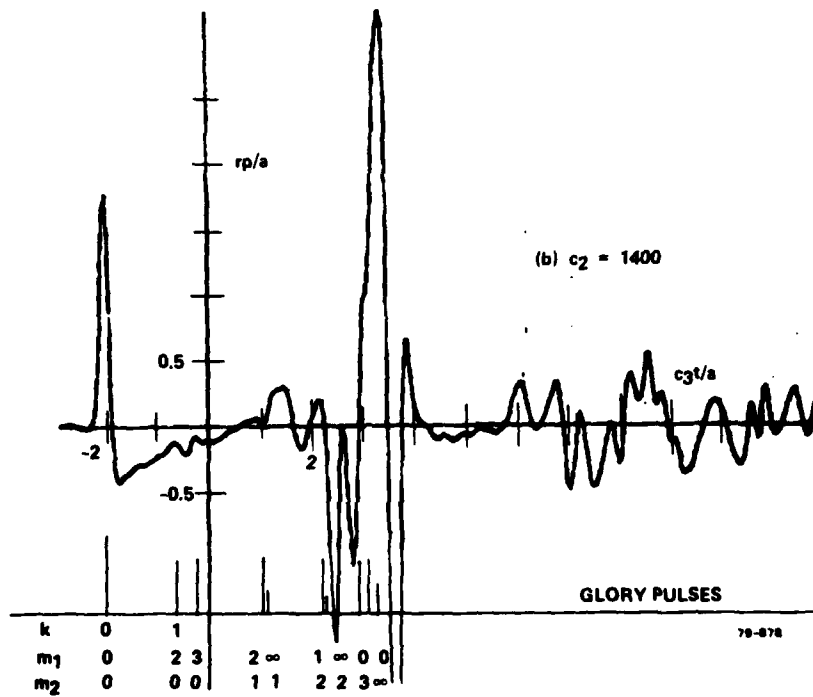
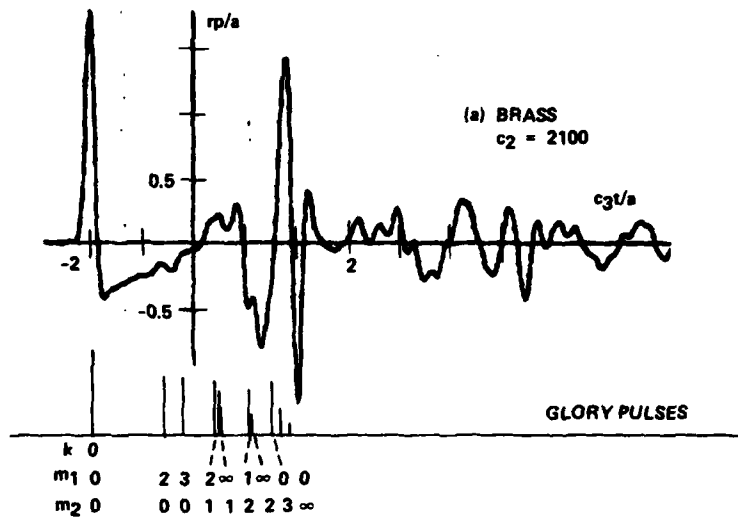


FIG. 3-7 Glory wave model – brass and variations.

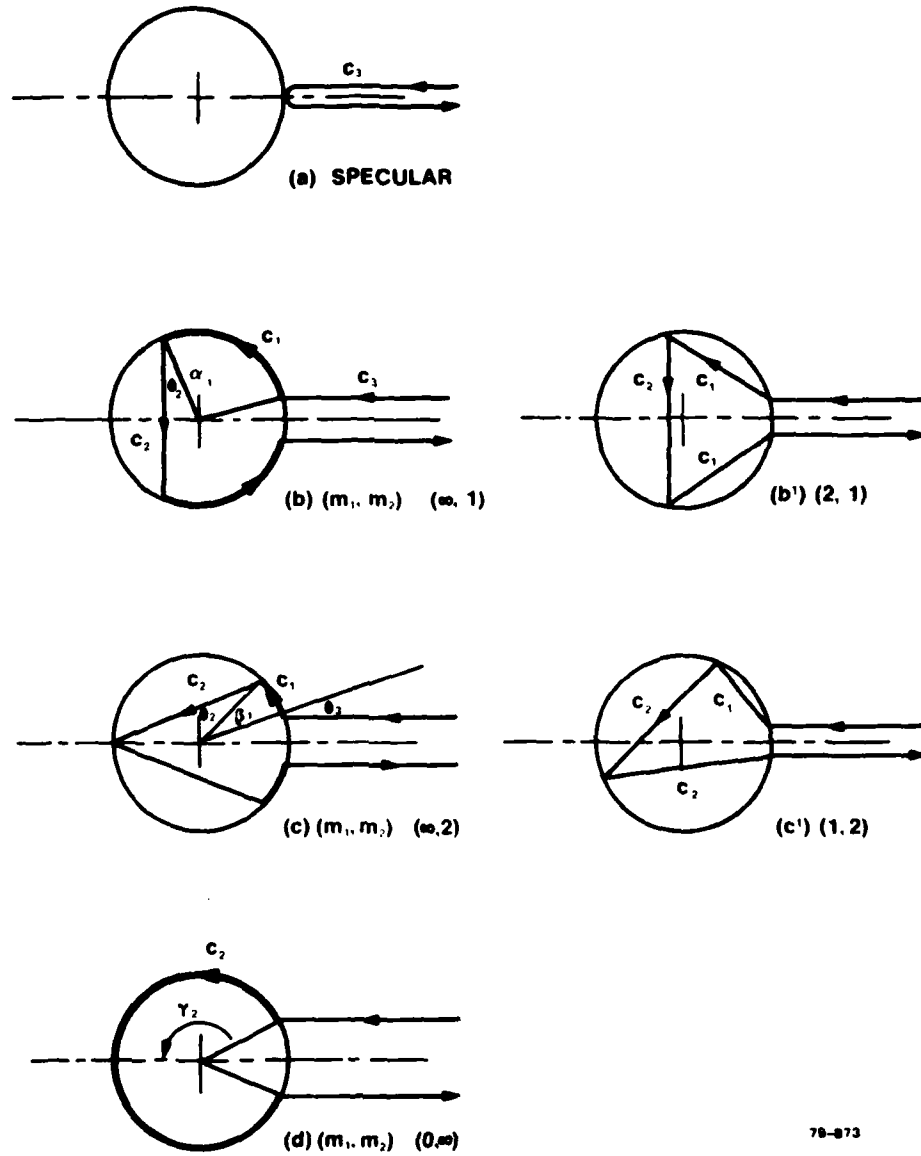


FIG. 3-8 Principal scattering modes involving shear waves.

For paths (b) and (c) we are at the critical angle for  $c_1$ . That is  $\theta_1 = 90^\circ$  and  $\theta_{3c1} = \sin^{-1}(c_3/c_1)$  and  $\theta_2 = \sin^{-1}(c_2/c_1)$ . The creep path length travelled at  $c_1$  is just sufficient to satisfy the requirement that the ray return to the source. (Actually, the creep wave at  $c_1$  is continually radiating so that all orientations of the path at  $c_2$  occur. Also, at other observation angles, the same model can be expected to apply with a different arc length at  $c_1$ .) The arc at  $c_1$  spans in case (b):  $\alpha_1 = \theta_2 + (\pi/2 - \theta_{3c1})$  and in case (c):  $\beta_1 = 2\theta_2 - \theta_{3c1}$ .

The return times are thus

$$t_b = 2a \left[ \frac{\alpha_1}{c_1} + \frac{\cos \theta_2}{c_2} - \frac{\cos \theta_{3c1}}{c_3} \right], \quad (3-50)$$

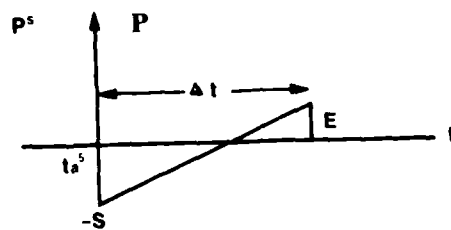
$$t_c = 2a \left[ \frac{\beta_1}{c_1} + \frac{2 \cos \theta_2}{c_2} - \frac{\cos \theta_{3c1}}{c_3} \right]. \quad (3-51)$$

Path (d) has the critical angle associated with  $c_2$ ,  $\theta_{3c2} = \sin^{-1}(c_3/c_2)$ , and half arc length  $\gamma_2 = (\pi - \theta_{3c2})$ . Hence the return time is

$$t_d = 2a \left[ \frac{\gamma_2}{c_2} - \frac{\cos \theta_{3c2}}{c_3} \right]. \quad (3-52)$$

A computer program was written to implement this model. The response for each mode is assumed to be of the form illustrated in Figure 3-9, namely impulse, step, ramp, and backswing (P, S, R, and E) such that the total area (DC response) is zero.

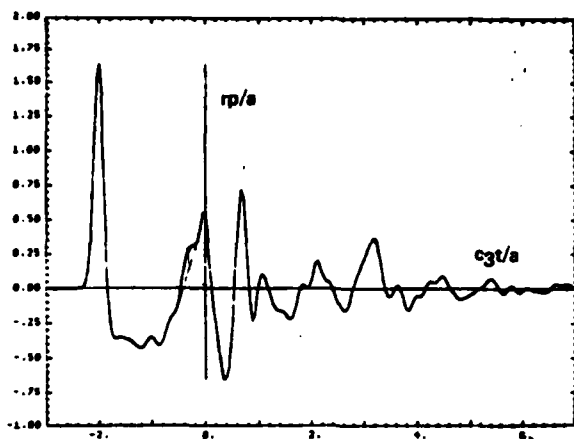
$$r(t) = \sum_k P_k \delta(t - t_k) + S_k u(t - t_k) + R_k (t - t_k) [u(t - t_k) - u(t - t_k + \Delta t)] + E_k u(t - t_k + \Delta t) \quad (3-53)$$



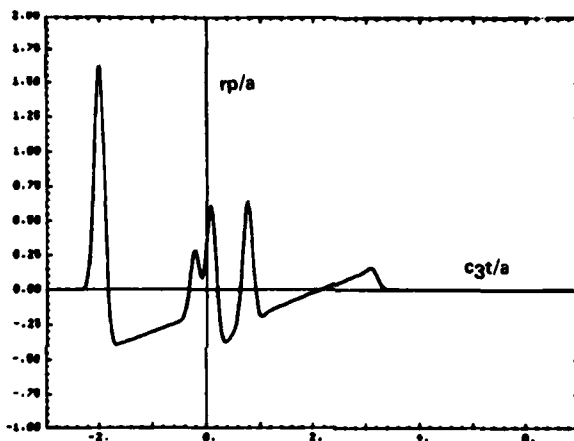
79-874

FIG. 3-9 Simplified impulse response.

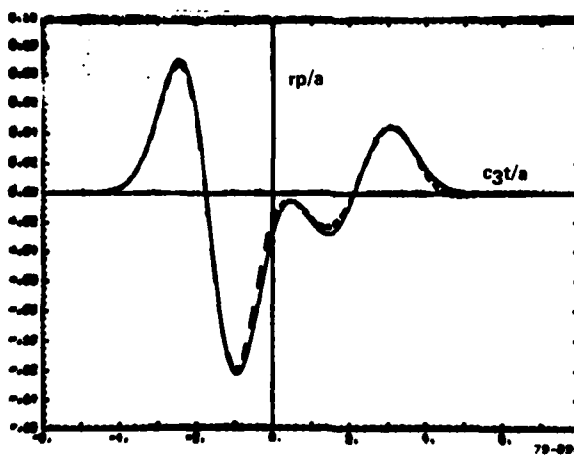
At this stage  $P$ ,  $S$ , and  $E$  are inputs to the program; with  $\Delta t = -2P/(E + S)$ ,  $R = (E - S)/\Delta t$ . It is expected that development of the methods in Sections 3-1 and 3-2 will yield theoretical values. The times of occurrence of these pulses are computed from the relations (3-49) to (3-52). It is seen in Figure 3-10 for aluminum that a simple representation for the impulse response can be found in this way. In the frequency domain (Figure 3-11), the model and actual response (as computed by Section 2 methods) agree in the main features. Brass is illustrated in Figures 3-12 and 3-13.



(a) CLASSICAL  
 $a_n = 8$



(b) MODEL  
 $a_n = 8$



(c)  $a_n = 1$   
--- CLASSICAL  
— MODEL

FIG. 3-10 Aluminum response model – time domain.

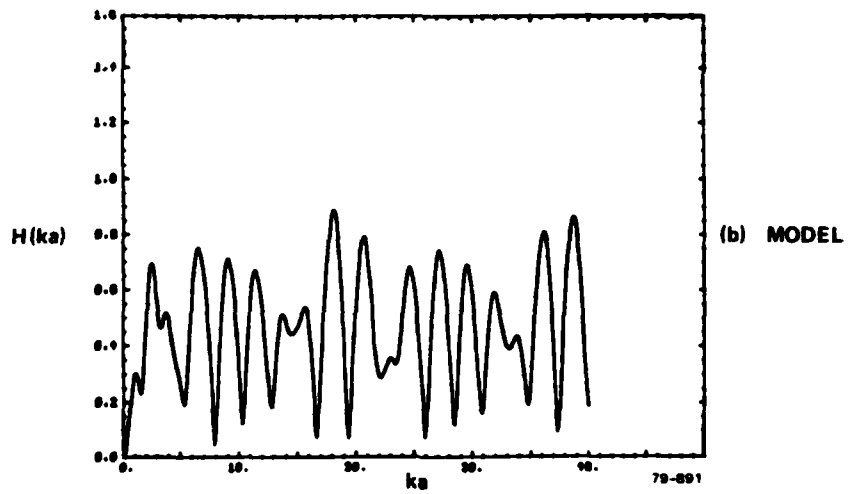
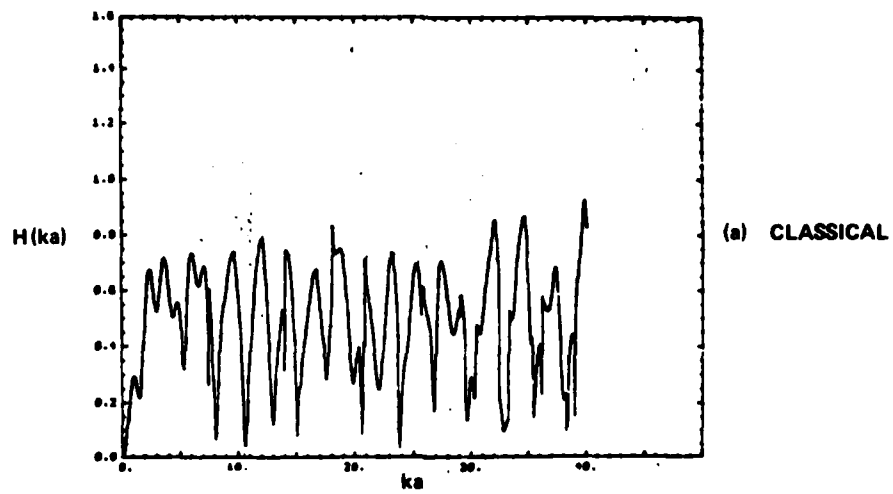


FIG. 3-11 Aluminum response model – frequency domain.

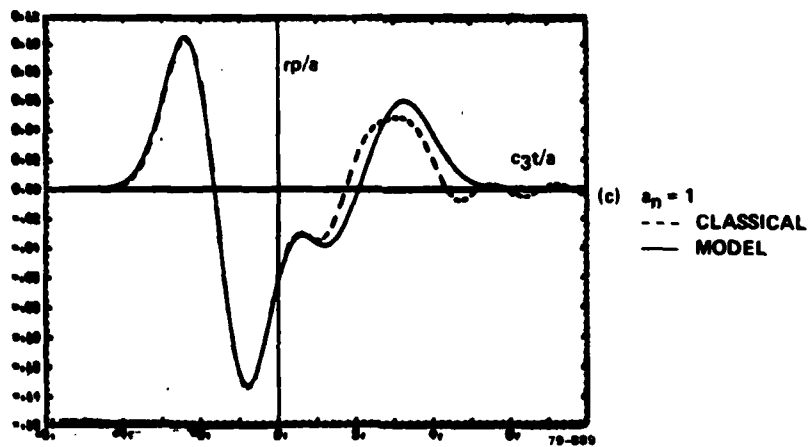
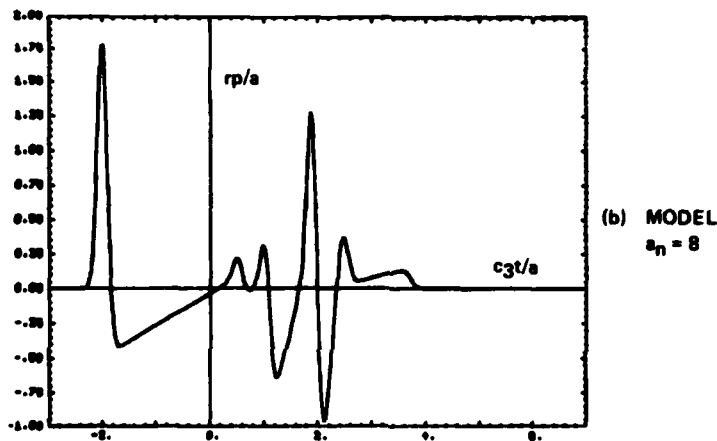
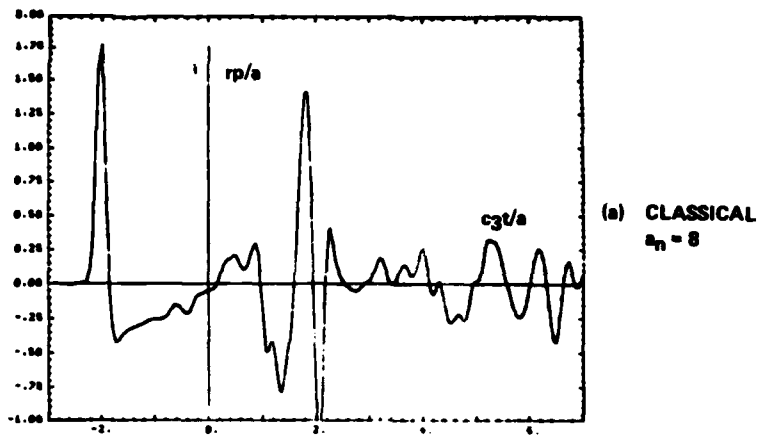


FIG. 3-12 Brass response model – time domain.

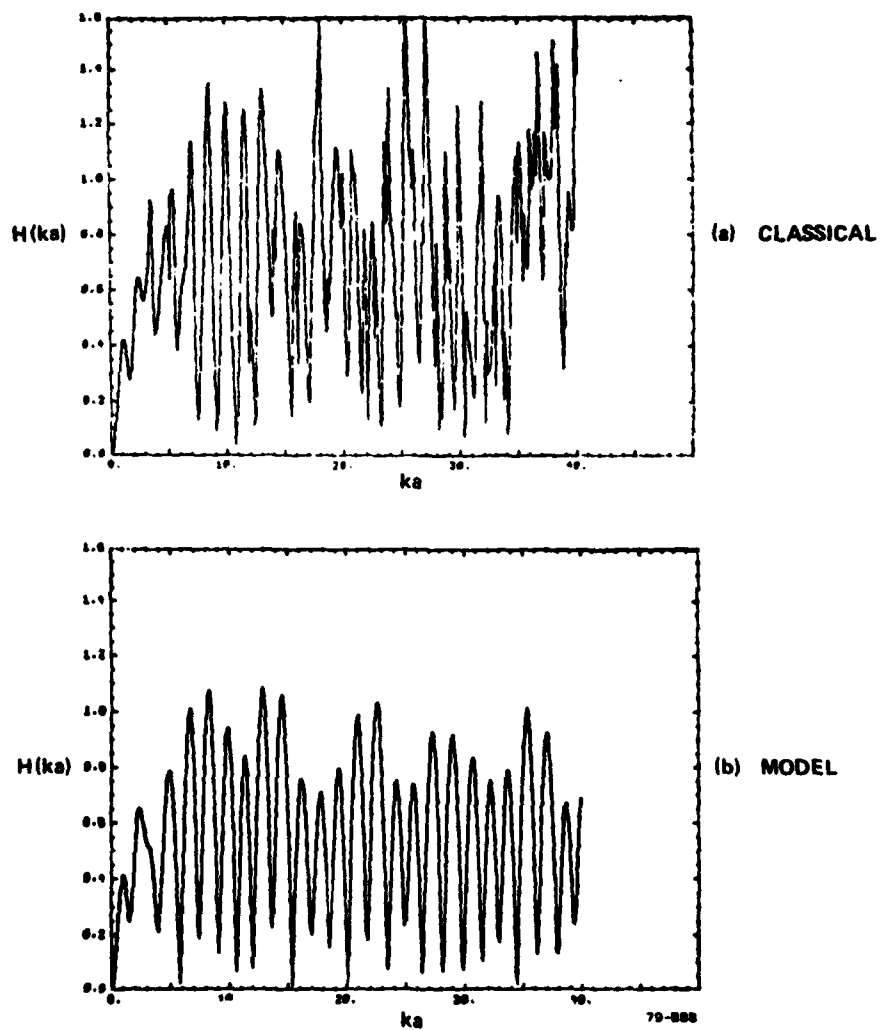


FIG. 3-13 Brass response model — frequency domain.

#### SECTION 4

##### SPACE-TIME INTEGRAL EQUATION APPROACH (SOLID TARGETS)

A major advantage of an integral equation formulation of the scattering problem is that it yields exact responses for targets of arbitrary three dimensional shape. The integral equation technique (STIE) used at the Sperry Research Center operates in the time domain, solving the problem by stepping in time rather than by matrix inversion. Using the excitation described in Section 2.2, the result is a smoothed impulse response. Such a time domain response is highly suggestive of target shape. If desired, the response can be deconvolved with the incident pulse and transformed to the frequency domain to obtain a frequency response. The latter is valid for values of  $ka$  from zero to an upper limit determined by the frequency content of the excitation pulse. The latter is limited primarily by computation time. To date most experience with this type of solution has been with electromagnetic scattering and with acoustic scattering from sound hard and sound soft targets [6, 13, 14]. It has been found that practical values on the upper frequency limit are  $ka = 6$  to 12.

To date the STIE approach has been applied with complete success to impenetrable targets such as conducting solids and thin surfaces in the electromagnetic case and to sound hard and sound soft targets in the acoustic case. Results have been published [6, 13, 14] for three dimensional targets of varying complexity.

In the present effort, this technique is extended to penetrable targets. The approach is reported in detail in reference 1, and will here be outlined in a somewhat more convenient form. At time of writing, targets penetrated only by compression waves are treated successfully, whereas numerical difficulties plague the solution when shear waves are added. We will first concentrate on the fluid target solution and present

computational results.

#### 4.1 FLUID TARGET FORMULATION

In an ideal fluid the excess pressure satisfies the wave equation

$$\ddot{p} = c_3^2 \nabla^2 p, \quad (4-1)$$

where  $c_3$  is the speed of sound. The pressure is related to particle displacement  $\vec{u}$  by

$$\nabla p = -\rho_3 \ddot{\vec{u}} \quad (4-2)$$

where  $\rho_3$  is the density (see [1], Section 2.1).

##### 4.1.1 Derivation of Integral Equation

Consider a closed surface  $S$  in the medium with pressure sources,  $p^i$ , originating outside of  $S$ . Using the Green's function

$$G(\vec{r}|\vec{r}', t|\tau) = \frac{1}{R} \delta(\tau - R/c_3 - t)$$

where  $\vec{R} = \vec{r} - \vec{r}'$ , a solution to the wave equation can be developed, known as the Kirchhoff integral representation:

$$p(\vec{r}, t) = p^i(\vec{r}, t) - \frac{1}{4\pi} \int_S \left\{ \frac{1}{R} \frac{\partial p(\vec{r}', \tau)}{\partial n'} - (\hat{n}' \cdot \hat{R}) L p(\vec{r}', \tau) \right\} ds' \quad (4-3)$$

where the integral is over the surface

$\hat{n}'$  is the unit normal out of the surface

$R$  is the magnitude of  $\vec{R} = \vec{r} - \vec{r}'$

$\hat{R}$  is the unit direction of  $\vec{R}$

$$L = \frac{1}{R^2} + \frac{1}{Rc_3} \frac{\partial}{\partial \tau}$$

$$\tau = t - R/c_3$$

The above is valid for  $\vec{r}$  outside of S.

Let the inside of S be source-free and filled with a fluid with properties  $c_1, \rho_1$ ; then (maintaining the same direction for  $\hat{n}$ )

$$p_1(\vec{r}, t) = \frac{1}{4\pi} \oint_S \left\{ \frac{1}{R} \frac{\partial p_1}{\partial n'}(\vec{r}', \tau_1) - (\hat{n}' \cdot \hat{R}) L_1 p_1(\vec{r}', \tau_1) \right\} ds' \quad (4-4)$$

for  $\vec{r}$  inside S, where

$$L_1 = \frac{1}{R^2} + \frac{1}{Rc_1} \frac{\partial}{\partial \tau_1}$$

$$\tau_1 = t - R/c_1$$

and  $p_1, \partial p_1/\partial n$  are the values just on the inside of the surface.

That is, the pressure can be calculated everywhere if the values of  $p$  and  $\partial p/\partial n$  are known on S. In particular, in the far field as  $R \rightarrow r \rightarrow \infty$ , the scattered part of the field is given by

$$r p^s(\vec{r}, t) = \frac{1}{4\pi} \oint \left\{ -\frac{\partial p}{\partial n}(\vec{r}', \tau) + (\hat{n}' \cdot \hat{r}) \frac{\partial p}{c_3 \partial \tau}(\vec{r}', \tau) \right\} ds' \quad (4-5)$$

To evaluate this expression, it is first required to solve (4-3) and (4-4) on S. A limiting procedure must be applied to make these valid on the surface since the term  $(\hat{n}' \cdot \hat{R}) L p$  in the integral becomes singular as  $r' \rightarrow r$ . This singularity is removed in the following way: consider the singular term separately and define the integral written as  $\oint ds'$  to have its

singular term removed. (Usually this is written as  $\int dS'$ .) Now require that (4-3), the "outside equation" results in  $p(\vec{r}) \equiv 0$  for  $\vec{r}$  inside  $S$ . This requirement remains to be justified. Comparing the results of evaluating (4-3) for  $\vec{r}$  just inside and just outside of  $S$ , we see that the non-singular parts of the equation  $I_{NS}$  give the same value at these two points, but that the singular portion changes sign (due to  $\hat{r} \cdot \hat{n}$ ). That is, we have

$$\begin{aligned} \vec{r} \text{ outside: } p &= p^i + I_{NS} - I_S \\ \vec{r} \text{ inside: } 0 &= p = p^i + I_{NS} + I_S \end{aligned} \quad (4-6)$$

Combining these, we obtain  $p = 2p^i + 2I_{NS}$ . The singular point has been removed and we have introduced a factor of 2. We thus obtain for  $\vec{r}$  on the (outside layer of the) surface  $S$ :

$$p(\vec{r}, t) = 2p^i(\vec{r}, t) - \frac{1}{2\pi} \int_S \left\{ \frac{1}{R} \frac{\partial p}{\partial n'}(\vec{r}', \tau) - (\hat{n}' \cdot \hat{R}) L p(\vec{r}', \tau) \right\} dS' \quad (4-7)$$

This equation contains two unknowns  $p$  and  $\partial p / \partial n$  so that another relation is needed to solve. In the case of an impenetrable target the requirement  $p = 0$  inside is exactly physically true so that  $p$  and  $\partial p / \partial n$  in (4-7) represent actual physical quantities. The additional boundary condition  $\partial p / \partial n = 0$  for sound-hard or  $p = 0$  for sound-soft then permits solution of (4-7).

In the case of the fluid target we apply an analogous argument, requiring inside equation (4-5) to yield  $p(\vec{r}) = 0$  for  $\vec{r}$  outside, resulting in

$$p_1(\vec{r}, t) = \frac{1}{2\pi} \int_S \left\{ \frac{1}{R} \frac{\partial p_1}{\partial n'}(\vec{r}', \tau_1) - (\hat{n}' \cdot \hat{R}) L_1 p_1(\vec{r}', \tau_1) \right\} dS' \quad (4-8)$$

We now have two integral equations in 4 unknowns.  $S$  is a surface of discontinuity with two sides. The two sides of  $S$  are related by the boundary conditions. Imposition of the boundary conditions justifies the above  $p = 0$  requirement and also permits the system (4-7), (4-8) to be solved. These conditions are

$$\left. \begin{aligned} p_1(\vec{r}, t) &= p(\vec{r}, t) \\ \frac{\partial p_1}{\rho_1 \partial n}(\vec{r}, t) &= \frac{\partial p}{\rho_3 \partial n}(\vec{r}, t) \end{aligned} \right\} \vec{r} \text{ on } S \quad (4-9)$$

corresponding to continuity of pressure and normal displacement.

#### 4.1.2 Numerical Implementation

To solve these equations numerically, the surface is divided into patches  $\Delta S_k$  and  $p$ ,  $\partial p / \partial t$ ,  $\partial p / \partial n$  are assumed to be constant in value over a patch. Time is also quantized. That is, for (4-7) at  $\vec{r}_i$ :

$$\begin{aligned} p(\vec{r}_i, t_j) &= 2p^i(\vec{r}_i, t_j) - \frac{1}{2\pi} \sum_{k \neq i} \left\{ \frac{1}{R_{ik}} \frac{\partial p}{\partial n}(\vec{r}_k, \tau_{ijk}) - (\hat{n}_k \cdot \hat{R}_{ik}) L_{ik} p(\vec{r}_k, \tau_{ijk}) \right\} \Delta S_k \\ &\quad - \gamma_i \frac{\partial p}{\partial n}(\vec{r}_i, t_j) + \epsilon_i p(\vec{r}_i, t_j) \end{aligned} \quad (4-10)$$

where  $\tau_{ijk} = t_j - R_{ik}/c_3$ . In the above, the integral over the "self-patch" which contains  $\vec{r}_i$  (i.e., for  $k = i$ ), has been performed analytically.

$$\frac{1}{2\pi} \int_{\Delta S_i} \frac{ds'}{R} = \sqrt{\frac{\Delta S_i}{\pi}} \equiv \gamma_i \quad (4-11)$$

$$\frac{1}{2\pi} \int_{\Delta S_i} (\hat{n}' \cdot \hat{R}) \left( \frac{1}{R^2} + \frac{1}{Rc} \frac{\partial}{\partial \tau} \right) p(\vec{r}', \tau) ds' = \frac{\gamma_i}{2} K_i p \equiv \epsilon_i p \quad (4-12)$$

where  $K_i$  is the average curvature of the patch at  $\vec{r}_i$ . The derivation of (4-11) is straightforward, by approximating the patch by a circle with radius  $\gamma_i$ . For (4-12) it is necessary to expand  $\vec{R}$  and  $\hat{n}$  in curvilinear coordinates (see Appendix in reference 13). A similar numerical expression is written for (4-8). Writing  $I$  and  $I_1$  for these sums (the "non-self integrals") and applying the boundary conditions, we obtain the system

$$\begin{aligned} (1 - \epsilon_i) p(\vec{r}_i, t_j) + \gamma_i \frac{\partial p}{\partial n}(\vec{r}_i, t_j) &= 2p^i(\vec{r}_i, t_j) - I(\vec{r}_i, t_j) \\ (1 + \epsilon_i) p(\vec{r}_i, t_j) - \gamma_i \frac{\rho_1}{\rho_3} \frac{\partial p}{\partial n}(\vec{r}_i, t_j) &= I_1(\vec{r}_i, t_j) \end{aligned} \quad (4-13)$$

This can be solved simultaneously for  $p$ ,  $\partial p / \partial n$  for time  $t_j$  at each  $\vec{r}_i$  on  $S$ . Note that the non-self integrals can be evaluated at time  $t_j$  since the arguments  $\tau$  are earlier than  $t_j$ . Hence (4-13) can be solved for all time by stepping in time.

The stepping in time procedure is valid so long as the distance  $\Delta R$  to the nearest patch is greater than  $c_1 \Delta t$  (or  $c_3 \Delta t$ , whichever is greater) for  $\Delta t =$  time step. It may be desirable to use smaller patches in regions of rapid change, for which  $\Delta R$  is smaller than the above limit. For these cases a local iterative procedure is used involving only these nearby patches: first the contributions from all the non-near (properly retarded) patches are calculated to each patch. These values are then used to determine the near-patch contributions by simple linear interpolation between the new values and those at the previous time point. Then, one more iteration of this process is sufficient to assure convergence. This procedure, involving only the nearby patches is quick and does not add much time to the overall solution.

Typical values for a target dimension is  $a = 1$  (representing, for instance, cylinder radius) and for the pulse length parameter  $a_n = 1$  (see equation 2-15). Then, for time expressed in sound-meters ( $c_3 = 1$ ),

a time step of  $\Delta t = .2$  (or even  $.3$ ) is adequate to obtain good results in the case of sound-hard or soft targets. Since the pulsewidth measured between 2% points is about  $W = 4/a_n = 4$ , this represents about 20 time steps per pulsewidth. The typical patch separation then is somewhat larger than 0.2. For the fluid case, the time step must be reduced by about the ratio  $c_3/c_1$ . It was found that  $\Delta t = .075$  was sufficiently fine.

In the integral (4-10) it is necessary to interpolate in the table of previously computed values of  $p$  to obtain  $p$  and  $\partial p/\partial t$  at time  $\tau$ . One way to do this is by fitting a fourth-order polynomial to the five values surrounding  $\tau$ . This worked very successfully and accurately for the sound-hard case. However, numerical inaccuracies tend to develop toward the end of the response in time which may be amplified by high order polynomial fitting, resulting in a rapidly growing instability. This effect was particularly noticeable for the sound-soft case. This problem can be eliminated by linearly smoothing the five points and then fitting a simple quadratic to the inner three points. This method causes a small loss in accuracy and hence requires the use of a somewhat smaller  $\Delta t$  (say  $.1$  for sound soft, or  $.05$  for fluid with  $c_1/c_3 = 4$ ).

#### 4.1.3 Responses of Right Circular Cylinders

Responses were computed by these methods for a fluid right circular cylinder with the properties of aluminum and brass but neglecting the shear velocity:

	$\rho_1$	$c_1$
"Fluid Al"	2.70 g/cm <sup>3</sup>	6200 m/s
"Fluid Brass"	8.39	4400
Medium (Water)	1.00	1480

the incident pulse was  $a_n = 1$ . Results are plotted in Figures 4-1 through 4-3. The cylinder has length/radius ratio  $L/a = 6/1$ . Time is in units of

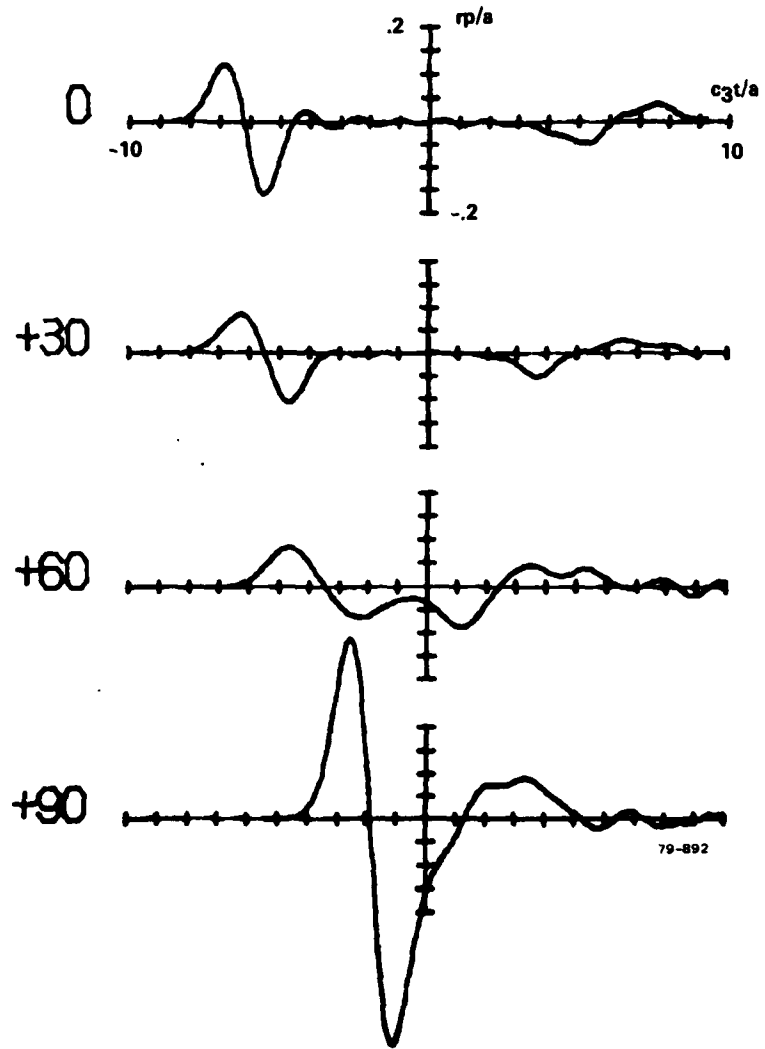


FIG. 4-1 STIE response for fluid aluminum right circular cylinder.

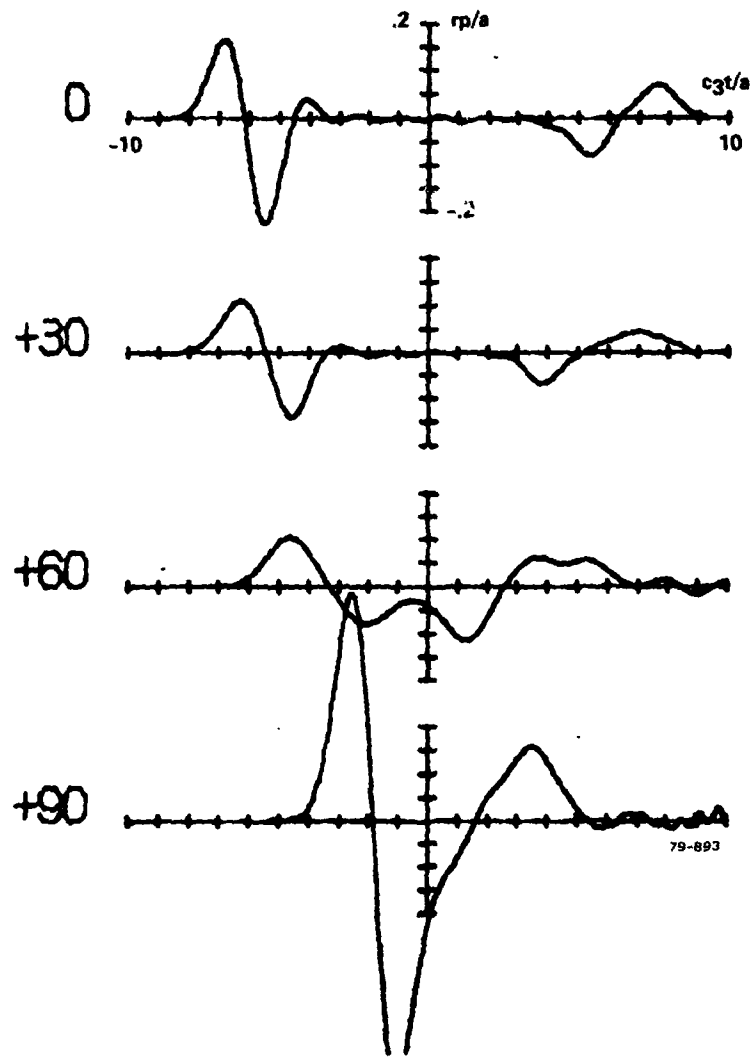


FIG. 4-2 STIE response for fluid brass right circular cylinder.

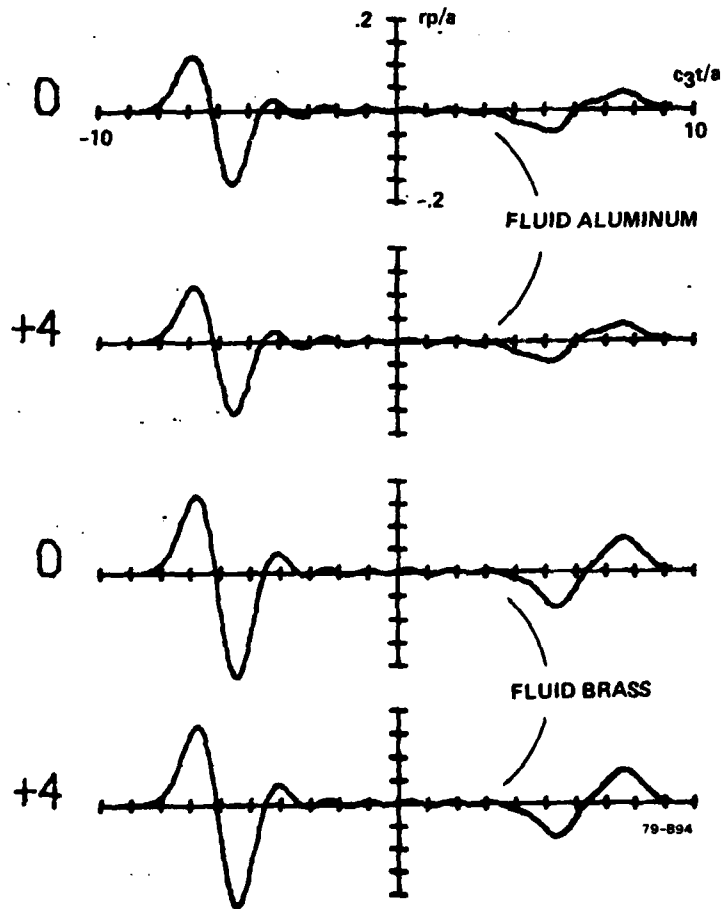


FIG. 4-3 STIE response – small angle deviation.

$c_3 t/a$ . Consider the  $0^\circ$  aspect; the initial part of the response is from the flat end of the cylinder and looks somewhat like the derivative of the incident pulse, centered on  $t = -6$ . The small peak at about  $t = -4$  can be interpreted as interaction with the edge. This part of the response is similar in shape to the response of a hard cylinder (see [13] or [1]) except for a reduction in amplitude. The small peak at  $t = -4$  is also somewhat earlier, indicating that edge effects occur at both  $c_1$  and  $c_3$ . The next major part of the return is the creep return at  $t = 6$  to  $8$ . This has been changed in shape and moved slightly earlier in comparison with the hard cylinder response. In between these two extreme times, the hard cylinder has a near-zero response, whereas the fluid target exhibits ringing. The latter must be interpreted as the result of internal reflections (end to end) of compression waves at  $c_1$ . As the aspect angle changes the two parts of the response move closer together.

A similar set of responses is given for brass in Figure 4-2. Also given, in Figure 4-3, is a comparison for each of these targets at the  $0^\circ$  and  $4^\circ$  aspects. The difference is extremely small.

#### 4.2 ELASTIC TARGET FORMULATION

A complete elastic target formulation must also include the effect of internal shear waves. As seen in Section 2, these can be the dominant effects. This formulation is treated in detail in [1] and will only be cursorily treated here. Instead of pressure it is easier to deal with the divergence of displacement. The two quantities are proportional:

$$p_1 = -c_1^2 \rho_1 (\nabla \cdot \vec{u}) \quad (4-14)$$

The equation of motion inside the solid is

$$\ddot{\vec{u}} = c_1^2 \nabla(\nabla \cdot \vec{u}) - c_2^2 \nabla \times \nabla \times \vec{u}, \quad (4-15)$$

from which it may be found (by taking the  $\nabla \times$  and  $\nabla \cdot$  of the above) that both  $(\nabla \cdot \vec{u})$  and  $(\nabla \times \vec{u})$  separately satisfy wave equations:

$$(\nabla \times \ddot{\vec{u}}) = c_2^2 \nabla^2 (\nabla \times \vec{u}) \quad (4-16)$$

In addition to equations (4-7) and (4-8), with  $p_1$  replaced by  $(\nabla \cdot \vec{u})$ , we have a vector Kirchhoff integral:

$$\nabla \times \vec{u}(\vec{r}, t) = \frac{1}{2\pi} \int_S \left\{ \frac{1}{R} \frac{\partial}{\partial n'} (\nabla \times \vec{u}') - (\hat{n}' \cdot \hat{R}) L_2 (\nabla \times \vec{u}') \right\} dS' \quad (4-17)$$

for  $\vec{r}$  on  $S$ . Here, the equation has already been specialized to the boundary  $S$ .

$$\nabla \times \vec{u}' \text{ means } \nabla \times \vec{u}(\vec{r}', \tau_2)$$

$$\tau_2 = t - R/c_2 .$$

Another form for this equation, which may be useful in practice is

$$\nabla \times \vec{u} = -\frac{1}{2\pi} \int_S \left\{ \frac{1}{R} (\hat{n}' \times \nabla \times \nabla \times \vec{u}') + L_2 \left( (\hat{n}' \cdot \nabla \times \vec{u}') \hat{R} + (\hat{n}' \times \nabla \times \vec{u}') \times \hat{R} \right) \right\} dS' \quad (4-18)$$

This form is obtained from (4-17) by vector manipulations and the use of the divergence theorem. (See Jackson [8], pp. 283.) It may be useful to observe that another equation can be written, namely for the  $(\nabla \times \nabla \times \vec{u})$ . The quantities  $(\nabla \times \vec{u})$ , and  $(\nabla \times \nabla \times \vec{u})$  now play somewhat similar roles to  $\vec{E}$  and  $\vec{H}$  of electromagnetics, so that techniques found useful there are possibly applicable here.

The boundary conditions are the two stated in Section 4.1, continuity of normal stress and normal displacement, although the first looks

somewhat more complicated for elastic solids (see [1]). An additional boundary condition on the shear states that the tangential shear stress is continuous across  $S$ . Since this quantity is zero in the fluid, it is zero at the solid side of  $S$ . The boundary conditions may be written (see [1] for derivation; here the form in which these relations are written is more precise):

$$-p = \rho_1 \left( c_1^2 - 2c_2^2 \right) (\nabla \cdot \vec{u}) + 2 \rho_1 c_2^2 \frac{\partial u_n}{\partial n} \quad (4-19)$$

$$-\frac{\partial p}{\rho_3 \partial n} = c_1^2 \frac{\partial}{\partial n} (\nabla \cdot \vec{u}) - c_2^2 (\nabla \times \nabla \times \vec{u})_n = \ddot{u}_n \quad (4-20)$$

$$0 = (\nabla \times \vec{u})_{\text{tan}} - 2 \frac{\partial}{\partial n} (\hat{n} \times \vec{u}) \quad (4-21)$$

where  $\hat{n}$  is the outward normal direction. The set of 2 scalar and one vector STIE's plus the two scalar and one vector boundary equations can be solved for the unknowns  $p$ ,  $\nabla \cdot \vec{u}$ ,  $\nabla \times \vec{u}$  and their normal derivatives. However it requires the formation, numerically, of certain space-derivatives on the surface of  $S$ , and the numerical solution of the equation of motion (4-15) [1]. The need for differentiation on a curved surface results in numerical instabilities in the solution, which have to date not been solved. Only the initial portion of the response from the region around the specular point can be computed successfully.

Figure 4-4 illustrates the status of the space-time integral equation calculation. Plotted is the surface pressure as a function of time  $p(c_3 t/a)$  for the smooth impulse incidence at several points on the surface. The pressure as predicted by the classical solution of Section 2 is plotted in part (a); the current status of the integral equation solution in part (b). The shape of  $p$  more or less follows that of the incident pulse with significant deviations. In particular, at the backside ( $\theta = 180^\circ$ ) there is a bump a little before  $t = 0$  which represents

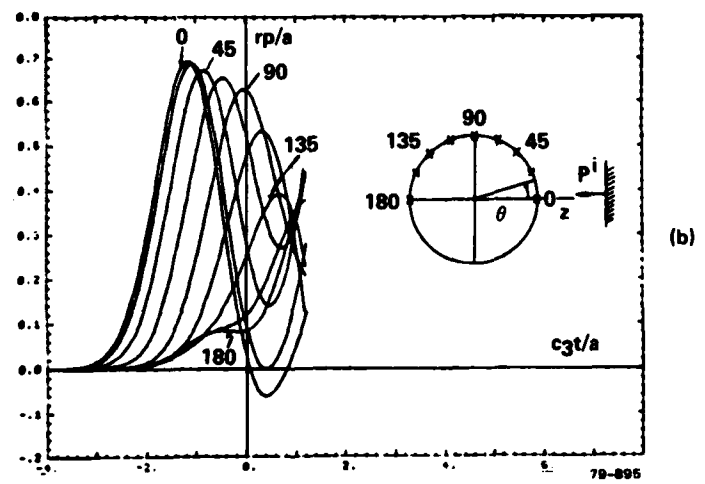
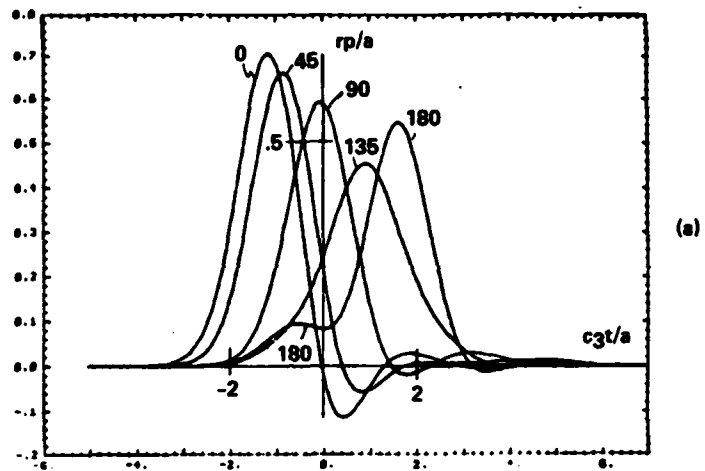


FIG. 4-4 Surface pressure for elastic sphere — classical and STIE.

transmission through the target at the shear velocity,  $c_2$ . It is seen that the initial part of the STIE calculation is correct; in particular the bump at  $\theta = 180^\circ$  is computed correctly. The latter is the respect in which elastic targets are distinguished from hard or fluid targets. Unfortunately, inaccuracies which rapidly develop into an instability start near  $\theta = 45^\circ$ . These inaccuracies have been identified as numerical differentiation problems; particularly since the quantity differentiated,  $\vec{u}$ , becomes large as time goes on, although the derivatives to be found remain relatively small. This problem has not yet been circumvented. The solution must lie in a formulation which avoids space-differentiation of the displacement  $\vec{u}$ . The far field computed from these surface values is shown in Figure 4-5, with the classical result shown dashed.

#### 4.3 THIN SHELL SPACE-TIME INTEGRAL EQUATION FORMULATION

A direct approach to solving the problem of scattering from an elastic shell with fluid interior and exterior is to formulate integral equations over both boundaries and applying boundary conditions on each. This two-boundary approach is taken in the classical solution of the next section. A computationally simpler approach is to attempt to find the limiting boundary condition between inside and outside media, and avoiding the need for solving any equations in the shell itself.

Consider the sphere of Figure 4-6 with outer and inner radii  $a$  and  $b$ . The boundary conditions can be written as

$$\begin{aligned}
 -p &= \rho_1 (c_1^2 - 2c_2^2) (\nabla \cdot \vec{u})^a + 2 \rho_1 c_2^2 \left( \frac{\partial u_r}{\partial r} \right)^a \\
 -p_4 &= \rho_1 (c_1^2 - 2c_2^2) (\nabla \cdot \vec{u})^b + 2 \rho_1 c_2^2 \left( \frac{\partial u_r}{\partial r} \right)^b
 \end{aligned}
 \tag{4-22}$$

and

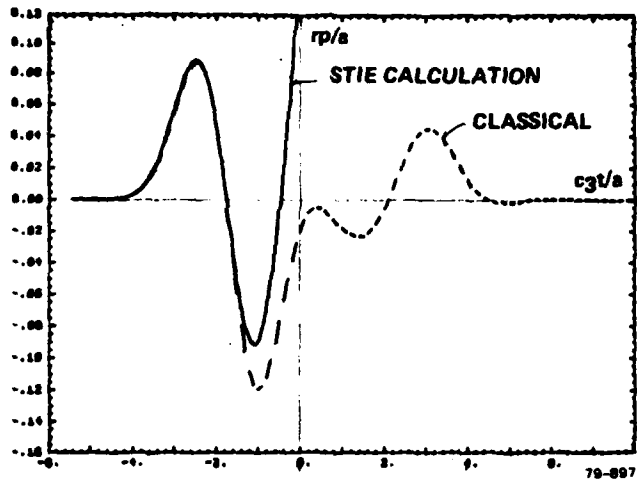


FIG. 4-5 Status of elastic STIE calculation – far field response.

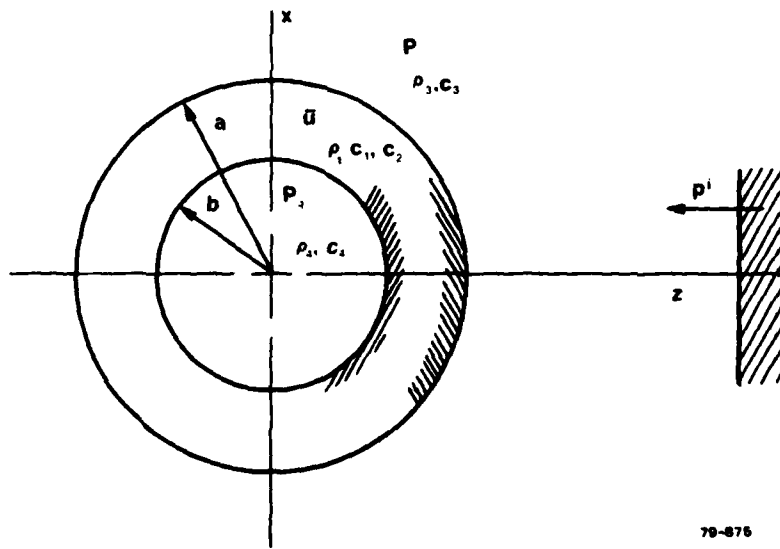


FIG. 4-6 Shell scattering problem.

$$\ddot{u}_r^a = -\frac{\partial p}{\rho_3 \partial r} = c_1^2 \frac{\partial}{\partial r} (\nabla \cdot \vec{u})^a - c_2^2 (\nabla \times \nabla \times \vec{u})_r^a, \quad (4-23)$$

$$\ddot{u}_r^b = -\frac{\partial p_4}{\rho_4 \partial r} = c_1^2 \frac{\partial}{\partial r} (\nabla \cdot \vec{u})^b - c_2^2 (\nabla \times \nabla \times \vec{u})_r^b;$$

where the superscripts a and b refer to the outer and inner surfaces. If we write  $(\nabla \times \nabla \times \vec{u})_n$  and the boundary condition (4-21) in spherical coordinates, we obtain

$$(\nabla \times \nabla \times \vec{u})_r^a = 2 \frac{\partial}{\partial r} (\nabla \cdot \vec{u})^a - 2 \frac{\partial}{\partial r} \left[ \frac{1}{r^2} \frac{\partial}{\partial r} (r^2 u_r) \right]^a \quad (4-24)$$

We use this to rewrite (4-23):

$$\begin{aligned} \ddot{u}_r^a &= -\frac{\partial p}{\rho_3 \partial r} = \left( c_1^2 - 2c_2^2 \right) \frac{\partial}{\partial r} (\nabla \cdot \vec{u})^a + 2 c_2^2 \frac{\partial}{\partial r} \left[ \frac{1}{r^2} \frac{\partial}{\partial r} (r^2 u_r) \right]^a \\ \ddot{u}_r^b &= -\frac{\partial p_4}{\rho_4 \partial r} = \left( c_1^2 - 2c_2^2 \right) \frac{\partial}{\partial r} (\nabla \cdot \vec{u})^b + 2 c_2^2 \frac{\partial}{\partial r} \left[ \frac{1}{r^2} \frac{\partial}{\partial r} (r^2 u_r) \right]^b. \end{aligned} \quad (4-25)$$

The aim is to find relations between  $p$ ,  $\frac{\partial p}{\partial r}$ ,  $p_4$ ,  $\frac{\partial p_4}{\partial r}$  by applying a limiting process so that the problem reduces to essentially the fluid-in-fluid problem of Section 4.1, but with different boundary conditions.

First, suppose the shell thickness,  $h$ , sufficiently thin so that we can use a first order Taylor expansion; for example

$$(\nabla \cdot \vec{u})^a = (\nabla \cdot \vec{u})^b + h \frac{\partial}{\partial r} (\nabla \cdot \vec{u})^b. \quad (4-26)$$

We will then rewrite the boundary conditions

$$p_4 - p = \rho_1 h (c_1^2 - 2c_2^2) \frac{\partial}{\partial r} (\nabla \cdot \vec{u}) + 2 \rho_1 h c_2^2 \frac{\partial^2 u_r}{\partial r^2} \quad (4-27)$$

$$\frac{\partial p_4}{\rho_4 \partial r} - \frac{\partial p}{\rho_3 \partial r} = h (c_1^2 - 2c_2^2) \frac{\partial^2}{\partial r^2} (\nabla \cdot \vec{u}) + 2 h c_2^2 \frac{\partial^2}{\partial r^2} \left[ \frac{1}{r^2} \frac{\partial}{\partial r} (r^2 u_r) \right]. \quad (4-28)$$

If both  $h$  and  $\rho$  are reduced to zero the problem reduces to the fluid-in-fluid problem with no shell. As a next level of approximation, let  $h \rightarrow 0$  and let  $u_r^b = u_r^a$ . Then

$$p_4 - p = \rho_1 h (c_1^2 - 2c_2^2) \frac{\partial}{\partial r} (\nabla \cdot \vec{u}) \quad (4-29)$$

$$\ddot{u}_r = - \frac{\partial p_4}{\rho_4 \partial r} = - \frac{\partial p}{\rho_3 \partial r} = (c_1^2 - 2c_2^2) \frac{\partial}{\partial r} (\nabla \cdot \vec{u}) . \quad (4-30)$$

or

$$p_4 - p = \rho_1 h \ddot{u}_r . \quad (4-29')$$

This represents the equation of motion of a membrane with no internal restoring forces. We can add restoring forces due to an ambient pressure difference,  $\tilde{\Delta p}$ , between inside and outside which results in a tension  $T = \tilde{\Delta p} (a/2)$ . Then we have

$$p_4 - p = \rho_1 h \ddot{u}_r - T \nabla_s^2 u_r . \quad (4-29'')$$

This is the equation of motion of a membrane under tension and can be solved in conjunction with the fluid-in-fluid integral equations.

We have simplified more than desired, however, since we wish the elastic properties of the shell to be included. Returning to equations (4-23), we note that we can also write by virtue of the boundary conditions [1]

$$(\nabla \times \nabla \times \vec{u})_r = -2 \nabla_s^2 u_r, \quad (4-31)$$

but it must be realized that the meaning of  $\nabla_s^2$  is dependent on the coordinate system. In spherical coordinates (with axial symmetry):

$$\nabla_s^2 u_r \equiv \frac{\partial^2 u_r}{r^2 \partial \theta^2} - \frac{\partial u_\theta}{r^2 \partial \theta} + \frac{\cos \theta}{r^2 \sin \theta} \left( \frac{\partial u_r}{\partial \theta} - u_\theta \right) \quad (4-32)$$

the above is actually a definition of  $\nabla_s^2$ , obtained from writing out  $(\nabla \times \nabla \times \vec{u})$  and applying the boundary condition in spherical coordinates. We then write (4-23) as

$$\ddot{u}_r = c_1^2 \frac{\partial}{\partial r} (\nabla \cdot \vec{u}) + 2 c_2^2 \nabla_s^2 u_r \quad (4-33)$$

and use this to eliminate  $\partial/\partial r (\nabla \cdot \vec{u})$  in equation (4-29). The result is

$$p_4 - p = (\rho_1 h) \left( 1 - 2 \frac{c_2^2}{c_1^2} \right) \left\{ \ddot{u}_r - 2 \frac{c_2^2}{c_1^2} \nabla_s^2 u_r \right\} \quad (4-34)$$

$$\ddot{u}_r = - \frac{\partial p}{\rho_3 \partial r} = - \frac{\partial p_4}{\rho_4 \partial r} \quad (4-25')$$

These equations can be used as the boundary conditions with the system of two space-time integral equations as written for the fluid case of Section 4.1. It requires the time-integration of  $\ddot{u}_r$  (which is no problem) and the numerical differentiation in the surface of  $u_r$ . Unfortunately, as was the case for the elastic target, the numerical differentiation causes instabilities.

In Figure 4.7 is plotted the result of the numerical implementation of the space-time integral equation solution using the membrane

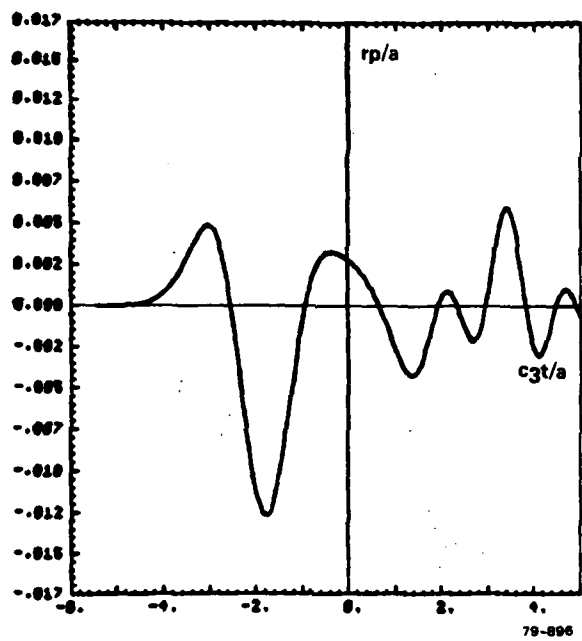


FIG. 4-7 STIE solution – scattering from spherical membrane.

boundary condition between similar fluids. As will be seen in the next section, this result is not a good model for a thin shell. While the general nature of the response is similar, its dominant frequency differs by a factor of 2. It is therefore necessary to solve the problem remaining with implementing boundary condition (4-34).

SECTION 5  
SPHERICAL HULLED TARGETS

5.1 CLASSICAL SOLUTION FOR THICK SHELL

The fluid-filled spherical thick shell problem can be solved by expansion in terms of eigenfunctions in a way completely analogous to the elastic solid of Section 2.1 [15]. Let the outer and inner radii be  $a, b$ ; and let the core have constants  $c_4, \rho_4$ . In addition to the incident and scattered pressure expansions, we have a compressional wave in the sphere core ( $\rho_4, c_4$ ). The eigenfunctions must be bounded at the origin and are therefore  $j_n(kr) P_n(\cos \theta)$ . In the shell, on the other hand, there no longer is the requirement that the eigenfunction be bounded at the origin. Or, alternatively we can say that the shell exhibits both inward and outward traveling waves. The shell solution thus contains both  $j_n$  and  $n_n$  (or, both  $h_n^{(1)}$  and  $h_n^{(2)}$ , whichever is more convenient).

Suppressing the time dependence  $e^{-i\omega t}$ , we thus have

$$p^i(\vec{r}) = P_0 \sum_{n=0}^{\infty} (2n+1) (-i)^n j_n(kr) P_n(\cos \theta) \quad (5-1)$$

$r \geq a$

$$p^s(\vec{r}) = P_0 \sum_{n=0}^{\infty} c_n h_n^{(1)}(kr) P_n(\cos \theta) \quad (5-2)$$

$r \geq a$

$$p^4(\vec{r}) = P_0 \sum_{n=0}^{\infty} f_n j_n(k_4 r) P_n(\cos \theta) \quad (5-3)$$

$r \leq b$

$$\psi(\vec{r}) = \sum_{n=0}^{\infty} \left( a_n j_n(k_1 r) + d_n n_n(k_1 r) \right) P_n(\cos \theta) \quad (5-4)$$

$b \leq r \leq a$

$$A_{\phi}(\vec{r}) = \sum_{n=0}^{\infty} \left( b_n j_n(k_2 r) + e_n n_n(k_2 r) \right) \frac{dP_n}{d\theta} \quad (5-5)$$

$b \leq r \leq a$

Again we have that in the elastic shell

$$\vec{u}(\vec{r}) = -\nabla\psi + \nabla \times \vec{A} \quad b \leq r \leq a \quad (5-6)$$

$$\rho_1 \ddot{\vec{u}}(\vec{r}) = (\lambda + 2\mu) \nabla(\nabla \cdot \vec{u}) - \mu \nabla \times \nabla \times \vec{u} \quad b \leq r \leq a \quad (5-7)$$

and that the total pressure in the external medium is

$$p = p^i + p^s \quad r \geq a \quad (5-8)$$

The unknowns are  $a_n, b_n, c_n, d_n, e_n, f_n$  for each mode  $n$ . The boundary conditions (2-6), (2-7) and (2-8) are applied both at  $r = a$  and at  $r = b$ . The result is a system of 6 equations in 6 unknowns analogous to the system (2-10):

$$M^n Z^n = V^n, \quad (5-9)$$

where  $Z^n$  is written for the vector of unknowns  $(a_n, b_n, \dots, f_n)$ . The matrix entries  $M_{ij}^n$  and the entries  $V_i^n$  for  $i, j \leq 3$  are exactly those of (2-11). To obtain the other  $M_{ij}^n$ , we can avoid a lot of writing by observing the following: each row is augmented by the coefficients of  $d_n$  and  $e_n$ , which are the same as the corresponding coefficients of  $a_n$  and  $b_n$  except for the use of  $n_n$  instead of  $j_n$ . That is:

replace  $j_n$  by  $n_n$  in  $M_{i1}^n$  to obtain  $M_{i4}^n$   $(i = 1, \dots, 6)$ ;

replace  $j_n$  by  $n_n$  in  $M_{i2}^n$  to obtain  $M_{i5}^n$   $(i = 1, \dots, 6)$ .

Also, equations 4, 5, and 6 are the same as 1, 2, 3, except that they are

evaluated at  $r = b$  instead of  $r = a$ ; and also all occurrences of  $\rho_3, c_3$  are replaced by  $\rho_4, c_4$ . That is: replace Bessel function arguments  $x, x_1, x_2$  by  $y, y_1, y_2$ , where

$$\begin{aligned} y &= k_4 b = \omega b / c_4 \\ y_1 &= k_1 b = \omega b / c_1 \\ y_2 &= k_2 b = \omega b / c_2 \end{aligned} \quad (5-10)$$

in

$$M_{1j}^n \text{ to obtain } M_{4j}^n,$$

$$M_{2j}^n \text{ to obtain } M_{5j}^n,$$

$$M_{3j}^n \text{ to obtain } M_{6j}^n \quad (\text{all for } j = 1, 2, 4, 5).$$

Further,  $M_{i6}^n = 0$  for  $i = 1, 2, 3$ ;  $M_{i3}^n = 0$  for  $i = 4, 5, 6$ ;

$$M_{46}^n = \beta_4 D_0 b^2 j_n(y),$$

$$M_{56}^n = -D_0 b^2 j_n'(y),$$

$$M_{66}^n = 0,$$

$$V_i^n = 0, \quad i = 4, 5, 6, \quad (5-11)$$

where

$$\beta_4 = \frac{\rho_4 c_4^2}{\rho_1 c_1^2}.$$

For example,

$$M_{45}^n = (n^2 + n) \alpha \left( y_2 n'_n (y_2) - n_n (y_2) \right) .$$

A number of degenerate cases can be obtained from these equations by letting the appropriate  $\rho$  or  $c$  go to  $\infty$  or 0, and thereby eliminating one or more unknowns and equations.

Degenerate Condition	Shell	Core	Equations (i)	Unknowns (j)
-	Elastic	Fluid	1,2,3,4,5,6	1,2,3,4,5,6
$\rho_4 \rightarrow \infty$	Elastic	Hard	1,2,3,5,6	1,2,3,4,5
$\rho_4 = 0$	Elastic	Soft	1,2,3,4,6	1,2,3,4,5
$b = 0$	Elastic	No	1,2,3	1,2,3
$c_2 = 0$	Fluid	Fluid	1,2,4,5	1,3,4,6
$c_2=0, \rho_4 \rightarrow \infty$	Fluid	Hard	1,2,5	1,3,4
$c_2=0, \rho_4=0$	Fluid	Soft	1,2,4	1,3,4
$c_2=0, b=0$	Fluid	No	1,2	1,3
$\rho_1 \rightarrow \infty$	Hard	No	2	3
$\rho_1 \rightarrow 0$	Soft	No	1	3

It is simplest to solve this set of equations by Gauss elimination and back substitution. Care must be taken, however, since the (complex) entries in  $M^n$  vary in magnitude from  $10^{20}$  to  $10^{-20}$ . Successful solution is achieved by normalizing  $M$  both by rows and by columns before applying the elimination procedure. The same considerations hold here as discussed in Section 2.1 with regard to the order of the Bessel functions.

Here the problem is somewhat more severe because of the larger range of Bessel function arguments. In the examples to follow, responses will be computed to  $ka = 20$  and smoothed impulse responses will be computed for pulsewidth parameter  $a_n = 4$ .

## 5.2 THIN SHELL LIMIT

The solution for the thin shell can be obtained nicely from the above without further modification. As the thickness  $h = a - b$  becomes small, greater accuracy can be obtained by noting that

$$M_{1j}^n = M_{4j}^n + h \frac{\partial}{\partial r} M_{4j}^n \quad (j = 1, 2, 4, 5) .$$

Row 4 can then be subtracted from row 1. The same can be done with rows 2 and 3. As  $h \rightarrow 0$ , some elements of  $M^n$  can be replaced by zero. However, this is not a great simplification since no unknowns are eliminated. In the calculations that follow, the unmodified thick shell computer program was used for the thin shell as well.

## 5.3 SHELL RESPONSES AS FUNCTIONS OF ELASTIC PARAMETERS

The sequence of plots in Figure 5-1 through 5-3 gives the magnitude of the frequency response of the spherical aluminum shell with parameter thickness. The thickness,  $h/a$  decreases from 1 to .001 through the sequence. The sequence 5-4 through 5-6 gives the same results in the time domain for smoothed impulse incidence with  $a_n = 4$ . It is seen that the thick shell has a more complex response than the solid. However, as the shell becomes thin, the response becomes simpler again, reducing in the limit to a sequence of spikes in the frequency domain. The magnitude of the response is proportional to  $h$  in the thin shell limit.

Whereas the response of a solid is perhaps best understood in the time domain as a sequence of pulses corresponding to various paths,

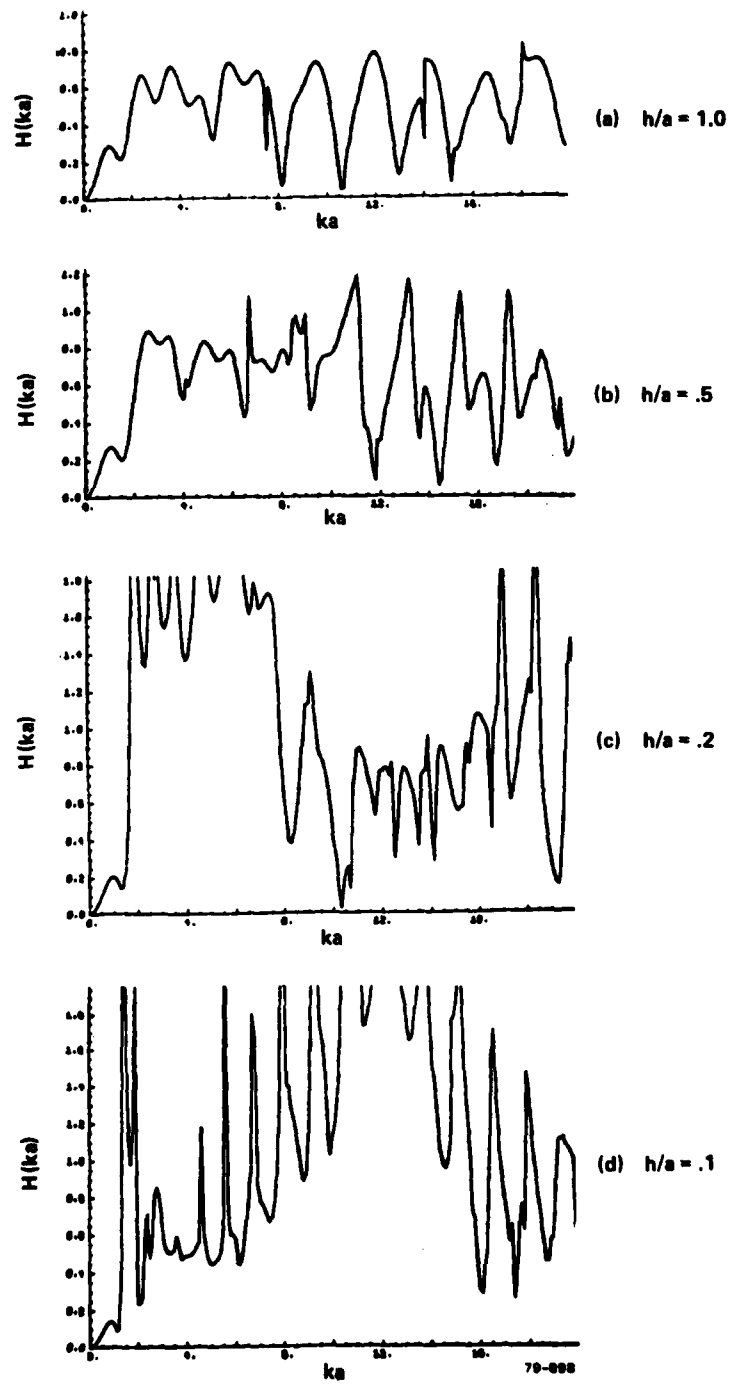


FIG. 5-1 Shell responses as a function of thickness — frequency domain, thick shell.

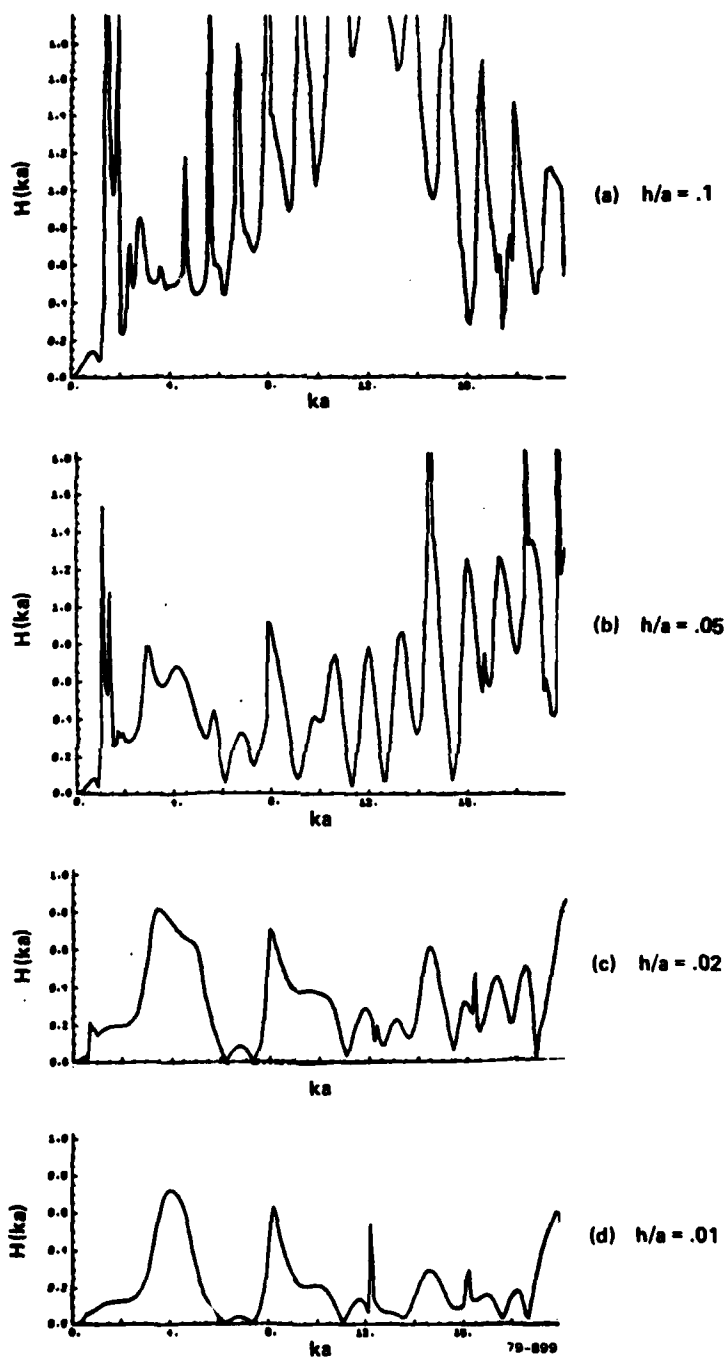


FIG. 5-2 Shell responses as a function of thickness – frequency domain, thin shell.

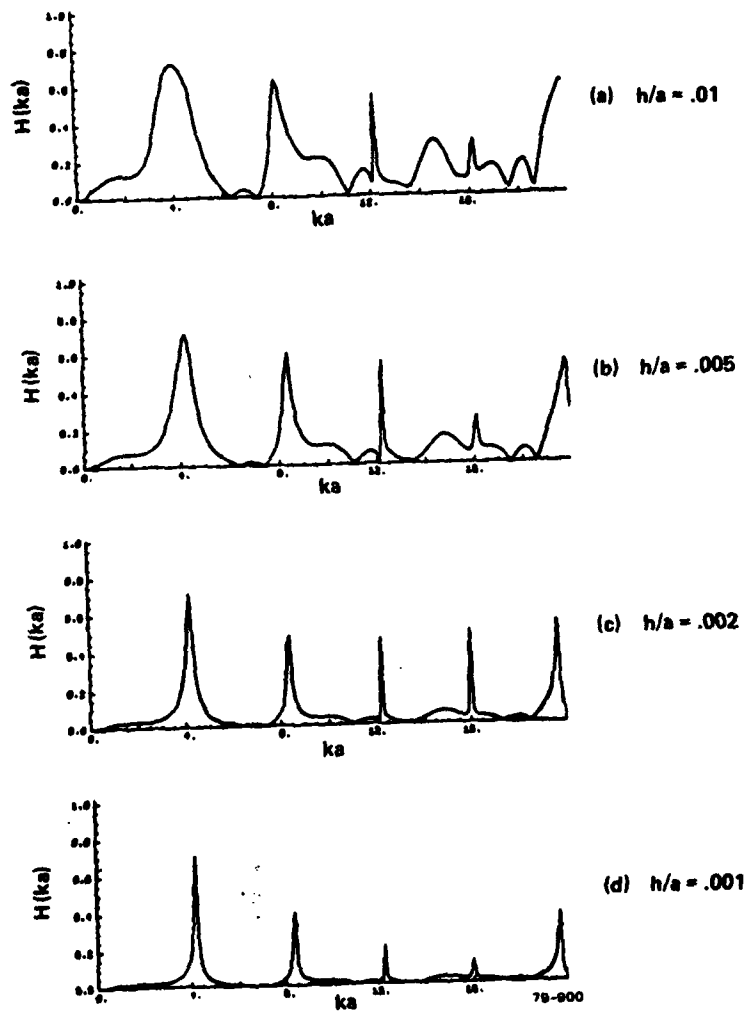


FIG. 5-3 Shell responses as a function of thickness – frequency domain, very thin shell.

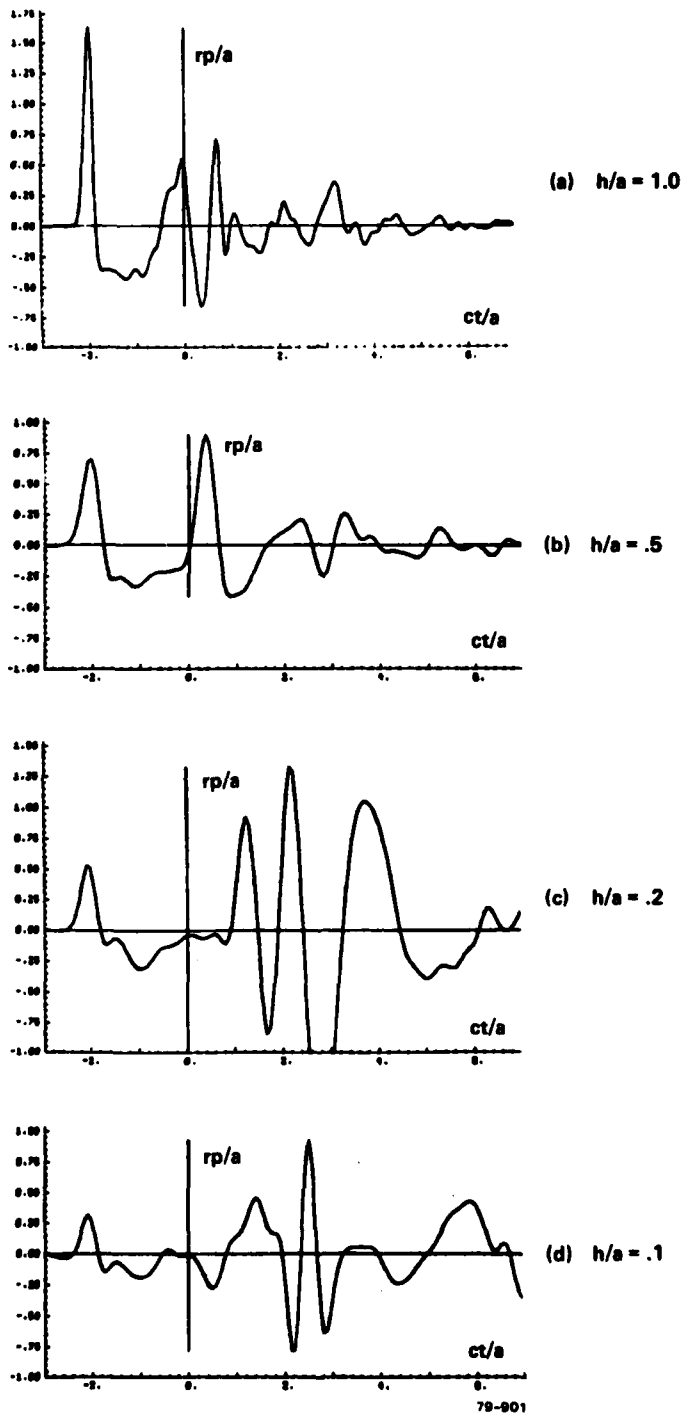


FIG. 5-4 Shell responses as a function of thickness — time domain,  $a_n = 4$ , thick shell.

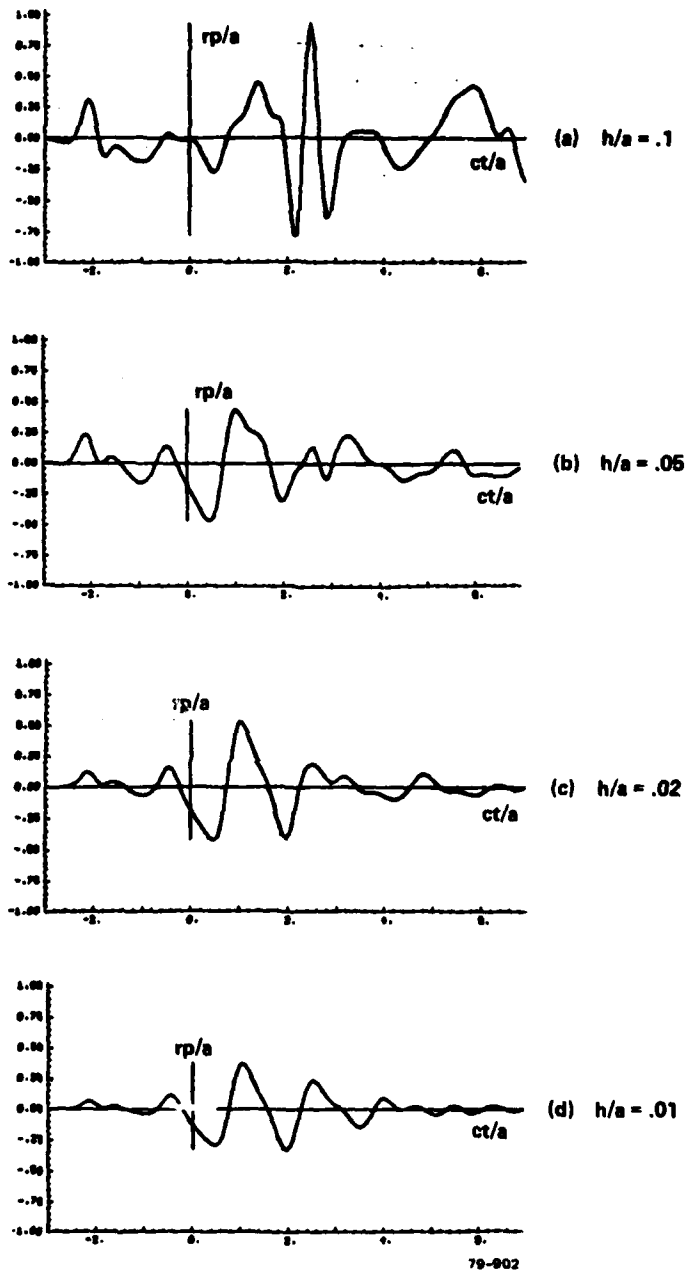


FIG. 5-5 Shell responses as a function of thickness — time domain,  $a_n = 4$ , thin shell.

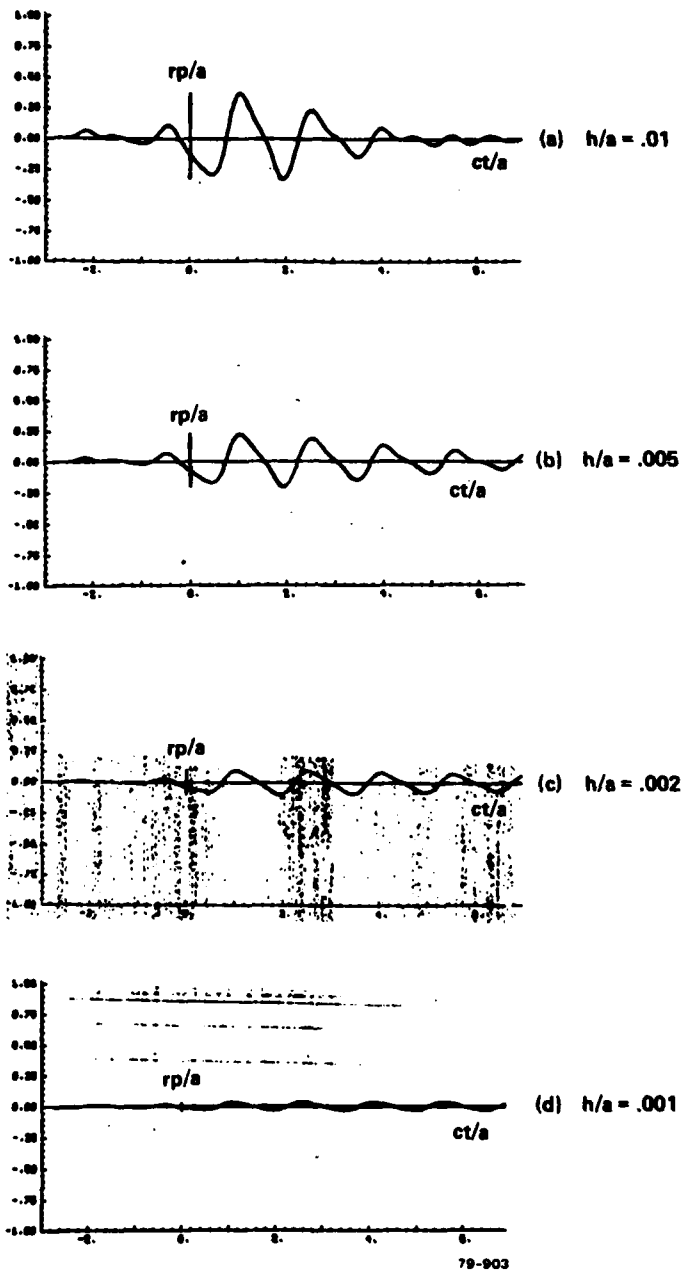


FIG. 5-6 Shell responses as a function of thickness – time domain,  $a_n = 4$ , very thin shell.

the very thin shell response is best understood in the frequency domain as a resonance with its overtones. The resonant frequency is dependent on both  $c_1$  and  $c_2$  as illustrated in Figure 5-7, where one of the elastic parameters of an aluminum shell with  $h = .001$  is changed at a time. If both  $\rho_1$  and  $h$  are changed in such a way that the surface density ( $\rho_1 h$ ) remains constant, then the response remains about constant (for the very thin shell). This is illustrated in Figure 5-8.

In all of the above examples, the core was water filled. It is interesting to see the effect of a different core. In Figure 5-9 the response of a soft sphere is compared to that of a soft core (that is, a gas-filled) spherical shell. The difference between the two responses is the same sequence of resonances already found for the water filled shell. In addition, a large very low frequency resonance is observed. The time domain response is given in Figure 5-10. A similar result is found if the core is a heavier fluid. Figure 5-11 illustrates the response of a glycerin core, which has a density about 1.25 times water. This resembles closely the response of a fluid sphere, but with the spikes characteristic of the shell superposed. The very low frequency spike is absent.

It is significant that a thin shell, surrounding a sound-soft or fluid target has a large effect on the response in the form of sharp resonances.

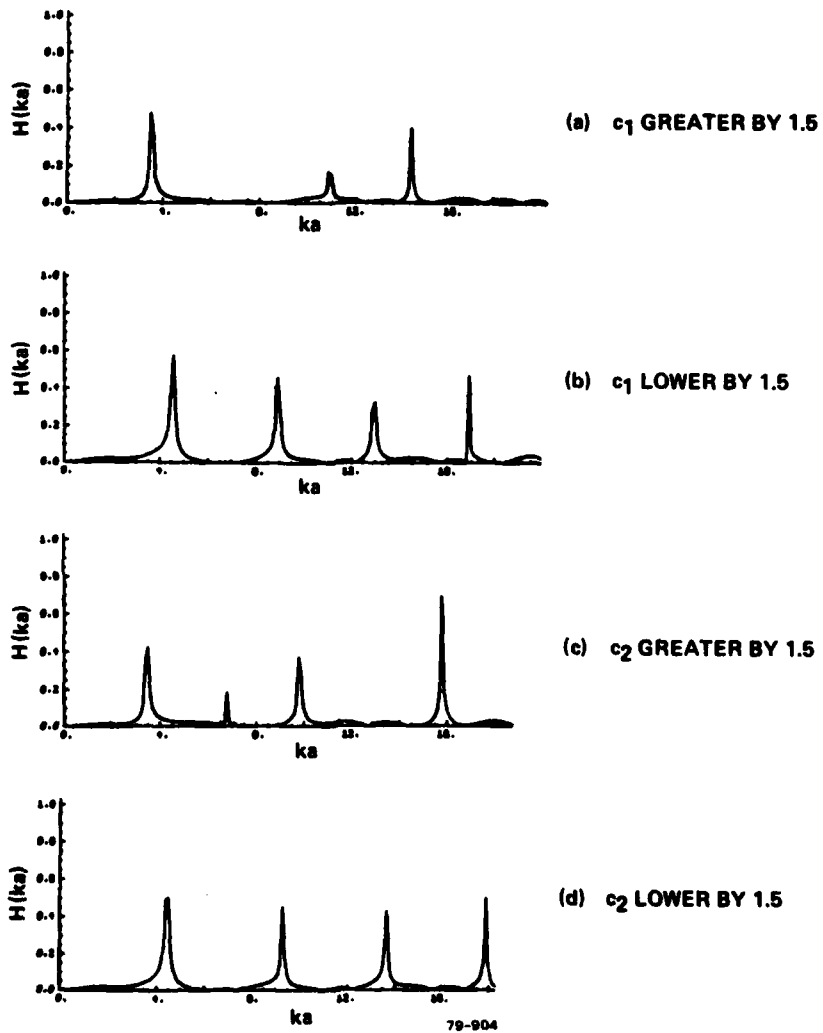


FIG. 5-7 Responses of very thin shell with variations in elastic parameters,  $h = 0.001$ .

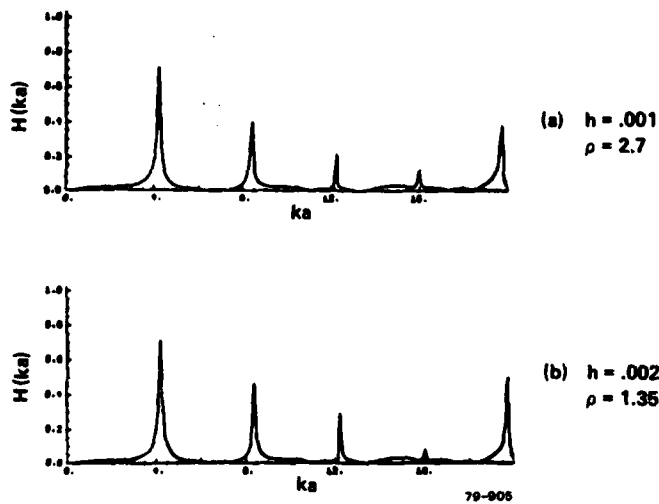


FIG. 5-8 Responses of very thin shell with variations in  $\rho$  and  $h$ , keeping  $\rho_1 h$  constant.

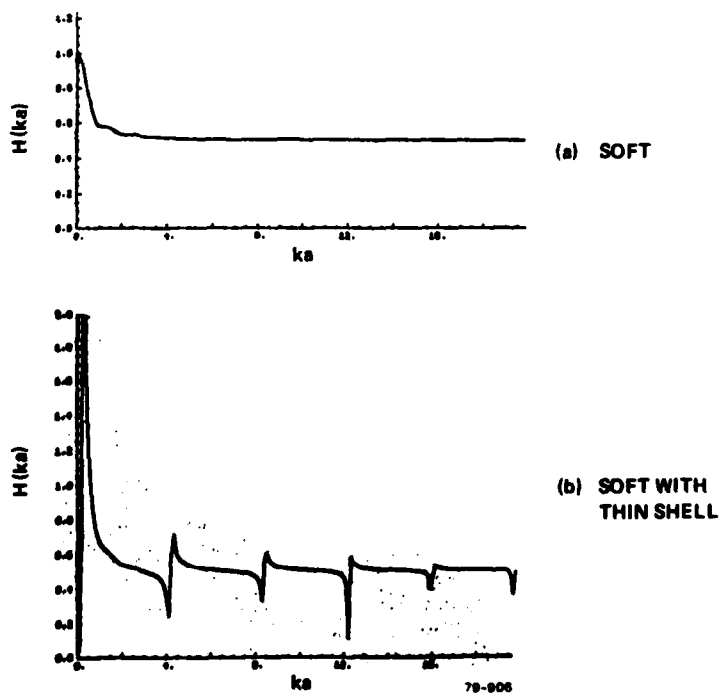


FIG. 5-9 Comparison of responses of soft sphere and soft core (gas-filled) spherical shell — frequency domain.

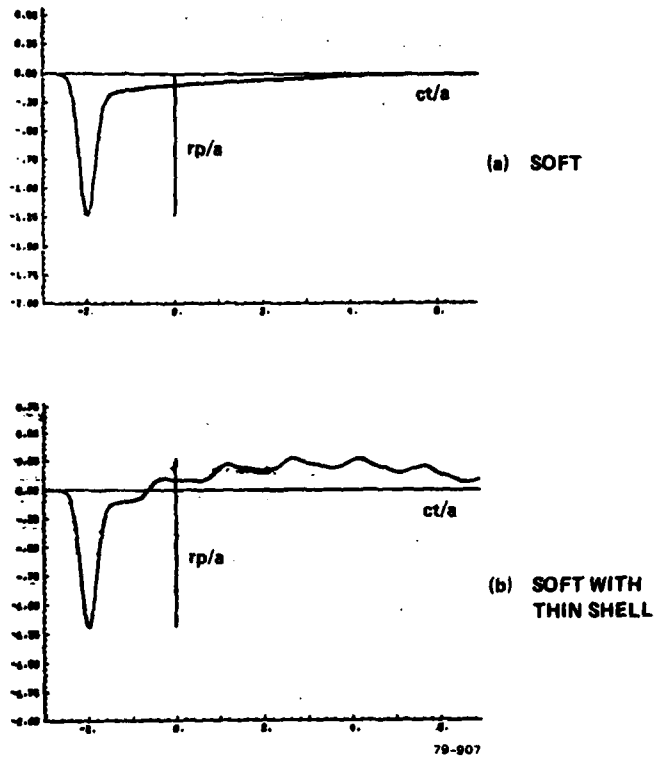


FIG. 5-10 Comparison of responses of soft sphere and soft core (gas-filled) spherical shell — time domain.

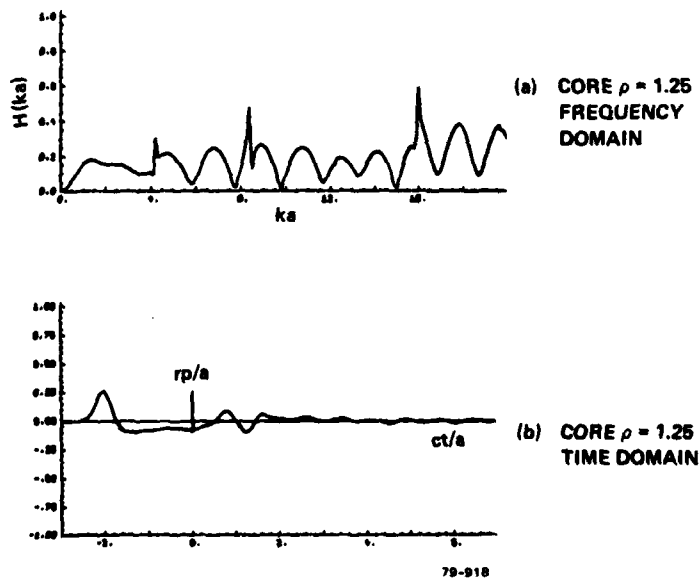


FIG. 5-11 Frequency and time domain responses of heavy core (glycerin-filled) spherical shell.

SECTION 6

REFERENCES

1. H. Mieras and C.L. Bennett, "Active Sonar Modeling," Sperry Research Center, Final Report Contract No. N61339-77-C-0105, August 1978.
2. V.C. Anderson, "Sound Scattering from a Fluid Sphere," JASA 22-4, July 1950.
3. J.J. Faran, "Sound Scattering by Solid Cylinders and Spheres," JASA 23-4, July 1951.
4. M. Goldstein and R.M. Thaler, "Recurrence Techniques for the Calculation of Bessel Functions," MTAC, 1959.
5. R. Hickling, "Analysis of Echoes from a Solid Elastic Sphere in Water," JASA 34-10, October 1962.
6. C.L. Bennett, A.M. Auckenthaler, R.S. Smith and J.D. DeLorenzo, "Space Time Integral Equation Approach to the Large Body Scattering Problem," Final Report, F30602-71-C-0162, RADC-CR-73-70, AD 763794, May 1973.
7. D. Brill and H. Uberall, "Acoustic Waves Transmitted through Solid Elastic Cylinders," JASA 50-3 (Part 2), p. 921, 1971.
8. J.D. Jackson, Classical Electromagnetics, Wiley, N.Y., 1962.
9. E.M. Kennaugh and R.L. Cosgriff, "The Use of Impulse Response in Electromagnetic Scattering Problems," 1958 IRE National Convention Record, Part 1, pp. 72-77.
10. C.L. Bennett, H. Mieras, S.L. Teeter, and J.P. Toomey, "Low EM Signature Response Techniques," Final Report Contract No. F30602-77-C-0166, October 1978.
11. H.C. Van de Hulst, Light Scattering by Small Particles, Wiley, N.Y., 1957.
12. H.C. Bryant and N. Jarmie, "The Glory," Scientific American, July 1974.
13. C.L. Bennett and R.M. Hieronymus, "Solution of Acoustic Space-Time Integral Equations for Soft and Hard Boundary Conditions," SCRC-RR-74-29, November 1974.

AD-A089 651

SPERRY RESEARCH CENTER SUDBURY MA  
TIME-DOMAIN SONAR TARGET RESPONSE MODELING. (U)  
OCT 79 H MIERAS, C L BENNETT  
SRC-CR-79-74

F/G 17/1

UNCLASSIFIED

N61331-78-C-0049

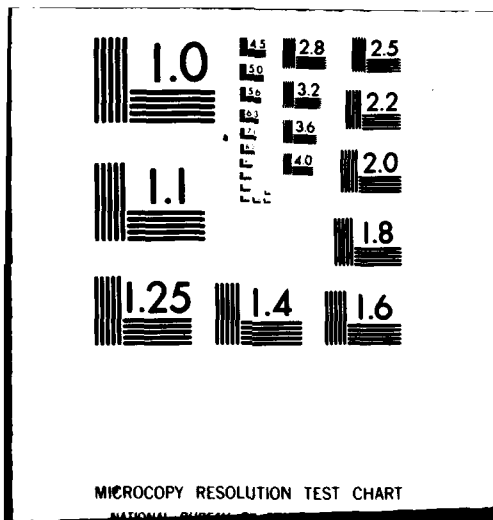
NL

2 of 2

2 of 2



END  
DATE  
FILMED  
10-80  
DTIC



MICROCOPY RESOLUTION TEST CHART

NATIONAL BUREAU OF STANDARDS-1963-A

14. H. Mieras and C.L. Bennett, "Solution of Acoustic Space-Time Integral Equations for Hard or Soft Targets in the Presence of Hard or Soft Planes," SCRC-RR-76-4, February 1976.
15. R.R. Goodman and R. Stern, "Reflection and Transmission of Sound by Elastic Spherical Shells," JASA 34-3, March 1962.

SECTION 7  
APPENDICES

7.1 ELASTIC CONSTANTS

Collected here are some useful relationships and equations to do with elastic properties.

- $\lambda, \mu$  Lamé Coefficients
- $Y, B, \mu$  Young's, Bulk, Shear Moduli
- $\sigma$  Poisson Ratio
- $c_1, c_2$  Longitudinal, Transverse Speeds
- $\rho$  Density

$$Y = 3B(1 - \sigma) = 2\mu(1 + \sigma)$$

$$\lambda = B - 2\mu/3$$

$$c_1^2 = \frac{\lambda + 2\mu}{\rho}$$

$$c_2^2 = \frac{\mu}{\rho}$$

$$c_1^2/c_2^2 = 2(1 - \sigma)/(1 - 2\sigma)$$

$$\sigma = \frac{(c_1^2 - 2c_2^2)/2}{(c_1^2 - c_2^2)}$$

In a fluid:  $\mu = 0, \sigma = 1/2, c_2 = 0$

$\vec{u}$  displacement

Equation of motion:

$$\ddot{\vec{u}} = c_1^2 \nabla(\nabla \cdot \vec{u}) - c_2^2 \nabla \times \nabla \times \vec{u} .$$

In fluid:  $p$  excess pressure,

$$p = -c_1^2 \rho(\nabla \cdot \vec{u}) , \nabla p = -\rho \ddot{\vec{u}} .$$

7.2 SCATTERING MODEL - COMPUTER PROGRAM

PROGRAM ASTROD-ASCROD-TPFS.  
LINES 001-022/17779-16:00 (U.)

100. PARAMETER IPR=4  
110. DIMENSION VZ(IPM),TPATH(3,IPM),PATH(3,IPM),IN3D(IPM)  
120. DIMENSION PZ(IPM),SZ(IPM),EZ(IPM),RZ(IPM),DELTAZ(IPM)  
130. PARAMETER MFORT=11, MFORT=20011, NUMM=MFORT/2  
140. COMPLEX R(MFORT), M(NUMM)  
150. DIMENSION V(MFORT), A(MNUM), A(MNUM), E(MNUM), AT(MFORT), T(MFORT)  
160. ST), SFORT(MNUM)

170. DIMENSION XXX(2), VVV(2)  
180. CHARACTER\*80 TITLE, LABEL  
190. CHARACTER\*48 VLABEL  
200. CHARACTER\*8 CDATE,CTIME

210. C----- CONSTANTS & PARAMETERS  
220. C  
230. C  
240. C  
250. C  
260. C  
270. C  
280. C  
290. C  
300. C

310. C----- END CONSTANTS  
320. C  
330. C  
340. C  
350. C  
360. C  
370. C  
380. C  
390. C  
400. C  
410. C  
420. C

430. C SINGLE MODEL FOR ACOUSTIC SCATTERING FROM ELASTIC SOLID SPHERE  
440. C THIS VERSION VALID ONLY FOR C1<2<C3  
450. C OTHER PATHS INVOLVING EXTERNAL CREEP ARE REQUIRED FOR  
460. C DIFFERENT RELATIONSHIPS BETWEEN THE C'S  
470. C USES THE MAIN PATHS OF THE GLORYWAVE MODEL TO DETERMINE THE  
480. C TIME OF THE RESPONSE  
490. C THE AMPLITUDE IN THIS VERSION IS INPUT -- IT IS EXPECTED TO  
500. C DETERMINE AMPLITUDES IN THE FUTURE BY REFRACTION THEORY  
510. C THE RESPONSE IS CONSIDERED COMPOSED OF PARTS DUE TO EACH PATH  
520. C EACH PART HAS A IMPULSE, STEP, RAMP, BACKSLING AND IS CONSTRAINED  
530. C TO HAVE ZERO INTEGRAL, SO THAT DC RESPONSE IS ZERO  
540. C IMPULSE, STEP, BACKSLING AMPLITUDES DETERMINE THE REST

550. C AUGUST 1979 W. MIERAS  
560. C NESC CONTRACT  
570. C  
580. C  
590. C  
600. C  
610. C  
620. C  
630. C  
640. C  
650. C  
660. C  
670. C  
680. C  
690. C  
700. C  
710. C  
720. C  
730. C  
740. C  
750. C  
760. C  
770. C  
780. C  
790. C  
800. C  
810. C  
820. C  
830. C  
840. C  
850. C  
860. C  
870. C  
880. C  
890. C  
900. C  
910. C  
920. C  
930. C  
940. C  
950. C  
960. C  
970. C  
980. C  
990. C  
1000. C

1010. C----- INPUT-----  
1020. C  
1030. C  
1040. C  
1050. C  
1060. C  
1070. C  
1080. C  
1090. C  
1100. C  
1110. C  
1120. C  
1130. C  
1140. C  
1150. C  
1160. C  
1170. C  
1180. C  
1190. C  
1200. C  
1210. C  
1220. C  
1230. C  
1240. C  
1250. C  
1260. C  
1270. C  
1280. C  
1290. C  
1300. C  
1310. C  
1320. C  
1330. C  
1340. C  
1350. C  
1360. C  
1370. C  
1380. C  
1390. C  
1400. C  
1410. C  
1420. C  
1430. C  
1440. C  
1450. C  
1460. C  
1470. C  
1480. C  
1490. C  
1500. C  
1510. C  
1520. C  
1530. C  
1540. C  
1550. C  
1560. C  
1570. C  
1580. C  
1590. C  
1600. C  
1610. C  
1620. C  
1630. C  
1640. C  
1650. C  
1660. C  
1670. C  
1680. C  
1690. C  
1700. C  
1710. C  
1720. C  
1730. C  
1740. C  
1750. C  
1760. C  
1770. C  
1780. C  
1790. C  
1800. C  
1810. C  
1820. C  
1830. C  
1840. C  
1850. C  
1860. C  
1870. C  
1880. C  
1890. C  
1900. C  
1910. C  
1920. C  
1930. C  
1940. C  
1950. C  
1960. C  
1970. C  
1980. C  
1990. C  
2000. C

210. WRITE(6,210)DENS,CMEB  
220. FORMAT(' SIMPLE MODEL FOR ACOUSTIC SCATTERING FROM',  
230. L' ELASTIC SPHERE '//  
240. 8' MEDIUM DENS,CMEB',F8.4,F8.0/  
250. 8' ENTER TARGET DENS,CLONG,CJSHEAR')  
260. READ(5,DENS,CCLONG,CJSHEAR)  
270. C1=CLONG/CMEB 0 RELATIVE VALUES  
280. C2=CJSHEAR/CMEB  
290. C3=1.  
300. RW=DENS/DENSM  
310. WRITE(6,220)DENS,CCLONG,CJSHEAR,RW,C1,C2  
320. FORMAT('8.4,2E8.0,10L, 8 RELATIVE TO MEDIUM',3E8.4)

330. C----- GLORY PATH CALCULATIONS-----  
340. C  
350. C  
360. C  
370. C  
380. C  
390. C  
400. C  
410. C  
420. C  
430. C  
440. C  
450. C  
460. C  
470. C  
480. C  
490. C  
500. C  
510. C  
520. C  
530. C  
540. C  
550. C  
560. C  
570. C  
580. C  
590. C  
600. C  
610. C  
620. C  
630. C  
640. C  
650. C  
660. C  
670. C  
680. C  
690. C  
700. C  
710. C  
720. C  
730. C  
740. C  
750. C  
760. C  
770. C  
780. C  
790. C  
800. C  
810. C  
820. C  
830. C  
840. C  
850. C  
860. C  
870. C  
880. C  
890. C  
900. C  
910. C  
920. C  
930. C  
940. C  
950. C  
960. C  
970. C  
980. C  
990. C  
1000. C

CRITICAL ANGLES CORRESPONDING TO C1  
SIN(C1-1./C1 0 SINES OF ANGLES  
RIN22INC2UE3

```

670. CTM3C1=SQRT(1.-STM3C1**2)      B COSINES
675. CTM2C1=SQRT(1.-STM2C1**2)
680. TM3C1=ASIN(STM3C1)
685. TM2C1=ASIN(STM2C1)

```

```

690. C CRITICAL ANGLE CORRESPONDING TO C2
700. STM3C2=1./C2
705. STM3C2=ASIN(STM3C2)
710. C
715. C
720. C
725. C
730. C
735. C
740. C
745. C
750. C
755. C
760. C
765. C
770. C
775. C
780. C
785. C
790. C
795. C
800. C
805. C
810. C
815. C
820. C
825. C
830. C
835. C
840. C
845. C
850. C
855. C
860. C
865. C
870. C
875. C
880. C
885. C
890. C
895. C
900. C
905. C
910. C
915. C
920. C
925. C
930. C
935. C
940. C
945. C
950. C
955. C
960. C
965. C
970. C
975. C
980. C
985. C
990. C
995. C
1000. C
1005. C
1010. C
1015. C
1020. C
1025. C
1030. C
1035. C
1040. C
1045. C
1050. C
1055. C
1060. C
1065. C
1070. C
1075. C
1080. C
1085. C
1090. C
1095. C
1100. C
1105. C
1110. C
1115. C
1120. C
1125. C
1130. C
1135. C
1140. C
1145. C
1150. C
1155. C
1160. C
1165. C
1170. C
1175. C
1180. C
1185. C
1190. C
1195. C
1200. C
1205. C
1210. C
1215. C
1220. C
1225. C
1230. C
1235. C
1240. C
1245. C
1250. C

```

```

770. C PATH 1 IS SPHERICAL BEAM
775. C
780. C
785. C
790. C
795. C
800. C
805. C
810. C
815. C
820. C
825. C
830. C
835. C
840. C
845. C
850. C
855. C
860. C
865. C
870. C
875. C
880. C
885. C
890. C
895. C
900. C
905. C
910. C
915. C
920. C
925. C
930. C
935. C
940. C
945. C
950. C
955. C
960. C
965. C
970. C
975. C
980. C
985. C
990. C
995. C
1000. C
1005. C
1010. C
1015. C
1020. C
1025. C
1030. C
1035. C
1040. C
1045. C
1050. C
1055. C
1060. C
1065. C
1070. C
1075. C
1080. C
1085. C
1090. C
1095. C
1100. C
1105. C
1110. C
1115. C
1120. C
1125. C
1130. C
1135. C
1140. C
1145. C
1150. C
1155. C
1160. C
1165. C
1170. C
1175. C
1180. C
1185. C
1190. C
1195. C
1200. C
1205. C
1210. C
1215. C
1220. C
1225. C
1230. C
1235. C
1240. C
1245. C
1250. C

```

```

870. C PATH 2 IS CRITICAL C1 (CROSS) WITH ONE CHORD AT C2
875. C
880. C
885. C
890. C
895. C
900. C
905. C
910. C
915. C
920. C
925. C
930. C
935. C
940. C
945. C
950. C
955. C
960. C
965. C
970. C
975. C
980. C
985. C
990. C
995. C
1000. C
1005. C
1010. C
1015. C
1020. C
1025. C
1030. C
1035. C
1040. C
1045. C
1050. C
1055. C
1060. C
1065. C
1070. C
1075. C
1080. C
1085. C
1090. C
1095. C
1100. C
1105. C
1110. C
1115. C
1120. C
1125. C
1130. C
1135. C
1140. C
1145. C
1150. C
1155. C
1160. C
1165. C
1170. C
1175. C
1180. C
1185. C
1190. C
1195. C
1200. C
1205. C
1210. C
1215. C
1220. C
1225. C
1230. C
1235. C
1240. C
1245. C
1250. C

```

```

970. C PATH 3 IS CRITICAL C1, WITH TWO CHORDS AT C2
975. C
980. C
985. C
990. C
995. C
1000. C
1005. C
1010. C
1015. C
1020. C
1025. C
1030. C
1035. C
1040. C
1045. C
1050. C
1055. C
1060. C
1065. C
1070. C
1075. C
1080. C
1085. C
1090. C
1095. C
1100. C
1105. C
1110. C
1115. C
1120. C
1125. C
1130. C
1135. C
1140. C
1145. C
1150. C
1155. C
1160. C
1165. C
1170. C
1175. C
1180. C
1185. C
1190. C
1195. C
1200. C
1205. C
1210. C
1215. C
1220. C
1225. C
1230. C
1235. C
1240. C
1245. C
1250. C

```

```

970. C PATH 4 IS CRITICAL C2
975. C
980. C
985. C
990. C
995. C
1000. C
1005. C
1010. C
1015. C
1020. C
1025. C
1030. C
1035. C
1040. C
1045. C
1050. C
1055. C
1060. C
1065. C
1070. C
1075. C
1080. C
1085. C
1090. C
1095. C
1100. C
1105. C
1110. C
1115. C
1120. C
1125. C
1130. C
1135. C
1140. C
1145. C
1150. C
1155. C
1160. C
1165. C
1170. C
1175. C
1180. C
1185. C
1190. C
1195. C
1200. C
1205. C
1210. C
1215. C
1220. C
1225. C
1230. C
1235. C
1240. C
1245. C
1250. C

```

```

1070. C TRAVERSAL TIMES
1075. C
1080. C
1085. C
1090. C
1095. C
1100. C
1105. C
1110. C
1115. C
1120. C
1125. C
1130. C
1135. C
1140. C
1145. C
1150. C
1155. C
1160. C
1165. C
1170. C
1175. C
1180. C
1185. C
1190. C
1195. C
1200. C
1205. C
1210. C
1215. C
1220. C
1225. C
1230. C
1235. C
1240. C
1245. C
1250. C

```

```

1140. C PARTS OF IMPULSE RESPONSE CORRESPONDING TO EACH PATH
1145. C
1150. C
1155. C
1160. C
1165. C
1170. C
1175. C
1180. C
1185. C
1190. C
1195. C
1200. C
1205. C
1210. C
1215. C
1220. C
1225. C
1230. C
1235. C
1240. C
1245. C
1250. C

```

```

1170. C
1175. C
1180. C
1185. C
1190. C
1195. C
1200. C
1205. C
1210. C
1215. C
1220. C
1225. C
1230. C
1235. C
1240. C
1245. C
1250. C

```

```

1210. C DERIVED PULSE PARAMETERS
1215. C
1220. C
1225. C
1230. C
1235. C
1240. C
1245. C
1250. C

```

```

1470. WRITE(6,250)(IP,PZ(IP),SZ(IP),EZ(IP),RZ(IP),DELTAZ(IP),
1475. A TZ(IP),THZ(IP),(TPATH(IC,IP),IC=1,3),IP=1,IPM)
1480. FORMAT(' IMPULSE RESPONSE PARAMETERS // IP PZ SZ
1485. A'EZ RZ DELTAZ TZ THZD PL1/C1 ',
1490. C PL2/Z2 PL3/Z3')
1495. FORMAT('X,11,10F7.3')
1500. C
1505. WRITE(6,270)
1510. FORMAT(' ENTER FREQUENCY STEP DM, MAX WM, SM,IMPULSE AN')
1515. READ(5,*)DM,WM,AN
1520. NUMBDM=DM*1.5
1525. NUM=MIN(NUM,NUMM)
1530. WM=NUMDM-DM
1535. WRITE(6,280)DM,WM,AN,NUM,MFORT
1540. FORMAT('H,FM=3.2F8.3,16,' VALUES, FFT ON,15,' POINTS')
1545. CALL FORT(0,MFORT,SFORT,0,LFORT) B SET UP FFT SINETABLES
1550. C
1555. C-----END INPUT-----AND CALC SET-UP-----
1560. C
1565. C COMPUTE FREQUENCY RESPONSE FOR EACH PAIR AND ADD TOGETHER IN M(W)
1570. C
1575. C CALL RESPNS(IPR,TZ,PZ,SZ,EZ,RZ,DELTAZ,DM,NUM,M)
1580. C
1585. C
1590. C
1595. C
1600. C
1605. C
1610. C
1615. C
1620. C
1625. C
1630. C
1635. C
1640. C
1645. C
1650. C
1655. C
1660. C
1665. C
1670. C
1675. C
1680. C
1685. C
1690. C
1695. C
1700. C
1705. C
1710. C
1715. C
1720. C
1725. C
1730. C
1735. C
1740. C
1745. C
1750. C
1755. C
1760. C
1765. C
1770. C
1775. C
1780. C
1785. C
1790. C
1795. C
1800. C
1805. C
1810. C
1815. C
1820. C
1825. C
1830. C
1835. C
1840. C
1845. C
1850. C
1855. C
1860. C
1865. C
1870. C
1875. C
1880. C
1885. C
1890. C
1895. C
1900. C
1905. C
1910. C
1915. C
1920. C
1925. C
1930. C
1935. C
1940. C
1945. C
1950. C
1955. C
1960. C
1965. C
1970. C
1975. C
1980. C
1985. C
1990. C
1995. C
2000. C

```



2440. C  
2450. 9J CONTINUE  
2460. STOP  
2470. END

END 010 750 10ANK 17115 00ANK

1070.5 ASCR0B-RESPNS,TPFS.

108. 0.2/17/72-16:01(0.2)

100. SUMOUTLINE RESPNS(N,TZ,PZ,SZ,EZ,RZ,DM,MU,M)  
110. DIMENSION TZ(N),PZ(N),SZ(N),EZ(N),RZ(N),DELTZ(N)  
120. COMPLEX N(N),CMI,CEA2,CR,JAY

130. C  
140. C ADD M RESPONSES IN FREQ DOMAIN  
150. C RESPONSE OCCURS AT TIME TZ, AND IS COMPOSED OF IMPULSE PZ.  
160. C STEP SZ, RAMP RZ, BACKSWING EZ AT TIME DELTZ,TZ  
170. C ASSUME RZ, DELTZ SET SUCH THAT DC RESPONSE M(0) IS ZERO  
180. C CALLED BY MODELING PROGRAM ASCR0B

190. C  
200. JAV=(0.,1.)  
210. DO 12 I=1,M  
220. M(I)=(0.,0.)  
230. DO 8 K=1,N 3 FOR M PULSES  
240. M=0.

250. DO 7 I=2,MM 9 AT ALL FREQ. EXCEPT M=0.  
260. V=M\*DM  
270. A2=-M\*Z(I,K)  
280. CEA2=CEBP(A2\*JAY)  
290. CMI=(0.,0.,0.,0.)

300. CR=PZ(K)\*CMI\*(SZ(K)-EZ(K)+CEA2)-RZ(K)\*(1.-CEA2)/M\*\*2  
310. M(I)=CR\*CEBP(A1\*JAV)\*M(I)  
320. C  
330. C  
340. C  
350. C

360. C  
370. C  
380. C  
390. C  
400. C  
410. C  
420. C  
430. C  
440. C  
450. C  
460. C  
470. C  
480. C  
490. C  
500. C  
510. C  
520. C  
530. C  
540. C  
550. C

END 010 750 10ANK 85 00ANK



FORT 155  
 FORT 159  
 FORT 160  
 FORT 161  
 FORT 162  
 FORT 163  
 FORT 164  
 FORT 165  
 FORT 166  
 FORT 167  
 FORT 168  
 FORT 169  
 FORT 170  
 FORT 171  
 FORT 172  
 FORT 173  
 FORT 174  
 FORT 175  
 FORT 176  
 FORT 177  
 FORT 178  
 FORT 179  
 FORT 180  
 FORT 181  
 FORT 182  
 FORT 183  
 FORT 184  
 FORT 185  
 FORT 186  
 FORT 187  
 FORT 188  
 FORT 189  
 FORT 190  
 FORT 191  
 FORT 192  
 FORT 193  
 FORT 194  
 FORT 195  
 FORT 196  
 FORT 197  
 FORT 198  
 FORT 199  
 FORT 200  
 FORT 201  
 FORT 202  
 FORT 203  
 FORT 204  
 FORT 205  
 FORT 206  
 FORT 207  
 FORT 208  
 FORT 209  
 FORT 210  
 FORT 211  
 FORT 212  
 FORT 213  
 FORT 214  
 FORT 215  
 FORT 216

60 N=2000  
 61 IF (A(1,1)) - 1) 20,20,0,0  
 62 WE ARE DOING TRANSFORM ONLY. SEE IF PRE-COMPUTED  
 63 S TABLE IS SUFFICIENTLY LARGE  
 64 1L 100 N=MP 20000,12  
 65 1L 10000  
 66 GO TO 200  
 67 SCRAMBLE A, BY SANDER'S METHOD  
 68 1L 10000  
 69 DO 22 L=2,M  
 70 22 2LJ=K(L-1)/2  
 71 DO 24 L=K,12  
 72 24 2LJ=2  
 73 NOTE EQUIVALENCE OF KL AND K(14-L)  
 74 PRIMARY SORT-  
 75 1J=2  
 76 DO 30 J1=2,K1,2  
 77 DO 30 J2=J1,K2,K1  
 78 DO 30 J3=J2,K3,K2  
 79 DO 30 J4=J3,K4,K3  
 80 DO 30 J5=J4,K5,K4  
 81 DO 30 J6=J5,K6,K5  
 82 DO 30 J7=J6,K7,K6  
 83 DO 30 J8=J7,K8,K7  
 84 DO 30 J9=J8,K9,K8  
 85 DO 30 J10=J9,K10,K9  
 86 DO 30 J11=J10,K11,K10  
 87 DO 30 J12=J11,K12,K11  
 88 DO 30 J13=J12,K13,K12  
 89 1F(13-J13)\*30,30  
 90 2' T=AC(IJ-1)  
 91 ALIA=13-A(IJ-1)  
 92 AC(IJ)=T  
 93 T=AC(IJ)  
 94 AC(IJ)=ALIA  
 95 30 14=14?  
 96 IF(15)22,2,36  
 97 DOING FOURIER ANALYSIS,SO DIV. BY N AND CONJUGATE.  
 98 32 FN = N  
 99 DO 36 J1=1,M  
 100 A(201-1) = A(201-1)/FN  
 101 34 A(201)=-A(201)/FN  
 102 SPECIAL CASE- L=1  
 103 DO 40 I=1,N,2  
 104 T = A(201-I)  
 105 A(201-1) = T + A(201-I)  
 106 40 40(1)=T-A(201-I)  
 107 T=40(1)  
 108 40(1) = 1 + A(201-I)  
 109 40 A(201-I) = T - A(201-I)  
 110 IF(M-1) 2,1, 50  
 111 SET FOR L=2  
 112 L=1,1-2  
 113 LEPT=200(L-1)  
 114 L=1,1  
 115 LEPT=200(L+1)  
 116 MPL=LEPT  
 117 MPL=LEPT  
 118 MPL = MP\* 200-L  
 119

FORT 217  
 FORT 218  
 FORT 219  
 FORT 220  
 FORT 221  
 FORT 222  
 FORT 223  
 FORT 224  
 FORT 225  
 FORT 226  
 FORT 227  
 FORT 228  
 FORT 229  
 FORT 230  
 FORT 231  
 FORT 232  
 FORT 233  
 FORT 234  
 FORT 235  
 FORT 236  
 FORT 237  
 FORT 238  
 FORT 239  
 FORT 240  
 FORT 241  
 FORT 242  
 FORT 243  
 FORT 244  
 FORT 245  
 FORT 246  
 FORT 247  
 FORT 248  
 FORT 249  
 FORT 250  
 FORT 251  
 FORT 252  
 FORT 253  
 FORT 254  
 FORT 255  
 FORT 256  
 FORT 257  
 FORT 258  
 FORT 259  
 FORT 260  
 FORT 261  
 FORT 262  
 FORT 263  
 FORT 264  
 FORT 265  
 FORT 266  
 FORT 267  
 FORT 268  
 FORT 269  
 FORT 270  
 FORT 271  
 FORT 272  
 FORT 273  
 FORT 274  
 FORT 275

```

181 C 00 130 L=20M
182 SPECIAL CASE- J=C
183 DO 80 I=2,N2+LEAP
184 I=1 + LEAP1
185 I2=I2+LEAP1
186 I3=I2+LEAP1
187 V=A(I-1)
188 A(I1-1) = T +A(I1-1)
189 A(I2-1) = T-A(I1-1)
190 V=A(I1)
191 A(I1) = T+A(I12)
192 A(I2) = T-A(I12)
193 V=-A(I13)
194 T1 = A(I1-1)
195 A(I1-1) = A(I1-1) - T
196 A(I13) = A(I11) - T1
197 A(I11-1) = A(I11-1) + T
198 80 AC(I1) = A(I1) + T1
199 IF(L-2) 120,120,90
200 KLAST=N2-LEAP
201 JJ=NPL
202 DO 110 J=4,LEAP1,2
203 MPJ=MJ-JJ
204 UR=S(MPJ)
205 U1=S(JJ)
206 ILAST=J+KLAST
207 DO 100 I=J,ILAST,LEAP
208 I=I+LEAP1
209 I2=I1+LEAP1
210 I3=I2+LEAP1
211 V=A(I2-1)*UR-A(I1)*U1
212 I1=A(I1-1)*U1+A(I2)*UR
213 A(I2-1)=A(I1-1)-T
214 A(I2) =A(I1) - T1
215 A(I1-1) =A(I1-1)+T1
216 A(I1) =A(I1)+T1
217 V=-A(I1-1)*U1-A(I3)*UR
218 I1=A(I1-1)*UR-A(I3)*U1
219 A(I1-1)=A(I1-1)-T
220 A(I3) =A(I1) -T1
221 A(I1-1)=A(I1-1)+T1
222 100 AC(I1) =A(I1) +T1
223 C END OF I LOOP
224 JJ=JJ+NPL
225 C END OF J LOOP
226 LEAP1=2*LEAP1
227 LEAP = 2*LEAP
228 150 NPL=NPL/2
229 C END OF L LOOP
230 IF(I15)145,201
231 C DOING FOURIER ANALYSIS. REPLACE A BY CONJUGATE.
232 DO 150 I=1,N
233 AC(2+I) =-A(2+I)
234 GO TO 1
235 RETURN
236 C *ALL TABLE OF S(J)=SIN(2*PI*J/MP),J=1,2,.....,NT-1,NT=NP/4
237 NP=N
238 NT=N/4
239
  
```

```

177      MT=2
178      IF (MT) 2,0,2,205
179      THETA=.7053981634
180      C      THETA=PI/2*(L+1)      FOR L=1
181      210  JSTEP = NI
182      C      JSTEP = 2*(MT-L+1) FOR L=1
183      215  JDI = NI/2
184      C      JDI = NI/2
185      220  JDI = L*(MT-L) FOR L=1
186      C      S(JDI) = SIN(THETA)
187      IF (MT-2) 260,220,220
188      220  DO 250 L=2,MT
189      THETA = THETA/2.
190      JSTEP = JSTEP
191      JDI = JDI
192      S(JDI) = SIN(THETA)
193      C      S(JDI) = COS(THETA)
194      JLAST=MT-JSTEP
195      IF (JLAST-JSTEP) 250,210,210
196      210  DO 240 J=JSTEP,JLAST,JSTEP
197      JC=NI-J
198      J=JLAST
199      240  S(J)=S(J)*S(JC)+S(JC)*S(JDI)*S(JC)
200      250  CONTINUE
201      260  IF (IES) 20,1,20
202      END

```

```

FORT 276
FORT 277
FORT 278
FORT 279
FORT 280
FORT 281
FORT 282
FORT 283
FORT 284
FORT 285
FORT 286
FORT 287
FORT 288
FORT 289
FORT 290
FORT 291
FORT 292
FORT 293
FORT 294
FORT 295
FORT 296
FORT 297
FORT 298
FORT 299
FORT 300
FORT 301

```